AEDC-TR-68-148

cy_l

COMPARISON OF A FIRST-ORDER TREATMENT OF HIGHER-ORDER BOUNDARY-LAYER EFFECTS WITH SECOND-ORDER THEORY AND EXPERIMENTAL DATA

Clark Houston Lewis

ARO, Inc.

October 1968

VON KÁRMÁN GAS DYNAMICS FACILITY
ARNOLD ENGINEERING DEVELOPMENT CENTER
AIR FORCE SYSTEMS COMMAND
ARNOLD AIR FORCE STATION, TENNESSEE

NOTICES

COMPARISON OF A FIRST-ORDER TREATMENT
OF HIGHER-ORDER BOUNDARY-LAYER EFFECTS
WITH SECOND-ORDER THEORY
AND EXPERIMENTAL DATA

Clark Houston Lewis

ARO, Inc.

This document has been approved for public release
and sale; its distribution is unlimited.

FOREWORD

The work reported herein was sponsored by Headquarters, Arnold Engineering Development Center (AEDC), Air Force Systems Command (AFSC), under Program Element 6540223F, Project 8953.

The results of research presented were obtained by ARO, Inc. (a subsidiary of Sverdrup & Parcel and Associates, Inc.), contract operator of the AEDC, AFSC, Arnold Air Force Station, Tennessee, under Contract F40600-69-C-0001. The research was conducted from June 1, 1966 to January 1, 1968, under ARO Project No. VW5819, and the manuscript was submitted for publication June 11, 1968.

This report was accepted as a dissertation by the University of Tennessee in partial fulfillment of the requirements for the degree of Doctor of Philosophy with a major in Engineering Science.

Some of the results reported in this dissertation were presented in a paper entitled "First- and Second-Order Boundary-Layer Effects at Hypersonic Conditions" read at the North Atlantic Treaty Organization's Advisory Group for Aerospace Research and Development (AGARD) Seminar on "Numerical Methods for Viscous Flows" held at the National Physical Laboratory, Teddington, England during September 18-21, 1967.

This technical report has been reviewed and is approved.

David C. Reynolds
2nd Lt, USAF
Research Division
Director of Plans
  and Technology

Edward R. Feicht
Colonel, USAF
Director of Plans
  and Technology

ABSTRACT

The axisymmetric nonsimilar compressible laminar boundary-layer equations including approximate transverse curvature terms were modified to treat inviscid external vorticity, slip and temperature jump as first-order quantities, and this is referred to as the first-order treatment. The effects of boundary-layer displacement were also treated. Primary interest was in predicting experimentally measurable quantities over the entire body length of nonanalytic shapes, and the analysis was not confined to the nose or stagnation region. A review is included of second-order boundary-layer theory and of recent developments in the numerical solution of second-order boundary-layer effects. Comparisons of predicted displacement-induced pressure distributions, heat-transfer distributions and zero-lift drag were made with results from second-order boundary-layer theory and experimental data for a spherically blunted 9-degree half-angle cone at free-stream Mach numbers of 9 and 18. At moderate to high Reynolds numbers, the comparisons showed good agreement between first- and second-order predictions and experimental results for drag and heat-transfer distributions; however, poor agreement was found between predicted and experimental displacement-induced pressure distributions. At low Reynolds numbers, both first- and second-order treatments substantially overpredicted the zero-lift drag. The range of applicability of the theories was established for the conditions treated by

inspection of the numerical results and by comparison of the numerical results with experimental zero-lift drag data. Separate and coupled first- and second-order boundary-layer effects were considered for experimentally measurable quantities. The first-order treatment showed, for example, that slip and temperature jump produced a small effect when considered as a separate effect; however, this effect became important and under certain conditions dominant when coupled with other effects at low Reynolds numbers. Limitations and difficulties in both first- and second-order boundary-layer treatments are discussed.

TABLE OF CONTENTS

LIST OF TABLES

LIST OF FIGURES

FIGURE   PAGE

NOMENCLATURE

Unless otherwise noted, all lengths are nondimensionalized by the nose
radius.

A_b Base area

A_1 Parameter defined by Equation 40f

a   Nose radius in second-order boundary-layer theory

a_1 Slip constant, $(\pi/2)^{1/2}$

B   Parameter in displacement thickness with external vorticity

         (see Appendix C)

R_n Nose bluntness parameter, r_n/r_b

B_{sh} Nose-to-shock radius ratio, r_n/r_{sh}

b_1 Slip constant, 3/4

C   Density viscosity product ratio, $\rho\mu/\rho_e\mu_e$

C_{D_f} Friction-drag coefficient referenced to base area

C_{D_p} Pressure-drag coefficient referenced to base area

C_{disp} Displacement term in continuity equation defined by

         Equation 38a

C_f Skin-friction coefficient, $2\tau_w/\rho_\infty U_\infty^2$

C_{LC} Longitudinal curvature term in continuity equation defined

         by Equation 38b

C_{STJ} Slip and temperature term in continuity equation defined

         by Equation 38a

C_{TVC} Transverse curvature term in continuity equation defined by Equation 38c

C_{vort} Vorticity term in continuity equation defined by Equation 38a

C_{∞} Coefficient in linear viscosity law, $(\mu_W/\mu_{\infty})(T_{\infty}/T_W)$

c_1 Slip constant, $(15/8)(\pi/2)^{1/2}$

c_p Constant pressure specific heat

E_{disp} Displacement term in energy equation defined by Equation 40d

E_{LC} Longitudinal curvature term in energy equation defined by Equation 40b

E_{STJ} Slip and temperature jump term in energy equation defined by Equation 40e

E_{TVC} Transverse curvature term in energy equation defined by Equation 40c

E_{vort} Vorticity term in energy equation defined by Equation 40a

e Error test in first-order momentum and energy equation solutions

F_S Parameter defined by Equation 86c

f Dimensionless stream function

f' Velocity ratio, u/u_e

g Stagnation enthalpy ratio, H/H_e

H Stagnation enthalpy

h Static enthalpy

h_{ref} Reference specific enthalpy, 2.119×10^8 ft^2/sec^2

j Index 0 or 1 for two-dimensional or axisymmetric flow, respectively

K	Parameter defined by Equation 85b; bound on $\phi'(n_\infty)$ in first-order treatment (see Appendix A)
k	The factor $1 + \kappa n$
L	Characteristic length (dimensional)
ℓ	Axial length of body (dimensional)
M	Mach number
M_{disp}	Displacement term in tangential momentum equation defined by Equation 39d
M_{LC}	Longitudinal curvature term in tangential momentum equation defined by Equation 39b
M_{STJ}	Slip and temperature jump term in tangential momentum equation defined by Equation 39e
M_{TVC}	Transverse curvature term in tangential momentum equation defined by Equation 39c
M_{vort}	Vorticity term in tangential momentum equation defined by Equation 39a
N	Inner expansion variable in second-order boundary-layer theory, n/ϵ; parameter in first-order treatment defined below Equation 78
n	Outer expansion variable in second-order boundary-layer theory, $n*/a*$
P	Inviscid outer flow pressure, $p*/\rho_\infty* U_\infty*^2$
Pr	Prandtl number
p	Pressure
p_o'	Free-stream normal shock pitot pressure

$\vec{Q}$ Total velocity vector

R   Inviscid outer flow density; radius parameter; gas constant

Re   Reynolds number, $\rho_\infty^* U_\infty^* r_n^*/\mu_\infty^*$

$\dot{Re}_{\infty,\ell}$ Reynolds number, $\rho_\infty U_\infty \ell/\mu_\infty$

Re_* Reynolds number, $\rho_* u_* r_n/\mu_*$

r   Radius

r_n Nose radius (dimensional)

S   Entropy

S_1' Entropy derivative in basic inviscid flow, $dS_1/d\Psi$

St   Stanton number, $q^*/[\rho_\infty^* U_\infty^* c_p^* (T_0^* - T_w^*)]$

s   Surface distance measured from stagnation point

T   Inviscid outer flow temperature, $T^*/(U_\infty^{*2}/c_p^*)$

T_{cs} First-order transverse curvature parameter

t   Inner flow temperature

U   Tangential component inviscid outer flow velocity

U_∞ Free-stream velocity

u   Tangential velocity

V   Normal component inviscid outer flow velocity

v   Normal velocity

$\bar{v}_\infty$ Hypersonic viscous interaction parameter, $M_\infty (C_\infty/Re_{\infty,\ell})^{1/2}$

x   Surface distance from stagnation point

y   Distance normal to surface

z   Axial distance from stagnation point

α Angle between tangent to surface and axis of symmetry

β Pressure gradient parameter, $(x/u_e) \, du_e/dx$

γ Ratio of specific heats, 1.4

δ Boundary-layer thickness

δ^* Boundary-layer displacement thickness, δ^{**}/a^*

δ^*_D Davis' displacement thickness, δ^*/ϵ

δ^*_V Displacement thickness with external vorticity

ϵ Van Dyke's expansion parameter defined by Equation 8

ζ Inviscid vorticity

η Transformation variable

η_∞ Edge of boundary layer in transformed plane

θ_c Cone half angle

κ Longitudinal curvature

λ Second viscosity coefficient

μ Dynamic viscosity coefficient

ρ Density

σ Prandtl number in second-order boundary-layer theory

τ Shear stress

Φ Dissipation function defined by Equation 5

ϕ Transformation variable, $f-\eta$

Ψ Outer stream function

ψ Transformation variable, $g-1$; inner stream function

Ω Vorticity index defined by Equation 79

Ω_1 Van Dyke's inviscid vorticity

ω Exponent in power viscosity law

SUBSCRIPTS

o	Stagnation conditions
1	First-order quantity
2	Second-order quantity
b	Base
disp	Displacement effect
e	At the edge of the boundary layer
eff	At the effective body surface
i	Inviscid
LC	Longitudinal-curvature effect
N	Derivative with respect to inner variable N
n	Derivative with respect to outer variable n
sh	Shock wave
STJ	Slip-and-temperature-jump effect
TVC	Transverse-curvature effect
vort	Vorticity effect
w	Wall
x	Derivative with respect to x-coordinate
y	Derivative with respect to y-coordinate
*	Sonic conditions
∞	At free-stream conditions

SUPERSCRIPTS

'	Derivative with respect to independent variable
*	Dimensional quantity in second-order theory

(k)   Iteration index in first-order displacement treatment

In the figures, open symbols and/or curves are used to denote numerical results and filled symbols denote experimental data.

CHAPTER I
INTRODUCTION AND DEFINITION OF TERMS USED

Before the introductory discussion of the problem is presented, a few terms will be defined which may not have a clear definition in the literature. After the terms are defined, the background to the problem will be given and the methods used and scope of the research reported in the dissertation will be described.

I. DEFINITION OF TERMS USED

Entropy layer. This is an inviscid layer of gas near the wall which has passed through the curved portion of the bow shock wave. The entropy in this layer decreases from a maximum along the wall to a minimum along a streamline passing through the inflection point in the bow shock wave (if one exists) and increases to the constant value behind a straight (conical) shock wave. This concept will be made clearer later in this chapter by consideration of the inviscid shock layer over a spherically blunted cone at hypersonic flight conditions.

First-order boundary-layer effects. Prandtl's classical boundary-layer equations for conservation of mass, momentum and energy for two-dimensional and axisymmetric flow are the basic first-order equations. If terms are added to this system of equations to approxi-

1

mate other effects or if the boundary conditions for the equations are modified, the resulting system of equations is called first order, and the numerical solution method is called a first-order treatment of higher-order boundary-layer effects. It is possible only a posteriori to determine the magnitude of any specific effect by comparison of solutions with and without the effect included. Moreover, in general, simple scaling laws do not exist to scale wall-measurable quantities such as skin-friction coefficient or heat-transfer rate; therefore, a series of calculations is necessary over the range of the variables of interest.

Second-order boundary-layer effects. If the flow variables such as velocity, temperature, density, pressure, etc. are expanded in terms of an appropriate small parameter and the resulting expansions are substituted into the Navier-Stokes equations, it is possible to obtain two systems of equations describing the flow. The lowest-order system is Prandtl's equations, which are called the classical first-order boundary-layer equations. These equations are nonlinear partial differential equations. A second system of linear partial differential equations is obtained where various terms can be identified with second-order boundary-layer effects of physical significance. The second-order effects are not all independent and uncoupled, but with one exception simple scaling laws can be obtained to scale the results.

Longitudinal curvature effect. When the surface of a body is

curved rather than flat in the direction of the free-stream velocity vector, centrifugal forces produce a pressure change normal to the surface. This curvature will influence both the inviscid and viscous flow fields; however, the effects on the inviscid flow field are usually larger, persist further downstream along the body, and are more easily treated numerically than are the effects on the viscous boundary layer.

Transverse curvature effect. A second curvature effect arises when axisymmetric bodies of revolution are considered. The boundary layer on a body of revolution grows less rapidly than the change in wall radius with axial distance far downstream along the body because of the transverse curvature effect. Moreover, the radial distance of points in the boundary layer from the axis of symmetry may not be assumed equal to the local wall radius when the ratio of the thickness of the boundary layer to the local wall radius cannot be assumed negligible.

Displacement effect. In classical boundary-layer theory, the properties at the edge of the boundary layer are obtained from the inviscid flow field solution over the geometric body without a boundary layer. The boundary layer retards the flow and displaces the stream-lines near the surface. This effect on the inviscid outer flow appears as the flow over the geometric body thickened by the boundary-layer displacement thickness. This displacement effect causes changes in the properties at the edge of the boundary layer.

External vorticity effect. At supersonic and hypersonic speeds, a blunt body produces a curved detached bow shock wave which in turn produces an inviscid rotational flow field. A boundary layer growing on a body under such a flow field would have different "edge" conditions because of the shock-generated inviscid external vorticity. This effect can be further subdivided into an entropy gradient effect and a stagnation enthalpy gradient effect. For most practical problems, it is satisfactory to treat the inviscid flow field as isoenergetic, and thus under these conditions only the entropy gradient effect needs to be considered.

Slip and temperature jump effects. Under highly rarefied flow conditions, the gas tangential velocity at the wall is not zero relative to the wall and the temperature of the gas at the wall is not the wall temperature value. A continuum analysis based on the Navier-Stokes equations can be applied if the wall boundary conditions on the tangential velocity and static temperature are modified to include the noncontinuum effects of velocity slip and temperature jump.

The roles of first- and second-order boundary-layer effects will be made clearer in the following discussion.

II. INTRODUCTION

As a high-speed vehicle enters the earth's atmosphere, the flow field about the vehicle changes from near free-molecule flow in the outer regions of the atmosphere through various noncontinuum regions to a more classical continuum inviscid outer flow and inner viscous

4

laminar and turbulent flow fields. At high speed the gas is not a simple ideal gas since chemical equilibrium and nonequilibrium effects on the thermodynamic properties are also important.

The part of this complex problem which will be of concern in this dissertation is the extension of classical laminar boundary-layer flow theory into the lower Reynolds number regime. In modern hypersonic wind tunnels, the aim is toward flight simulation since flight duplication is almost never achieved. It is also worth noting that in these hypersonic test facilities, the flow fields over blunt-nosed bodies are almost always laminar since the effect of the blunt nose reduces the local Reynolds number in the flow field, and thus natural transition from laminar to turbulent flow seldom occurs.

The incentive for this research began in 1959 with some unexpectedly high drag measurements found in testing a slender blunt cone in the hotshot tunnels of the von Karman Gas Dynamics Facility (VKF). The application of simple boundary-layer theory failed to predict the experimentally observed data. Whitfield and Griffith [1][1] developed an approximate theory for predicting total zero-lift drag based upon the boundary-layer theory of Cohen and Reshotko [2,3], displacement effects based on the work of Lees and Probstein [4] and and Probstein [5], and transverse curvature (TVC) considerations as treated by Probstein and Elliott [6]. The method briefly was as

---

[1]Numbers in square brackets refer to similarly numbered references in the bibliography.

5

follows: First, the friction drag and displacement thickness were computed by the Cohen and Reshotko integral method [3] and a correlation of experimental pressure distributions. Then, with the aid of the above-mentioned theories [4,5,6] the displacement-induced pressure and friction drags and transverse-curvature-induced friction drag were computed. Whitfield and Griffith assumed that the theories of Probstein [5] and Probstein and Elliott [6] which were developed for sharp cones could also be applied to spherically blunted cones by assuming that the local, induced skin friction at the sphere-cone junction was the same as would exist at the same point on a sharp cone (i.e., τ_W (blunt sphere-cone junction, θ_c) = τ_W (sharp, θ_c)). In addition, constant boundary-layer edge properties were assumed over the conical afterbody. The justification for the noted assumptions a posteriori was that the induced effects were small, the corrections were in the proper direction, and the agreement between analysis and experiment was good. The calculations were made using both perfect ($\gamma = 1.4$) and equilibrium gas models. The highly approximate nature of the theoretical model used by Whitfield and Griffith [1] was recognized; however, a correlation parameter was defined and a method developed which correlated well the experimental drag data at $M_\infty \simeq 19$. The agreement between Whitfield and Griffith's prediction and experimental data can be seen from Figure 1.

The good agreement which Whitfield and Griffith found between their predictions and the experimental data was considered somewhat fortuitous since several boundary-layer effects were not considered
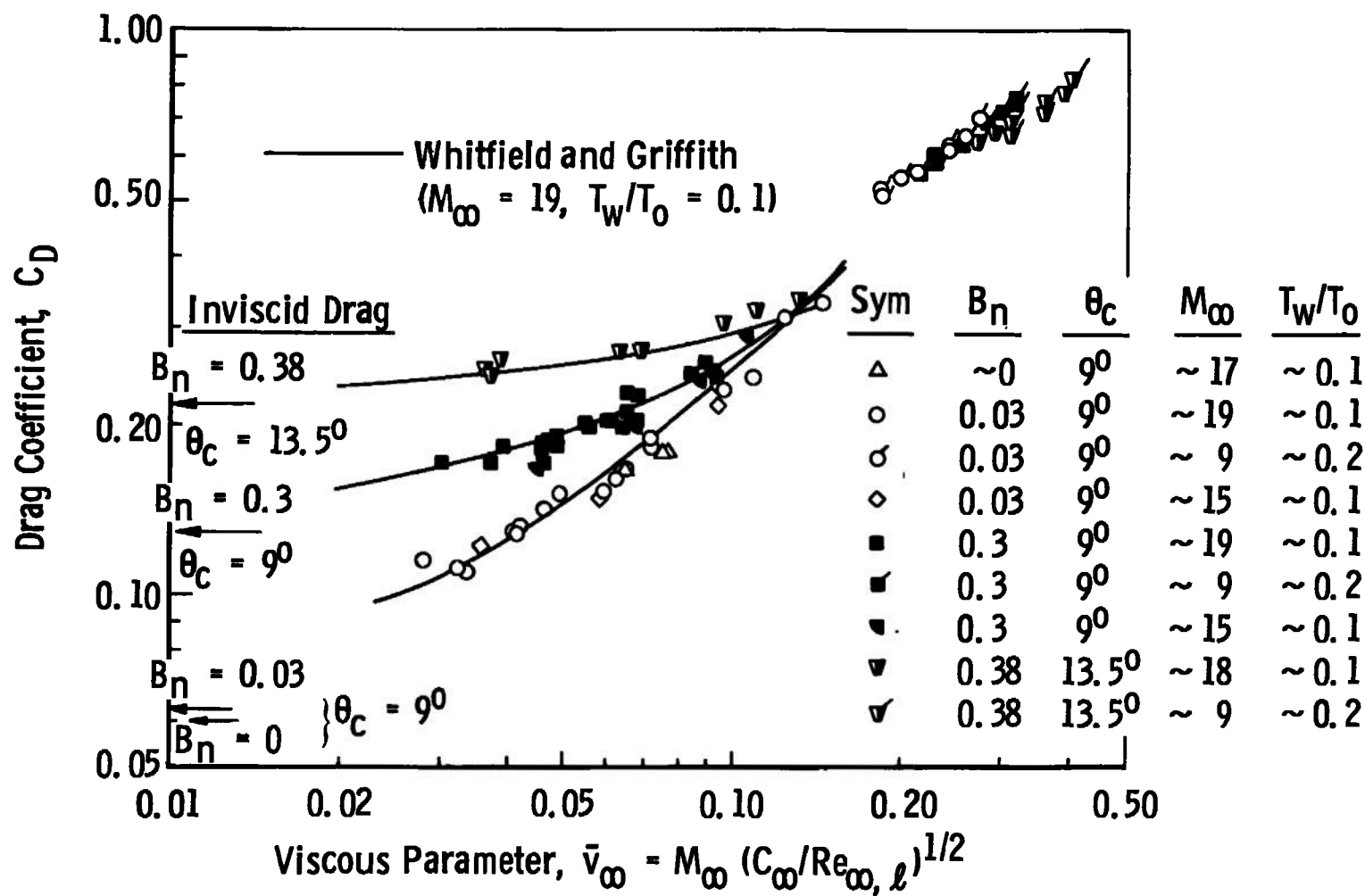
Fig. 1 Comparison of Hypersonic, Cold Wall, Zero-Lift Drag of Blunt, Slender Cones
in Continuum and Rarefied Flow Regimes (from Whitfield and Griffith [1])

by them and some of those treated were considered in a highly approxi-
mate manner. The next attempt at improving the theoretical model and
numerical solutions was made by Lewis and Whitfield [7]. The basic
model used by Lewis and Whitfield was the nonsimilar laminar boundary-
layer theory of Clutter and Smith [8] including approximate transverse
curvature terms and an inviscid outer flow field. The viscous boundary-
layer and inviscid outer flow fields were coupled in the following
manner. The inviscid blunt body and characteristics solutions were
obtained using the method of Inouye, Rakich and Lomax [9]. The surface
pressure distribution over the geometric body was then used to determine
the conditions at the edge of the boundary-layer. The "effective body"
as seen by the outer flow was obtained by perturbing the geometric body
by the displacement thickness as follows:

$$r_{eff} = r_w + \delta^* \cos \alpha$$

The inviscid blunt body and characteristics solutions were obtained
over an approximate effective body and another boundary-layer solution
was obtained. This process was continued until there was negligible
change in the pressure distribution over the body.

At the time of the calculations by Lewis and Whitfield, they
found it possible only to treat spherical-nosed bodies in the inviscid
blunt body solution, and thus the spherical nose was expanded or
contracted by the displacement thickness at the starting line (M_i =
1.05) for the characteristics solution. Moreover, approximate curve
fit procedures were developed for describing the effective body

downstream of the starting line.

The theoretical model and numerical treatment used by Lewis and Whitfield [7] were superior to those used by Whitfield and Griffith [1]; however, the results obtained for prediction of zero-lift drag were in poorer agreement with the experimental data as shown in Figure 2. A comparison of drag components computed by Whitfield and Griffith and by Lewis and Whitfield is shown in Figure 3. The skin-friction drag and transverse-curvature-induced drag components predicted by Whitfield and Griffith were each about 15 per cent larger than those predicted by Lewis and Whitfield. The minor drag components due to displacement-induced friction and pressure drags were in better agreement; however, their contributions were about one order of magnitude less than the first two components discussed.

The defects in both the analyses by Whitfield and Griffith and by Lewis and Whitfield were recognized and in fact sustained the interest for the work described herein. Both analyses were approximate but based upon what were considered some of the best theoretical models and numerical methods available at the time the studies were made. Both theoretical models approximately treated TVC and displacement; Lewis and Whitfield included the nonsimilar boundary-layer effects, whereas Whitfield and Griffith used the similar boundary-layer solutions and integral method of Cohen and Reshotko [2,3].

Those involved in the above-described analyses of the experimental drag data were aware of the hazard of application of approximate analyses outside of ranges where they were developed and tested.
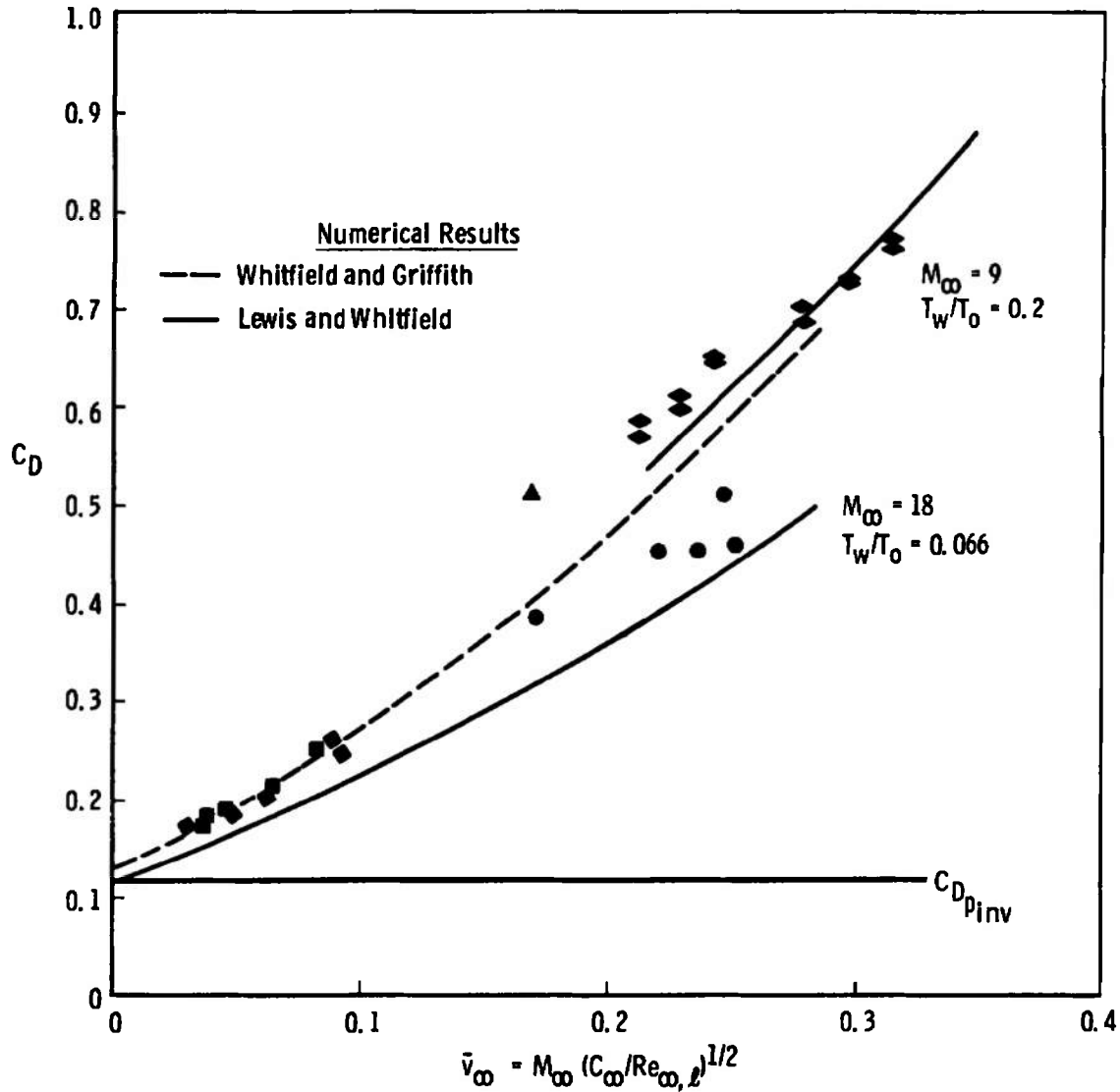
Fig. 2 Comparison of Experimental and Predicted Zero-Lift Drag for a 9-degree
Sphere-Cone at M_∞ = 9 and 18 (from Lewis and Whitfield [7])

——— Lewis and Whitfield
– – – Whitfield and Griffith

a. Friction Drag without Viscous
   Interaction or Transverse Curvature

b. Transverse-Curvature-Induced
   Friction Drag

c. Viscous-Induced Friction Drag

d. Viscous-Induced Pressure Drag
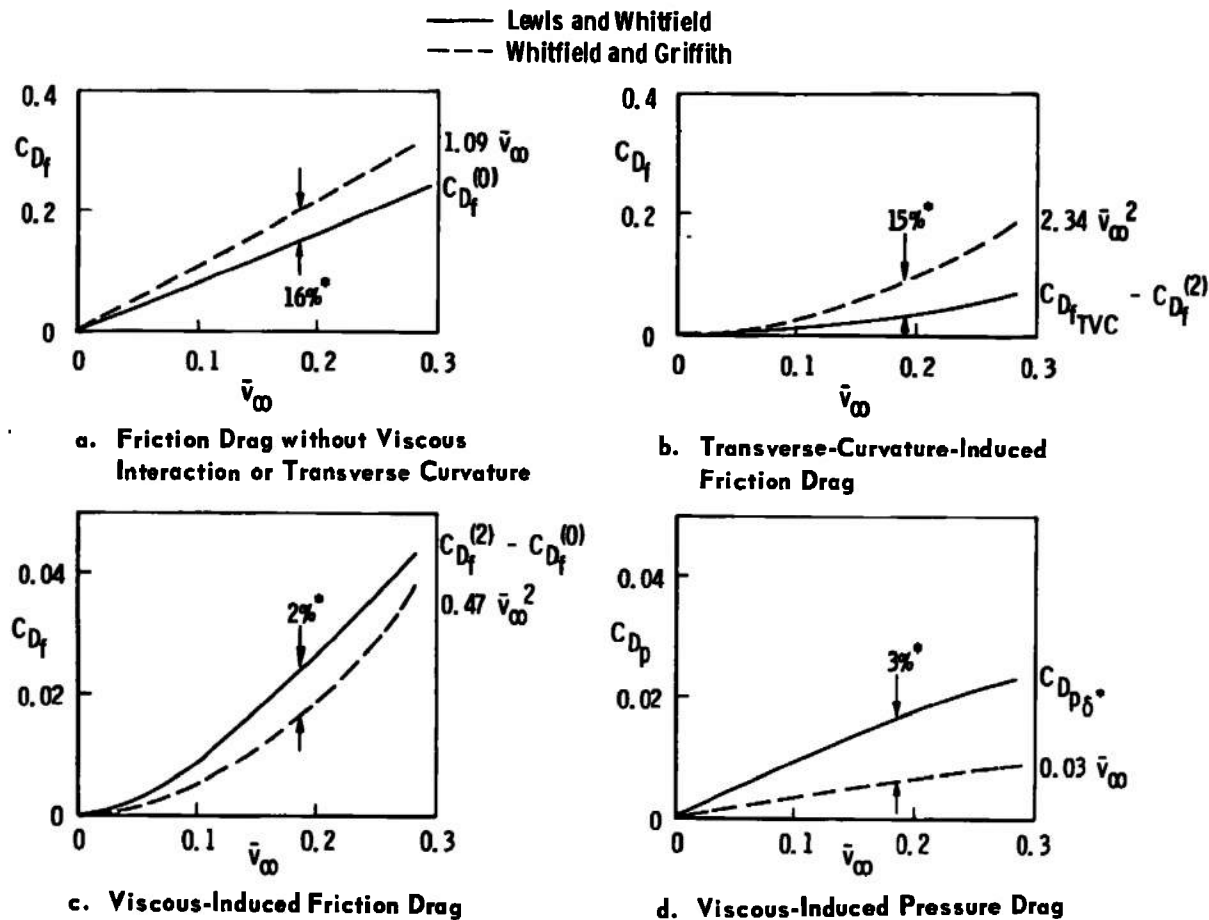
Fig. 3 Comparison of Drag Components According to Lewis and Whitfield's
Analysis with the Previous Analysis of Whitfield and Griffith (from
Lewis and Whitfield [7])

*Percentages are of total drag $C_{D_f}^{(2)} + C_{D_p}^{(2)}$ with
superscripts denoting the interation index used by
Lewis and Whitfield [7].

The work of Lewis and Whitfield has been extended to include the effects of vorticity interaction as first suggested by Ferri and Libby [10] and more fully described by Hayes [11] and Hayes and Probstein [12]. The effect of inviscid external vorticity is simple conceptually. When the Reynolds number is sufficiently low, the laminar boundary layer entrains the high temperature, low density gas which crossed the curved bow shock. The velocity at the "edge" of the boundary layer increases above that along the inviscid wall streamline, and the velocity gradient at the edge of the boundary layer is first increased and then decreased depending on the length of the body and Reynolds number or boundary layer-to-shock layer thickness.

To help clarify the physical aspects of shock-generated inviscid external vorticity, some typical results from a condition where vorticity effects are large are presented and discussed. The uncoupled inviscid and viscous flow fields over a 15-degree half-angle spherically blunted cone at $M_\infty = 18$ are shown in Figure 4. Lines of minimum entropy and "edge" of the entropy layer are shown in the inviscid shock layer. The term "edge" of the entropy layer as used herein denotes a line above which the entropy is nearly constant and within one per cent of the constant conical limit. The shock wave has an inflection point where the shock angle is a minimum, the shock is weakest, and the entropy increase across the bow shock wave is a minimum. Since the entropy is constant along streamlines, the entropy will be a minimum along the streamline which passes through the shock-wave inflection point. The
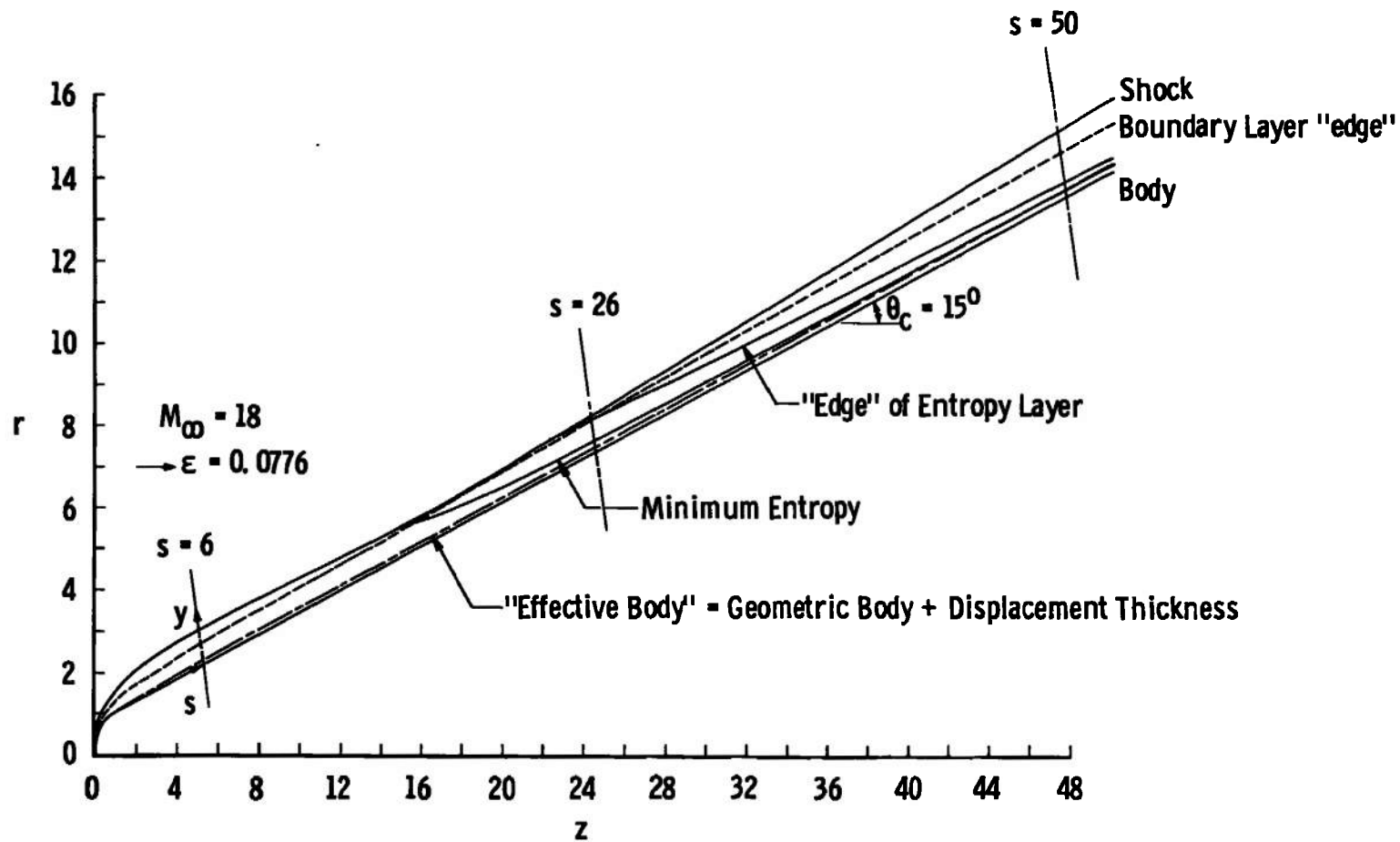
Fig. 4 Unperturbed Inviscid Shock Layer and Viscous Boundary Layer over a
Spherically Blunted 15-degree Half-Angle Cone at M_∞ – 18 and
T_w/T_o = 0.066

classical or first-order boundary-layer thickness is shown where the Reynolds number was chosen such that the boundary-layer thickness would be less than the shock layer thickness, and the boundary-layer displacement thickness is also shown. Although not distinguishable in this figure, the boundary-layer displacement thickness is negative over the spherical nose. For the conditions shown in Figure 4, the boundary layer is thinner than the shock layer over the entire body and thinner than the entropy layer in the nose region, but the boundary layer becomes thicker than the entropy layer for s > 26. Downstream of this point the thickness of the entropy layer decreases monotonically whereas the shock and boundary-layer thicknesses increase. It should be emphasized that the flow fields shown in Figure 4 were calculated on the basis of being completely uncoupled, and the conditions were chosen to illustrate some of the features of the flow fields.

The results from the characteristics solution were interpolated normal to the body at several axial stations, and the resulting velocity, temperature, pressure, and entropy distributions are shown in Figures 5-8. The results were nondimensionalized by the value of the variables along the inviscid wall for convenience of presentation. Since the sphere-cone tangent point was at z = 0.741, the profiles at z = 0.75 represent supersonic flow (M_i = 2.15 at z = 0.75) over the spherical nose where the effects of longitudinal curvature on the normal pressure gradient are evident. The flow field near the wall adjusts quickly, but the nose influence persists until z > 7.5 in the flow field near the shock wave. For thin boundary layers over the
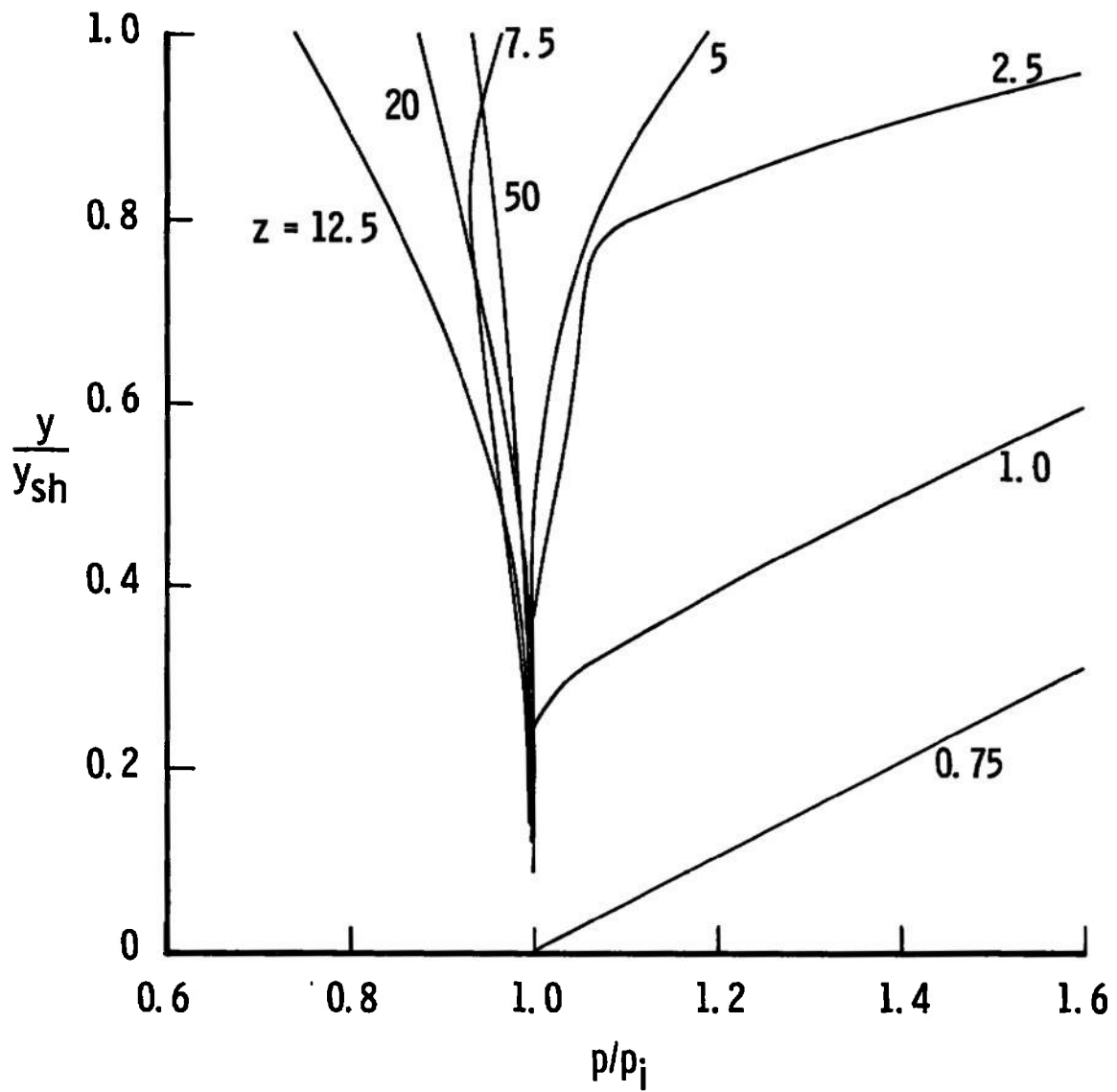
Fig. 5 Pressure Distribution Through an Inviscid Unperturbed Shock Layer Over a
15-degree Half-Angle Cone at M_∞ = 18
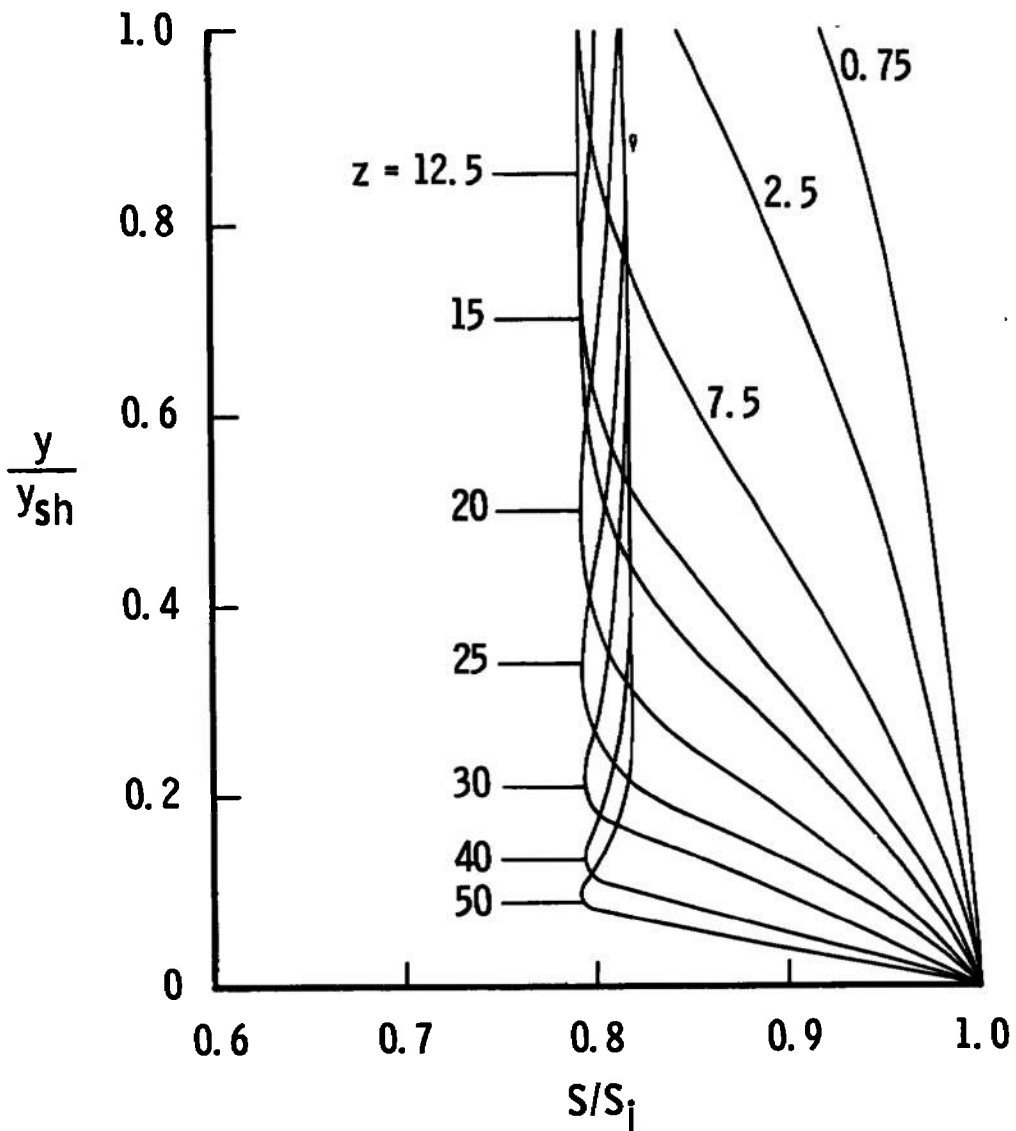
Fig. 6 Entropy Distribution Through on Inviscid Unperturbed Shock Layer Over a
15-degree Half-Angle Cone at M_∞ = 18
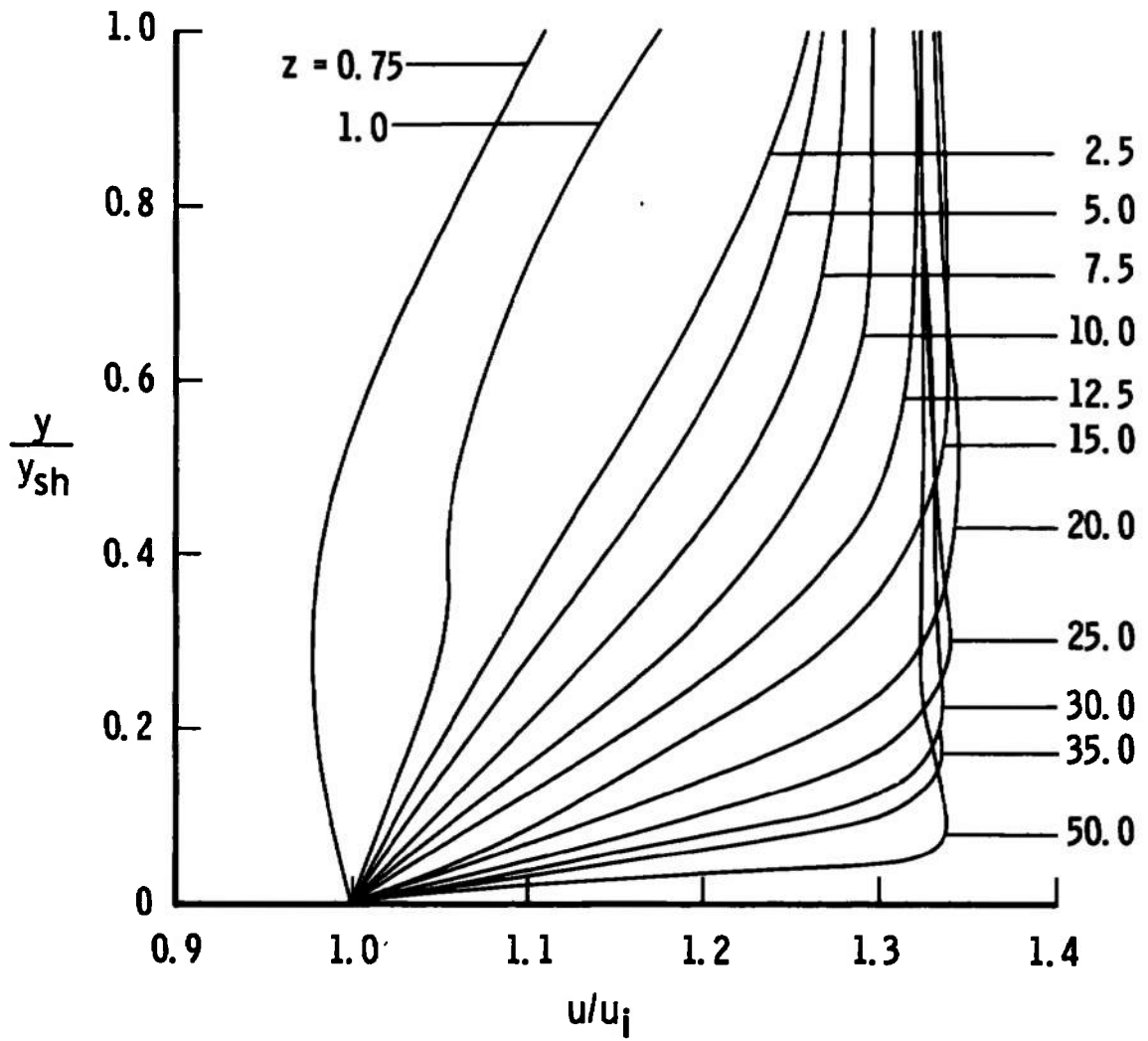
Fig. 7 Velocity Distribution Through an Inviscid Unperturbed Shock Layer Over a
15-degree Half-Angle Cone at M_∞ = 18
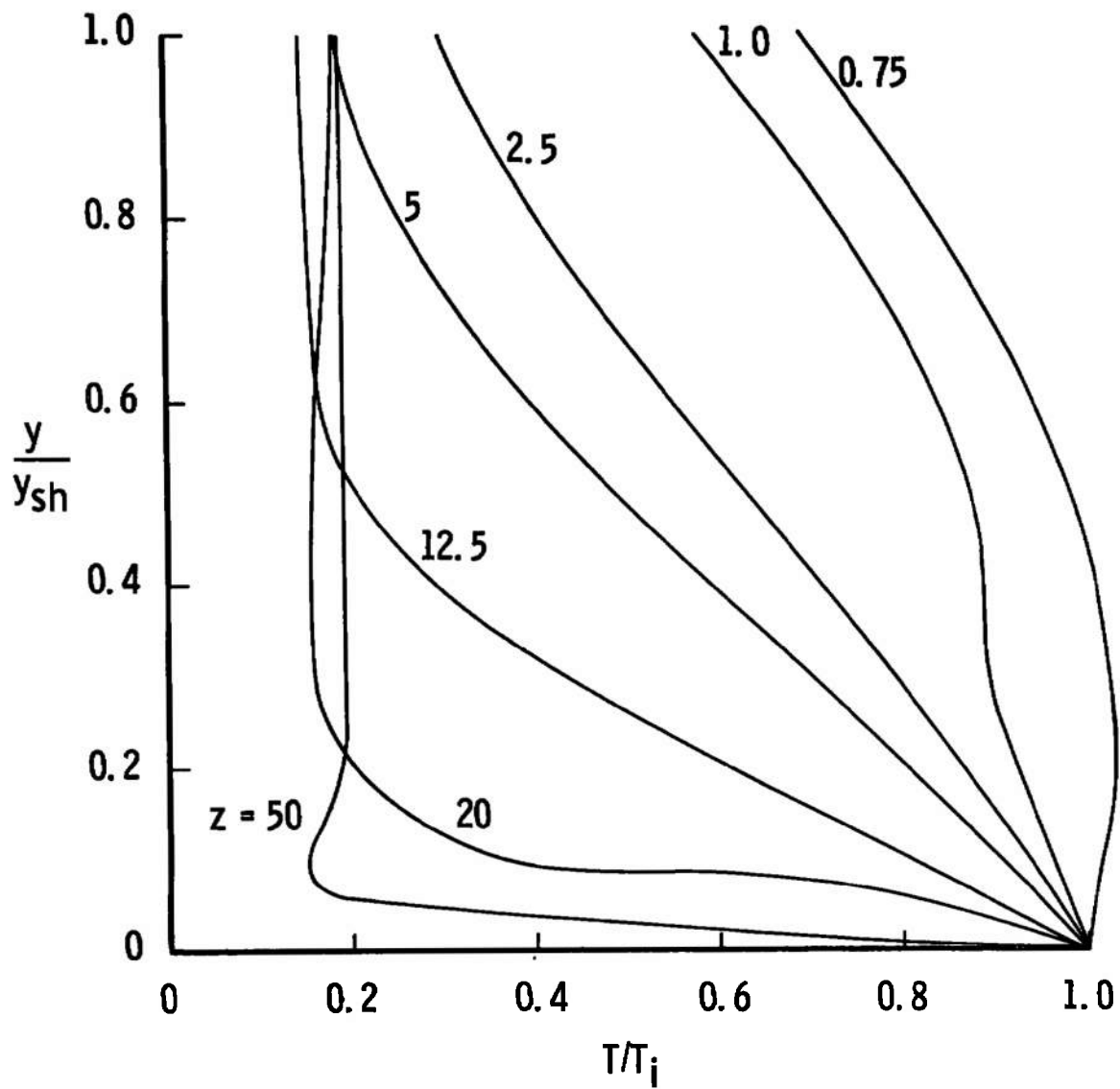
Fig. 8 Temperature Distribution Through an Inviscid Unperturbed Shock Layer Over
a 15-degree Half-Angle Cone at $M_\infty = 18$

conical afterbody ($\delta/y_{sh} < 0.3$), the usual boundary-layer assumption of $\partial p/\partial y = 0$ is supported by these data.

Primary interest, however, in these data is in the development of the velocity and temperature profiles and their relationship to the entropy profiles. The formation of the entropy layer can be seen from Figure 6. The monotonic increase in the velocity and decrease in the temperature gradients at the wall can be seen from Figures 7 and 8. The effects of these gradients in second-order boundary-layer theory will be discussed in Chapter II. Far downstream on the cone ($z > 20$) and even for thin boundary layers ($\delta/y_{sh} < 0.5$), the inviscid velocity at the "edge" of the boundary layer would be about 30 per cent greater than the inviscid wall value, and the temperature would only be about 20 per cent of the inviscid wall value. These large changes in edge conditions are not usually considered in boundary-layer analyses.

It is important to note that the 15-degree half-angle cone was chosen to magnify the effects of the entropy layer by compressing the effects nearer the nose than would be the case for smaller half-angle cones. However, in addition to considering these effects on the inviscid flow field, it is important to consider the effects of the coupling between the entropy and boundary layers.

The coupling of the inviscid outer flow and viscous boundary layer flow complicates the picture described above, and some of the difficulties caused by this coupling are considered in this dissertation. Also, at sufficiently low Reynolds numbers noncontinuum effects should be considered especially as they affect the wall boundary

19

conditions on the velocity and temperature profiles.

About the time of the presentation of the results by Lewis and Whitfield [7], Davis and Flügge-Lotz [13] published a report on second-order boundary-layer effects on hyperboloids and paraboloids at infinite Mach number and spheres at a Mach number of ten. The theory of Van Dyke [14] was used with an implicit finite difference scheme originally proposed by Flügge-Lotz and Blottner [15] for treating the classical first-order boundary layer over two-dimensional bodies. As will be shown in this dissertation, the theory of Van Dyke when coupled with the implicit finite difference method of Davis and Flügge-Lotz gives a powerful tool for extending classical boundary-layer theory to lower Reynolds number.

More recently Adams [16] used the Levy-Lees transformation [17] to solve the first- and second-order boundary-layer theory again with the finite difference method of Davis and Flügge-Lotz. Adams also developed an approximate method based on the Newtonian theory for the pressure distribution over hyperboloids and paraboloids. The essential difference between the second-order treatments of Davis and Flügge-Lotz and that of Adams was in the treatment of the displacement effect. Adams was able to treat analytic bodies of arbitrary length whereas Davis and Flügge-Lotz were restricted to the nose region since in their method the effective body was approximated by shifting and expanding the original body by the displacement thickness. Although the shifted and expanded body technique was useful and had some advantages over other methods, it was limited to the nose region since it did not provide

satisfactory fits of the effective body over regions far removed from the stagnation region. The method developed by Adams was limited to analytic bodies since it was based on the Newtonian impact theory and was thus not applicable to spherically blunted cones.

A method has recently been developed by Marchand, Lewis, and Davis [18] for treating the second-order displacement effect over nonanalytic shapes such as spherically blunted cones. The method used by Marchand, Lewis, and Davis for treating the displacement effect will be described later herein, and the remaining second-order effects followed Davis and Flügge-Lotz exactly except for the effects of vorticity which were coupled to the displacement effect.

The primary goal of this dissertation will be to present a comparison of a first-order treatment of second-order boundary-layer effects with treatments of Van Dyke's second-order theory and a comparison of both treatments with experimental data. From these comparisons some conclusions will be drawn regarding the ranges of applicability of the theories.

In Chapter II the theory of higher-order boundary-layer effects is given. A review of Van Dyke's second-order theory is presented including a discussion of the asymptotic matching principle. The source of the various second-order effects is indicated, and the coupling between second-order vorticity and displacement is shown.

The first-order treatment of higher-order boundary-layer effects is given in Chapter III. The effects of vorticity, slip and temperature jump (considered as a single effect), and displacement are described.

The effect of first-order transverse curvature was developed by Clutter and Smith, and the approximate nature of the treatment caused by an error in the original theoretical development is discussed.

Numerical results and discussion will be presented in Chapter IV. The conditions treated by the first- and second-order theories will be given, and the numerical results will be presented and discussed.

Comparisons of the numerical results from the first- and second-order theories will be made with experimental data and the results discussed in Chapter V.

The conclusions from the study will be given in Chapter VI. From the comparison of numerical results and experimental data, the ranges of applicability of the theories will be discussed, and the need for future work will be indicated.

Separate effects and problems will be treated in appendixes. The numerical treatment of the first-order boundary-layer theory is described in Appendix A. The method used to treat first- and second-order displacement effects is described in Appendix B. Finally, the effect of vorticity on the displacement thickness is derived in Appendix C.

CHAPTER II
REVIEW OF SECOND-ORDER BOUNDARY-LAYER THEORY

The second-order boundary-layer theory of Van Dyke [14] is reviewed to indicate the salient features of the theory and the roles of the various second-order effects. The critical role of the matching of the inner and outer expansions, based on Van Dyke's asymptotic matching principle, is discussed.

In the second-order boundary-layer theory, Van Dyke [14] identified seven separate second-order effects which were longitudinal curvature, transverse curvature, slip, temperature jump, entropy gradient, stagnation enthalpy gradient, and displacement.[1] The separation of the effects of vorticity and displacement is somewhat arbitrary; however, the presentation given below follows Van Dyke's treatment.

I. SECOND-ORDER BOUNDARY-LAYER EQUATIONS

The Navier-Stokes equations are written in the orthogonal coordinate system (s,n) shown in Figure 9, where s is the non-dimensional distance along the surface, n is the nondimensional distance normal to the surface, $\kappa(s)$ is the longitudinal surface curvature, and

---

[1] A brief physical explanation of each of the second-order boundary-layer effects is given in Chapter I.
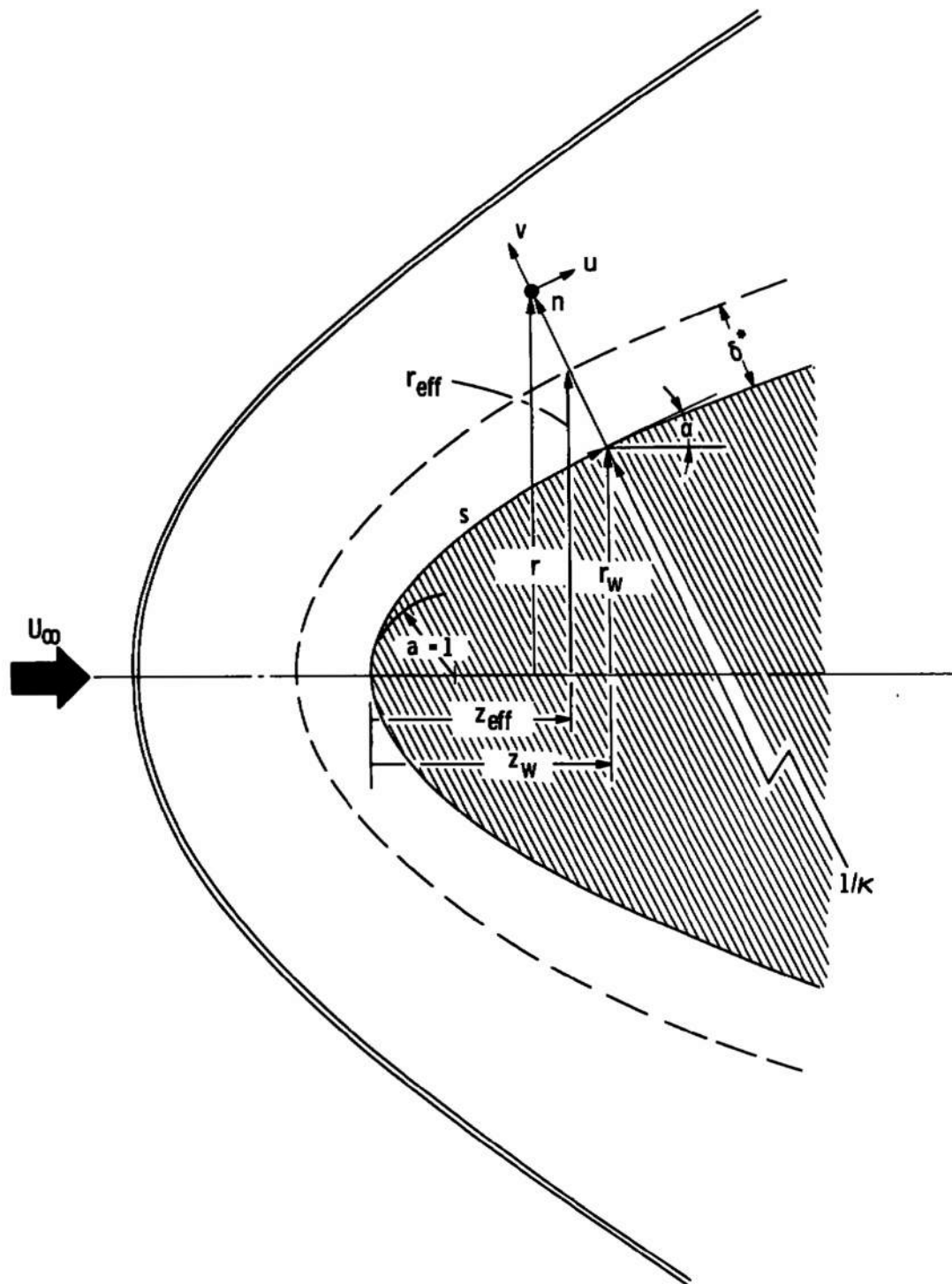
Fig. 9 Coordinate System for the Second-Order Boundary-Layer Theory

$r_w(s)$ is the radius of the axisymmetric body where all lengths are non-dimensionalized by the nose radius of curvature a^*. Further, all velocities are referred to U_∞^*, pressure to $\rho_\infty^* U_\infty^{*2}$, density to ρ_∞^*, temperature to U_∞^{*2}/c_p^*, entropy to c_p^*, enthalpy to U_∞^{*2}, and viscosity to the value of μ at $T^* = U_\infty^{*2}/c_p^*$.

The continuity equation becomes

$$(r^j \rho u)_s + (kr^j \rho v)_n = 0 \qquad (1)$$

where subscripts denote differentiation and $j = 0$ for two-dimensional flow and $j = 1$ for axisymmetric flow. The radius $r = r_w + n \cos \alpha$ and the function $k = 1 + \kappa n$ are used for convenience.

The Navier-Stokes momentum equations become

$$\epsilon^{-2} [\rho(uu_s/k + vu_n + \kappa uv/k) + p_s/k] = \{\mu[u_n + (v_s - \kappa u)/k]\}_n$$

$$+ (2/k) [\mu(u_s + \kappa v)/k]_s + \mu(2\kappa/k + j \cos \alpha/r)[u_n + (v_s - \kappa u)/k]$$

$$+ [2j\mu r_s/(kr)] [(u_s + \kappa v)/k - ur_s/(kr) - v \cos \alpha/r]$$

$$+ (1/k) \{\lambda[(u_s + \kappa v)/k + v_n + j (ur_s/k + v \cos \alpha)/r]\}_s \qquad (2)$$

and

$$\epsilon^{-2} [\rho(uv_s/k + vv_n - \kappa u^2/k) + p_n] = 2(\mu v_n)_n + \{\mu[u_n + (v_s - \kappa u)/k]\}_s$$

$$+ 2\mu(\kappa/k + j \cos \alpha/r)v_n - 2\mu\kappa(u_s + \kappa v)/k^2$$

$$- 2j\mu(ur_s/k + v \cos \alpha)/r^2 + j\mu r_s [u_n + (v_s - \kappa u)/k]/(kr)$$

$$+ \{\lambda[(u_s + \kappa v)/k + v_n + j (ur_s/k + v \cos \alpha)/r]\}_n \qquad (3)$$

The energy equation is

$$\epsilon^{-2} \left[\rho(uT_s/k + vT_n) - (up_s/k + vp_n) \right] = \sigma^{-1} (\mu T_s/k)_s/k$$

$$+ \sigma^{-1} (\mu T_n)_n + j\sigma^{-1} \mu T_s r_s/(k^2 r) + \sigma^{-1} (\kappa/k + j \cos \alpha/r) T_n + \Phi \qquad (4)$$

where σ is the Prandtl number, and the dissipation function is

$$\Phi = \mu\{2[(u_s + \kappa v)/k]^2 + 2v_n^2 + 2jr^{-2} (ur_s/k + v \cos \alpha)^2$$

$$+ [u_n + (v_s - \kappa u)/k]^2\}$$

$$+ \lambda [(u_s + \kappa v)/k + v_n + jr^{-1} (ur_s/k + v \cos \alpha)]^2 \qquad (5)$$

The nondimensional equation of state is

$$p = (\gamma-1)\rho T/\gamma \qquad (6)$$

The viscosity law is

$$\mu = \mu(T) \qquad (7)$$

The second coefficient of viscosity is λ.

Van Dyke defined the expansion parameter ϵ to be

$$\epsilon \equiv \left[\frac{\mu^* (U_\infty^{*2}/c_p^*)}{\rho_\infty^* U_\infty^* a^*} \right]^{1/2} = \left[\frac{\mu^* [(\gamma-1)M_\infty^2 T_\infty^*]}{Re_\infty \; \mu^* (T_\infty^*)} \right]^{1/2} \qquad (8)$$

If a power viscosity law $\mu \propto T^\omega$ is assumed, then

$$\epsilon = \left[\frac{[(\gamma-1)M_\infty^2]^\omega}{Re_\infty} \right]^{1/2}$$

Thus with $\gamma = 1.4$, $\epsilon = 0.6325\ M_\infty/Re_\infty^{1/2}$ for the linear viscosity law ($\omega = 1.0$), and $\epsilon = 0.795\ (M_\infty/Re_\infty)^{1/2}$ for the square root viscosity law ($\omega = 0.5$).[2]

The outer (outside the boundary layer) flow variables in the Navier-Stokes equations (including continuity and energy equations in the system) are expanded in powers of ϵ as follows:

$$u(s,n;\epsilon) \sim U_1(s,n) + \epsilon U_2(s,n) + \ldots \tag{9a}$$

$$v(s,n;\epsilon) \sim V_1(s,n) + \epsilon V_2(s,n) + \ldots \tag{9b}$$

$$p(s,n;\epsilon) \sim P_1(s,n) + \epsilon P_2(s,n) + \ldots \tag{9c}$$

$$\rho(s,n;\epsilon) \sim R_1(s,n) + \epsilon R_2(s,n) + \ldots \tag{9d}$$

$$T(s,n;\epsilon) \sim T_1(s,n) + \epsilon T_2(s,n) + \ldots \tag{9e}$$

Substituting Equations 9 into Equations 1-6 and equating terms in ϵ^o gives

$$(r^j R_1 U_1)_s + (kr^j R_1 V_1)_n = 0 \tag{10}$$

$$R_1(U_1 U_{1s}/k + V_1 U_{1n} + \kappa U_1 V_1/k) + P_{1s}/k = 0 \tag{11}$$

$$R_1(U_1 V_{1s}/k + V_1 V_{1n} - \kappa U_1{}^2/k) + P_{1n} = 0 \tag{12}$$

---

[2]With linear viscosity law, the expansion parameter is related to the hypersonic interaction parameter $\bar{V}_\infty$, by $\epsilon = 0.6325\ \bar{V}_\infty \times \sqrt{[\ell/(r_n C_\infty)]}$.

$$R_1(U_1T_{1s}/k + V_1T_{1n}) - (U_1P_{1s}/k + V_1P_{1n}) = 0 \qquad (13)$$

and

$$P_1 = (\gamma - 1) R_1 T_1/\gamma \qquad (14)$$

which are the first-order inviscid flow equations.

The stream function is defined in the usual way

$$r^j R_1 U_1 = \Psi_{1n}$$

and

$$kr^j R_1 V_1 = -\Psi_{1s} \qquad (15)$$

The entropy S_1 and stagnation enthalpy H_1 are constant along streamlines and can be written

$$S_1 = S_1(\Psi_1), \text{ and } H_1 = T_1 + \frac{1}{2} U_1^2 = H_1(\Psi_1) \qquad (16)$$

The second-order equations are obtained by equating terms in ϵ^1, and the tangential momentum equation is

$$R_1[(U_1U_2)_s/k + V_1U_{2n} + V_2U_{1n} + \kappa(U_1V_2 + U_2V_1)/k]$$

$$+ R_2(U_1U_{1s}/k + V_1U_{1n} + \kappa U_1V_1/k) + P_{2s}/k = 0 \qquad (17)$$

This equation, typical of the system of equations, is linear in the second-order terms and inviscid since viscous terms in the Navier-Stokes equations are of third-order being multiplied by ϵ^2. Thus, a third-order expansion would introduce viscous terms in the equations for the outer flow.

The normal derivatives of V_1 and P_1 at the surface are obtained by evaluating Equations 10 and 12 at $n = 0$, and one finds

$$V_{1n} = - \left[(r_w{}^j R_1)^{-1} (r_w{}^j R_1 U_1)_s \right]_{n=0} \tag{18}$$

and

$$P_{1n} = [\kappa R_1 U_1{}^2]_{n=0} \; . \tag{19}$$

The normal component of the tangential velocity U_1 is obtained from the vorticity of the outer flow which is

$$\Omega_1 = - U_{1n} + (V_{1s} - \kappa U_1)/k \tag{20}$$

Crocco's vortex theroem [12] is

$$\vec{Q}_1 \times \vec{\Omega}_1 = \nabla H_1 - T_1 \nabla S_1 \tag{21}$$

at the surface, and substituting Equations 15 and 16 into Equation 21 gives

$$\Omega_1 = r_w{}^j R_1 (T_1 S_1{}' - H_1{}') \text{ at } n = 0 \tag{22}$$

where prime denotes $d/d\Psi_1$.

Substituting Equation 20 into Equation 22, one can obtain

$$U_{1n} = - \kappa U_1 - r_w{}^j R_1 (T_1 S_1{}' - H_1{}') \tag{22a}$$

to be evaluated at $n = 0$.

The normal gradients of T_1 and R_1 are obtained by differentiating Equations 16 and 14 with respect to n, using Equation 22a, and evaluating the results at the wall yields

$$T_{1n} = [\kappa U_1^2 + r_w^j R_1 U_1 T_1 S_1']_{n=0} \tag{23}$$

and

$$R_{1n} = \left[R_1 U_1 \left(\frac{\kappa}{\gamma-1} \frac{U_1}{T_1} - r_w^j R_1 S_1' \right) \right]_{n=0} \tag{24}$$

The outer expansion fails at the surface since the highest derivatives in the Navier-Stokes equations were lost in the expansion. Therefore, an inner expansion is needed which is valid near the surface although it will be invalid far from the wall. The inner expansion is obtained by defining an expansion of the form

$$u(s,n;\epsilon) \sim u_1(s,n) + \epsilon u_2(s,N) + \ldots \tag{25}$$

$$v(s,n;\epsilon) \sim \epsilon v_1(s,N) + \epsilon^2 v_2(s,N) + \ldots \tag{26}$$

$$p(s,n;\epsilon) \sim p_1(s,N) + \epsilon p_2(s,N) + \ldots \tag{27}$$

$$\rho(s,n;\epsilon) \sim \rho_1(s,N) + \epsilon \rho_2(s,N) + \ldots \tag{28}$$

$$T(s,n;\epsilon) \sim t_1(s,N) + \epsilon t_2(s,N) + \ldots \tag{29}$$

where $n = \epsilon N$.

The viscosity is expanded in a series in T as follows:

$$\mu(T) \sim \mu(t_1) + \epsilon \mu'(t_1) t_2 + \ldots \tag{30}$$

Substituting the inner expansion Equations 25-30 into the Navier-Stokes Equations 1-7 and equating terms in ϵ^0 gives the first-order equations, which are

$$(r_w{}^j \rho_1 u_1)_s + (r_w{}^j \rho_1 v_1)_N = 0 \tag{31}$$

$$\rho_1 (u_1 u_{1s} + v_1 u_{1N}) + p_{1s} - (\mu u_{1N})_N = 0 \tag{32}$$

$$p_{1N} = 0 \tag{33}$$

$$\rho_1 (u_1 t_{1s} + v_1 t_{1N}) - (u_1 p_{1s} + v_1 p_{1N})$$

$$- \sigma^{-1} (\mu t_{1N})_N - \mu u_{1N}{}^2 = 0 \tag{34}$$

and

$$p_1 = \frac{\gamma-1}{\gamma} \rho_1 t_1 \tag{35}$$

which are Prandtl's compressible boundary-layer equations.

Equating terms in ϵ^1 yields the second-order boundary-layer equations, which are

$$[r_w{}^j (\rho_1 u_2 + \rho_2 u_1)]_s + [r_w{}^j (\rho_1 v_2 + \rho_2 v_1)]_N$$

$$= C_{vort} + C_{LC} + C_{TVC} + C_{disp} + C_{STJ} \tag{36}$$

$$\rho_1 (u_1 u_{2s} + u_2 u_{1s} + v_1 u_{2N} + v_2 u_{1N}) + \rho_2 (u_1 u_{1s} + v_1 u_{1N})$$

$$- (\mu u_{2N} + \mu' u_{1N} t_2)_N$$

$$= M_{vort} + M_{LC} + M_{TVC} + M_{disp} + M_{STJ} \tag{37}$$

$$\rho_1 (u_1 t_{2s} + u_2 t_{1s} + v_1 t_{2N} + v_2 t_{1N}) + \rho_2 (u_1 t_{1s} + v_1 t_{1N})$$

$$- u_2 p_{1s}(s,0) - (\mu \sigma^{-1} t_2)_{NN} - 2\mu u_{1N} u_{2N} - \mu' u_{1N}{}^2 t_2$$

$$= E_{vort} + E_{LC} + E_{TVC} + E_{disp} + E_{STJ} \tag{38}$$

$$P_2 = \frac{\gamma-1}{\gamma} (\rho_1 t_2 + \rho_2 t_1) \tag{39}$$

and

$$P_{2N} = \kappa \rho_1 u_1^2 \tag{40}$$

where

$$C_{vort} = C_{disp} = C_{STJ} = 0 \tag{38a}$$

$$C_{LC} = - \kappa r_w^j (N \rho_1 v_1)_N \tag{38b}$$

$$C_{TVC} = - j[(r_w^{j-1} \cos\alpha N\rho_1 u_1)_s + (r_w^{j-1} \cos\alpha N\rho_1 v_1)_N] \tag{38c}$$

$$M_{vort} = - r_w^j [R_1^2 T_1 S_1' V_2]_{n=0} \tag{39a}$$

$$M_{LC} = \kappa[N(\mu u_{1N})_N + \mu u_{1N} - \mu' u_1 t_{1N}$$

$$- N\rho_1 v_1 u_{1N} - \rho_1 u_1 v_1]$$

$$- [\kappa (R_1 U_1^2)_{n=0} A_1]_s \tag{39b}$$

$$M_{TVC} = j \cos\alpha \, \mu \, u_{1N}/r_w \tag{39c}$$

$$M_{disp} = [R_1(U_1 U_2)_s + R_2 U_1 U_{1s}]_{n=0} \tag{39d}$$

$$M_{STJ} = 0 \tag{39e}$$

$$E_{vort} = r_w^j u_1 [R_1^2 T_1 S_1' V_2]_{n=0} \tag{40a}$$

$$E_{LC} = \kappa[N\rho_1 u_1 t_{1s} + \sigma^{-1}\mu \, t_{1N} + \rho_1 u_1^2 v_1$$

$$- N u_1 P_{1s}(s,0) - 2\mu \, u_1 u_{1N}]$$

$$+ u_1 [\kappa (R_1 U_1^2)_{n=0} A_1]_s \tag{40b}$$

$$E_{TVC} = j\sigma^{-1} \cos \alpha \, \mu \, T_{1N}/r_w \qquad (40c)$$

$$E_{disp} = -u_1 [R_1(U_1 U_2)_s + R_2 U_1 U_{1s}]_{n=0} \qquad (40d)$$

$$E_{STJ} = 0 \qquad (40e)$$

and

$$A_1 = N + \int_N^\infty [1 - \rho_1 u_1^2/(R_1 U_1^2)_{n=0}] dN. \qquad (40f)$$

The subscripts vort, disp, LC, TVC, and STJ denote contributions due to vorticity, displacement, longitudinal curvature, transverse curvature, and slip and temperature jump, respectively. The differential equations are linear, but not all of the effects are independent since, for example as will be discussed below, the $V_2(s,0)$ in Equation 39a is related to the displacement effect through the displacement thickness δ^*.

The second coefficient of viscosity λ is of third-order (that is, in terms multiplied by ϵ^2) and thus does not appear.

Neglecting surface mass transfer, the boundary condition along the surface requires

$$v(s,0) = 0 \qquad (41)$$

Van Dyke [14] obtained the remaining surface boundary conditions from Street [20] including first-order slip-flow conditions as follows:

$$u(s,0) = \epsilon^2 \left[\frac{\mu}{p} \left[a_1 \left(\frac{\gamma-1}{\gamma} T \right)^{1/2} u_n + b_1 \frac{\gamma-1}{\gamma} T_s \right] \right]_{n=0} \qquad (42)$$

and

$$T(s,0) = T_w + \epsilon^2 \left[c_1 \frac{\mu}{p} \left(\frac{\gamma-1}{\gamma} T \right)^{1/2} T_n \right]_{n=0} \tag{43}$$

where $a_1 = (\pi/2)^{1/2}$, $b_1 = 3/4$, and $c_1 = (15/8)(\pi/2)^{1/2}$ when a hard sphere, monatomic gas model with unit accommodation coefficients is assumed.

If the surface temperature is prescribed as $T_w(s)$, then substitution of the inner expansion Equations 24-30 into the wall boundary conditions Equations 41-43 gives

$$u_1(s,0) = v_1(s,0) = 0 \tag{44}$$

$$u_2(s,0) = a_1 \left[\frac{\mu}{p_1} \left(\frac{\gamma-1}{\gamma} t_1 \right)^{1/2} u_{1N} \right]_{N=0} \tag{45}$$

$$v_2(s,0) = 0 \tag{46}$$

$$t_1(s,0) = t_w(s) \tag{47}$$

$$t_2(s,0) = c_1 \left[\frac{\mu}{p_1} \left(\frac{\gamma-1}{\gamma} t_1 \right)^{1/2} t_{1N} \right]_{N=0} \tag{48}$$

Van Dyke [14] gives corresponding expressions when the temperature gradient at the wall is prescribed.

II. ASYMPTOTIC MATCHING CONDITIONS

The outer boundary conditions will depend on the problem to be solved; however, the outer expansion fails to satisfy the wall boundary condition and, in general, the inner expansion fails as $N \to \infty$. It is

34

fundamental to the method of matched asymptotic expansions that there exist an overlap region where both inner and outer expansions are valid, and thus both expansions can be matched in this region.

Van Dyke [19] described the asymptotic matching principle as follows:

> The m-term inner expansion of (the n-term outer expansion) = the n-term outer expansion of (the m-term inner expansion). (49)

By his definition, the m-term inner expansion of the n-term outer expansion is obtained by rewriting n-terms of the outer expansion in inner variables (N in second-order boundary-layer theory), expanding asymptotically in small ϵ, and truncating the result after m nonzero terms. The converse of the procedure is used on the right-hand side of Equation 49.

To demonstrate the matching procedure, the tangential velocity component is considered first. Applying the matching principle with $n = m = 1$ gives the matching conditions for the first-order boundary-layer theory. According to the matching principle,

1-term outer expansion: $U_1(s,n)$

     rewritten in inner variables: $U_1(s,\epsilon N)$

     expanded for small ϵ: $U_1(s,0) + N\epsilon U_{1n}(s,0) + \ldots$

     1-term inner expansion: $U_1(s,0)$

1-term inner expansion: $u_1(s,N)$

     rewritten in outer variables: $u_1(s,n/\epsilon)$

expanded for small ϵ: $\qquad$ $u_1(s,\infty)$

1-term outer expansion: $\qquad$ $u_1(s,\infty)$

Equating the results one obtains

$$u_1(s,N) \sim U_1(s,0) \text{ as } N \to \infty \qquad\qquad (50a)$$

In the same manner, one finds the following matching conditions:

$$p_1(s,N) \sim P_1(s,0) \qquad\qquad (50b)$$
$$\rho_1(s,N) \sim R_1(s,0) \quad\Big\}\ \text{as } N \to \infty \qquad\qquad (50c)$$
$$t_1(s,n) \sim T_1(s,0) \qquad\qquad (50d)$$

The behavior of v_1 as $N \to \infty$ is found by solving the first-order boundary-layer equations.

The matching with $m = 1$ and $n = 2$ gives the matching condition due to the displacement thickness. Again applying the asymptotic matching principle to the normal velocity component v yields the following:

1-term inner expansion: $\qquad$ $\epsilon v_1(s,N)$

$\quad$ rewritten in outer variables: $\epsilon v_1(s,n/\epsilon)$

$\quad$ expanded for small ϵ: $\quad$ $\epsilon v_1(s,\infty)$

$\quad$ 2-term outer expansion: $\quad$ $\epsilon v_1(s,\infty)$

2-term outer expansion: $\qquad$ $V_1(s,n) + \epsilon V_2(s,n)$

$\quad$ rewritten in inner variables: $V_1(s,\epsilon N) + \epsilon V_2(s,\epsilon N)$

$\quad$ expanded for small ϵ: $\quad$ $V_1(s,0) + \epsilon N V_{1n}(s,0) + \ldots$

$$+ \epsilon[V_2(s,0) + \epsilon N V_{2n}(s,0) + \ldots]$$

1-term inner expansion: $\epsilon[V_2(s,0) + NV_{1n}(s,0)]$

Equating the results gives

$$V_2(s,0) = \lim_{N \to \infty} [v_1(s,N) - NV_{1n}(s,0)] \qquad (51)$$

where use was made of the boundary condition $V_1(s,0) = 0$.

Matching with m = n = 2 gives the remaining matching conditions as follows:

$$u_2(s,N) \sim U_2(s,0) + NU_{1n}(s,0) \qquad (52a)$$

$$p_2(s,N) \sim P_2(s,0) + NP_{1n}(s,0) \qquad (52b)$$

$$\rho_2(s,N) \sim R_2(s,0) + NR_{1n}(s,0) \qquad (52c)$$

$$t_2(s,N) \sim T_2(s,0) + NT_{1n}(s,0) \qquad (52d)$$

$$v_1(s,N) \sim V_2(s,0) + NV_{1n}(s,0) \qquad (52e)$$

where each of Equations 52 is evaluated as $N \to \infty$.

Equation 51 can be related to the boundary-layer displacement thickness δ^* as follows: The definition of the displacement thickness is

$$\delta^* = \int_0^\infty [1 - \rho_1 u_1/(R_1 U_1)_{n=0}]dN \qquad (53)$$

Using the inner expansion stream function $\psi_{1N}(s,N) = r_w^j \rho_1 u_1$, and $\Psi_{1n}(s,0) = \psi_{1N}(s,N)$ as $N \to \infty$, one obtains

$$\delta^* = \lim_{N \to \infty} [N - \psi_1(s,N)/\Psi_{1n}(s,0)] \tag{54}$$

Multiplying by $r_w^j R_1(s,0)U_1(s,0) = \Psi_{1n}(s,0)$ and differentiating with respect to s yields

$$(r_w^j R_1(s,0)U_1(s,0)\delta^*)_s$$

$$= \lim_{N \to \infty} [N\psi_{1sN}(s,N) - \psi_{1s}(s,N)]$$

$$= \lim_{N \to \infty} [N(-r_w^j \rho_1 v_1)_N + r_w^j \rho_1 v_1]$$

$$= \lim_{N \to \infty} [r_w^j \rho_1 v_1 - r_w^j N(\rho_1 v_{1N} + v_1 \rho_{1N})] \tag{55}$$

where the last term in the last expression is zero since the gradient of the first-order density vanishes as $N \to \infty$. The final result is

$$(r_w^j R_1(s,0)U_1(s,0)\delta^*)_s = r_w^j R_1(s,0)V_2(s,0) \tag{56}$$

where Equation 51 has been used. This final expression provides a means of evaluating the second-order normal velocity component $V_2(s,0)$ once the first-order outer flow and displacement thickness are known. As described by Van Dyke [14] and Davis and Flügge-Lotz [13], this relation is important in second-order boundary-layer theory since it relates the displacement effect through δ^* with the vorticity effect through $V_2(s,0)$.

It is instructive to consider the matching conditions in a slightly different way which indicates the second-order effects involved. From Davis and Flügge-Lotz, these conditions are as

follows:

$$u_2(s,N) \sim - r_w{}^j N[R_1 T_1 S_1']_{n=0} - \kappa N[U_1]_{n=0} + [U_2]_{n=0}$$

and

$$t_2(s,N) \sim r_w{}^j N[R_1 T_1 U_1 S_1']_{n=0} + \kappa N[U_1{}^2]_{n=0} + [T_2]_{n=0}$$

to be evaluated as $N \to \infty$, and where the terms on the right-hand side of each expression are due to vorticity, longitudinal curvature and displacement, respectively.

This rather extensive review of second-order boundary-layer theory has been given to indicate the various second-order effects and their relationship to first-order theory. The critical role of the matching of inner and outer expansions has also been indicated in addition to the coupling which exists between the displacement and vorticity effects.

The first- and second-order equations were solved numerically by Van Dyke [14] at the stagnation point of a sphere at infinite Mach number. Later Davis and Flügge-Lotz [13] using an implicit finite difference method, solved the stagnation region for hyperboloids and paraboloids at infinite Mach number and for a sphere at $M_\infty = 10$. The conditions considered by Van Dyke gave a displacement thickness near zero, and he neglected that effect. The results of the method used by Davis and Flügge-Lotz for treating the displacement effect (the shifted and expanded body) was independent of the expansion parameter ϵ, and thus the results could be scaled in ϵ. This result is generally

not possible to obtain because the effects of displacement are dependent on the perturbation of the inviscid outer flow which is a global rather than local effect.

Because of the coupling of displacement and vorticity, the effect has been treated as either a displacement or vorticity effect. The effect is more clearly seen by considering the second-order inviscid pressure gradient which is

$$P_{2s}(s,0) = -[R_1(U_1U_2)_s + R_2U_1U_{1s} - r_w{}^jR_1{}^2T_1V_2S_1']_{n=0} \tag{59}$$

where the last term arises due to the coupling between vorticity and displacement (see Equation 56). According to the second-order theory, the term may be considered as either a displacement or vorticity effect. Van Dyke [21] calls the effect a "displacement pressure" effect if the term is considered as a displacement effect and as a "displacement speed" effect if treated as a vorticity effect. Both Van Dyke [14] and Davis and Flügge-Lotz treated the term as a displacement speed (vorticity) effect. Recently Adams [16] and Marchand, Lewis, and Davis [18] treated analytic bodies and spherically blunted cones, respectively, by both methods. It was observed first by inspection of the numerical results and later proved by Adams [16] that the displacement pressure treatment results were not unique but were affected by where the outer boundary conditions were imposed.[3] The displacement speed treatment,

---

[3]The term unique will be used to denote second-order results which were not affected by the location of the outer edge of the boundary layer or the matching point for the inner and outer flow field solutions.

however, gave results independent of the matching point or edge of the first-order boundary layer. The disadvantage of the displacement speed treatment was that it gave unrealistic, separate vorticity and displacement effects. Adams [16] and Marchand, Lewis, and Davis [18] suggested that the only proper physical treatment was a combined vorticity-displacement interaction. A significant disadvantage in the combined vorticity-displacement interaction is that it makes comparison with other theoretical or numerical treatments more difficult. It should be noted that although the displacement pressure results were found to be nonunique, comparison of results for the sum of displacement plus vorticity effects between the two treatments showed errors of about 5 per cent in the displacement pressure results for the wall shear stress. Because the errors found by Adams [16] and Marchand, Lewis, and Davis [18] were small and since the displacement speed treatment gave unrealistically large displacement effects (treated as a separate effect), the second-order results used for comparison with the first-order treatment of vorticity and displacement came from a displacement pressure treatment.

CHAPTER III
FIRST-ORDER TREATMENT

The first-order treatment of higher-order boundary-layer effects presented herein is based on a modification to the nonsimilar boundary-layer theory of Clutter and Smith [8]. The modification includes addition of the separate or combined effects of the vorticity inter-action theory of Hayes and Probstein [12] and the slip and temperature jump wall boundary conditions of Van Dyke [14]. In addition, the approximate treatment of transverse curvature by Clutter and Smith and the effects of displacement are also considered.

An error exists in the transverse curvature term in the Clutter and Smith theory which is retained in the present treatment. The reasons for not correcting the error were twofold. First, to correct the error without redefining the transformation variables would have introduced several additional terms and substantially complicated the numerical solutions. The error has recently been corrected by Jaffe, Lind, and Smith [22] by means of new transformation variables. The second reason for not changing the Clutter and Smith variables was the widespread use of the computing machine program throughout the country in engineering applications. It was felt desirable to establish the error caused in wall shear stress, for example, using the Clutter and Smith method. Comparisons will be given in a later chapter which will show the magnitude of the error in the integrated friction drag.

The first-order boundary-layer equations are given in this chapter with derivations of the effects of vorticity and slip and temperature jump (STJ). The method of solution of the first-order boundary-layer equations is described in Appendix A.

I. BOUNDARY-LAYER EQUATIONS

The first-order steady-flow equations for an axisymmetric laminar boundary layer in the coordinate system shown in Figure 10 including transverse curvature are as follows:

$$(r\rho u)_x + (r\rho v)_y = 0 \tag{60}$$

$$\rho(uu_x + vu_y) = -p_x + \frac{u}{r} r_y u_y + (\mu u_y)_y \tag{61}$$

$$\rho(uH_x - vH_y) = \frac{1}{r} r_y \left[\frac{\mu}{Pr} H_y + \mu(1 - 1/Pr)uu_y\right]$$

$$+ \left[\frac{\mu}{Pr} H_y + \mu(1 - 1/Pr)uu_y\right]_y \tag{62}$$

Clutter and Smith use the following transformations:

$$\eta = (u_c/\rho_* u_* x)^{1/2} \int \rho \, dy \tag{63a}$$

and

$$x = x \tag{63b}$$

They also defined a stream function ψ by

$$\rho ru = (\psi r)_y \quad \text{and} \quad \rho vr = -(\psi r)_x \tag{64}$$

The dimensionless stream function f is then defined as
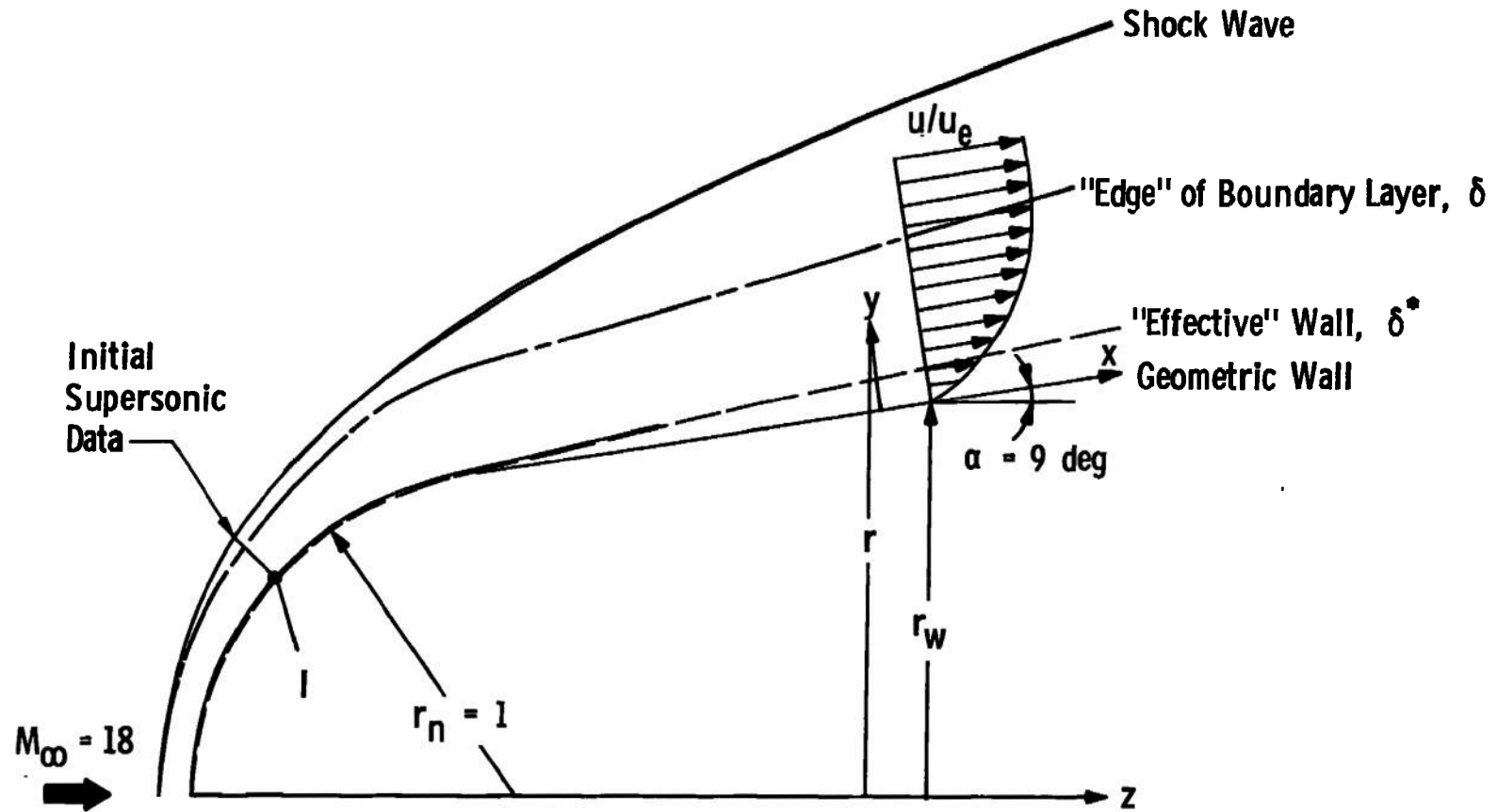
Fig. 10 Coordinate System for the First-Order Boundary-Layer Treatment of a Highly Cooled Spherically Blunted Cone at Hypersonic Conditions

$$\partial f/\partial \eta = f' = u/u_e \tag{65}$$

Then they state the following relation between f and ψ:

$$\psi = (\rho_* \mu_* x u_e)^{1/2} f \tag{66}$$

which is incorrect. The correct expression should read

$$\psi r = (\rho_* \mu_* u_e x)^{1/2} \int r f' d\eta \tag{67}$$

If $r = r(x)$ only, then Equation 67 would reduce to Equation 66 as given by Clutter and Smith; however, such is not the case since $r(x,y) = r_w(x) + y \cos \alpha$. This error was later recognized by Clutter and Smith [23] but not corrected until the recent work of Jaffe, Lind, and Smith [22]. Following Clutter and Smith, Equation 66 is assumed, and transformation of Equation 61 gives

$$(C_* r)^{-1} (Crf'')' + \beta(\rho_e/\rho - f'^2)$$

$$+ [(\beta+1)/2 + R]ff'' - x(f'f'_x - f''f_x) = 0 \tag{68}$$

where

$$C = \rho\mu/\rho_e\mu_e \tag{69a}$$

$$C_* = \rho_*\mu_*/\rho_e\mu_e \tag{69b}$$

$$\beta = (x/u_e)du_e/dx \tag{69c}$$

and

$$R = (x/r) \partial r/\partial x \tag{69d}$$

45

The no-slip boundary condition is

$$f'(0) = 0 \tag{70}$$

Neglecting mass transfer at the wall gives

$$f_w = f(0) = 0 \tag{71}$$

The remaining boundary condition is

$$f'(\eta \to \infty) = f'(\infty) = 1 \tag{72}$$

if first-order vorticity is neglected.

After defining the enthalpy ratio $g = H/H_e$, the energy equation is transformed to the x, η-plane and becomes

$$(C_* r)^{-1} \{ r[C/Pr]g' + (u_e^2/H_e)C(1-1/Pr)f'f''] \}'$$

$$= - [(\beta+1)/2 + R]fg' + x(f'g_x - g'f_x) \tag{73}$$

with the boundary conditions

$$g(\infty) = 1 \tag{74a}$$

and either $\quad g(0) = g_w(x)$ or $g'(0) = g'_w(x)$ \hfill (74b)

Clutter and Smith introduced the further transformations

$$\phi' = f' - 1 \text{ and } \psi = g - 1 \tag{75}$$

to improve the accuracy of numerical calculations. They also defined a transverse curvature T_{cs} by

$$(1/r)\partial r/\partial \eta = T_{cs} \rho_e/\rho \tag{76}$$

In terms of these new variables, the momentum equation becomes

$$(C\phi'')' = -T_{cs}(\rho_e/\rho)C\phi'' + C_*\beta[\phi'^2 + 2\phi' + 1]$$

$$- C_*N(\phi+\eta)\phi'' + C_*x[(\phi'+1)\phi'_x - \phi''\phi_x]$$

$$+ \{C_*(\rho_e/\rho)x(\rho_*/\rho_e)(u_*/u_e)^2 [(\gamma-1)/\gamma]$$

$$\cdot [H_e/u_*^2 - 1/2] \, d(p/p_*)/dx\} \tag{77}$$

and the energy equation is

$$\{(C/Pr)\psi' + (u_e^2/H_e) C[(1-1/Pr)(\phi'+1)\phi'']\}'$$

$$= -T_{cs}(\rho_e/\rho) \{(C/Pr)\psi' + (u_e^2/H_e) C[(1-1/Pr)(\phi'+1)\phi'']\}$$

$$- C_*N(\phi+\eta)\psi' + C_*x[(\phi'+1)\psi_x - \psi'\phi_x] \tag{78}$$

where $N = (\beta+1)/2 + R_o$

II. EXTERNAL VORTICITY EFFECTS

Inclusion of vorticity does not alter the basic equations but only the boundary conditions. Hayes and Probstein [12, page 370] define a vorticity index

$$\Omega = \underline{\frac{\text{vorticity at the outer edge of the boundary layer}}{\text{average vorticity across the boundary layer}}}$$

$$= \frac{\zeta_e}{\rho_e u_e} \int_0^{\eta=1} \rho \, dy \tag{79}$$

where ζ_e is the inviscid vorticity at the outer edge of the boundary layer. It should be noted that the vorticity index defined by Equation 79 will include the effect of displacement when coupled with vorticity since the properties are then to be evaluated at effective body surface.

From Crocco's vorticity law in terms of Van Dyke's variables, the inviscid vorticity becomes

$$\zeta_w = (\partial U_1^*/\partial y^*)_w = (U_\infty^*/r_n^*)\partial U_1/\partial y$$

$$= - (U_\infty^*/r_n^*) \, [r_w^{\ j} RTS_1{}']_e \qquad (80)$$

where the entropy gradient is obtained from Van Dyke [14] as

$$S_1'(0) = \frac{-1.6(M_\infty{}^2 - 1)^2 \, B^2{}_{sh}}{(2.8 \, M_\infty^2 - 0.4)(2 + 0.4 \, M_\infty^2)}$$

assuming $\gamma = 1.4$ with $B_{sh} = r_n/r_s$ (see Equations 20 and 22). A second-order expansion of the velocity leads to

$$u(x,y;\epsilon) = u_1(x,y) + \epsilon u_2(x,y)$$

$$\sim U_1(x,0) + \epsilon U_2(s,0) - y[r_w^{\ j} R_1 T_1 S_1']_{y=0} \qquad (81)$$

where use was made of Equations 22a, 50a, and 52a.

The vorticity index in the Clutter-Smith transformed plane becomes

$$\Omega = \frac{\zeta_e}{\rho_e u_e} \int_0^{\eta=1} \rho \, dy = \frac{\zeta_e}{\rho_e u_e} \left[\frac{\rho_* \mu_* \, x}{u_e} \right]^{1/2} \qquad (82)$$

Substituting Equation 80 into Equation 82 yields

$$\Omega = - \frac{(U_{\infty}^{*}/r_n^{*})}{\rho_{\infty}^{*} \ U_{\infty}^{*}} \left[\frac{r_w^{\ j} \ R \ T \ S_1'}{RU} \right]_e \left[\frac{\rho_* \mu_* \ x}{u_e} \right]^{1/2} \tag{83}$$

Dividing Equation 81 by $u_e/U_{\infty} = U_1(x,0) + \epsilon U_2(x,0)$, substituting Equations 63a and 83, and evaluating the result as $y \to \infty$ yields

$$\frac{u(x,\infty)}{u_e(x)} = f'(\infty) = 1 + \Omega(x) \int_0^\infty \frac{\rho_e}{\rho} \, d\eta \tag{84}$$

for the outer boundary condition on the momentum equation including external vorticity.

It should be noted from Equation 84 that the boundary condition $f'(\infty)$ must be obtained by iteration since the integral is unknown a priori. The numerical procedure used for solution of the first-order boundary-layer equations is described in Appendix A. The procedure used by Clutter and Smith is convenient when iteration is required, since the basic method is iterative somewhat unlike the implicit finite-difference scheme of Flügge-Lotz and Blottner.

The vorticity index Ω can be written as

$$\Omega = Kr_w^{\ j} \left[(H_e/u_*^2) - \frac{1}{2} (u_e/u_*)^2 \right] x^{1/2} (u_*/u_e)^{3/2} \tag{85a}$$

where

$$K = - (\rho_*/\rho_{\infty})(u_*/u_{\infty})S_1'/(Re_*)^{1/2} \tag{85b}$$

independent of x.

Thus one finds that $\Omega \sim x^{3/2}$ as $x \to \infty$ for spherically blunted

cones. This index is not to be confused with

$$\dot{\Omega}_1 = r_w^j \ R_1 T_1 S_1' = [\gamma/(\gamma-1)] r_w^j P_1 S_1'$$

defined by Van Dyke [14] for the inviscid vorticity. Davis and Flügge-Lotz [13] noted that $\Omega_1 \sim x$ for large x since $S_1'(0) =$ constant and $P_1 \to$ constant far downstream on most analytic bodies and all spherically blunted cones.

III. FIRST-ORDER SLIP AND TEMPERATURE JUMP EFFECTS

From second-order boundary-layer theory, Van Dyke [14] showed that the slip-flow boundary conditions are

$$u(0) = [\mu/p \ (\pi RT/2)^{1/2} \ \partial u/\partial y]_w$$

and

$$T(0) = T_w + (15/8)[\mu/p \ (\pi RT/2)^{1/2} \ \partial T/\partial y]_w$$

when the hard-sphere model for the gas was used to evaluate the coefficients.[1]

Transforming the equations to the x, η-plane and expressing in terms of convenient variables for inclusion in the Clutter and Smith numerical scheme gives

$$f'(\eta=0) = \frac{\rho\mu}{\rho_* \mu_*} \ \frac{\rho_*}{\rho_w} \ F_s \ f''(\eta=0) \qquad (86a)$$

---

[1]The second term in the wall slip velocity boundary conditions (Equation 42) is of third order (i.e. of order ϵ^2) and was not considered. However, for the constant wall temperature conditions treated, the term would have been zero in any event.

$$h(\eta=0) = h_w + \frac{15}{8}\,\frac{\rho\mu}{\rho_*\mu_*}\,\frac{\rho_*}{\rho}\,F_s\,\frac{\partial h}{\partial\eta} \qquad (86b)$$

where

$$F_s = \left(\pi\,\frac{\gamma}{\gamma-1}\,\frac{u_*^2}{2h_{ref}}\,\frac{h_{ref}}{h_w}\,\frac{u_e}{u_*}\,\frac{1}{Re_*}\,\frac{1}{x}\right)^{1/2} \qquad (86c)$$

Subscript w denotes properties evaluated at the no-slip wall conditions. The fluid properties should be evaluated at the slip conditions as described by Patterson [24]; however, to make direct comparison with the second-order results, the properties were consistently evaluated at the no-slip wall conditions. In recent calculations for flow over a sharp cone at low Reynolds number conditions, Mayne, Gilley, and Lewis [25], using a modified version of the Jaffe, Lind, and Smith [22] theory and slip-flow equations similar to those used herein, evaluated the fluid properties at the slip conditions. Unpublished comparison of results using fluid properties evaluated at both the slip and no-slip conditions showed small differences in the wall shear stress.

The STJ boundary conditions in Equations 86 must be obtained by iteration since the solution yields $f''(\eta=0)$ and $\partial h/\partial y \neq g'(\eta=0)$ with STJ. As in the case with external vorticity, inclusion in the Clutter and Smith numerical scheme presents no difficulty, and the method of inclusion is described in Appendix A.

IV. DISPLACEMENT EFFECT

In a recent paper, Van Dyke [26] discussed the role of the

displacement effect in higher-order boundary-layer theory. He indicated that the first discussion of higher-order effects was given by Prandtl [27, page 90] when he described the displacement effects of the flat-plate boundary layer on the uniform outer flow as follows:

> The displacement of the stream-lines by the amount δ^* produces a slight alteration in the potential flow which was made the basis of the calculations. Instead of the simple parallel flow, the flow around a parabolic cylinder of thickness $2\delta^*$ should be introduced, which would slightly alter the pressure distribution. The above calculation would have to be repeated for this new pressure distribution and if necessary the process repeated on the basis of the new measure of displacement so obtained. Such calculations have so far not been performed; they would, in any case, make little difference in the regions where the calculations are usually applied in practice. They would however, become necessary if the transition to smaller Reynolds numbers $U_\infty \rho_\infty L / \mu_\infty$ were attempted.

Van Dyke [26], in describing the difficulty in treating the displacement effect, noted the global rather than the local nature of the effect. He termed the effect due to classical boundary-layer theory plus the flow due to displacement as "one-and-a-half-order-theory." However, the term first-order displacement effect will be used herein to describe the effect since the choice of title is arbitrary and not derived by analysis.

No modification to the basic boundary-layer equations is required to treat the first-order displacement effect. The treatment of first- and second-order displacement effects is given in Appendix B, where the method of treating the perturbed inviscid outer flow is described.

CHAPTER IV

NUMERICAL RESULTS AND DISCUSSION

Comparisons of first- and second-order treatments of transverse curvature, vorticity, slip and temperature jump (as a single effect), and displacement will be presented in this chapter. A sensitive quantity for such comparisons is the effect on zero-lift drag, and thus this will be used primarily for comparison of numerical results in this chapter and with experimental data in the next chapter. The effects of viscosity law are also easily shown by comparison of second-order solutions in physical variables using a square-root viscosity law and solutions in transformed Levy-Lees variables using the Sutherland viscosity law.[1] Unless otherwise noted, all solutions used perfect gas (γ = 1.4), constant Prandtl number (Pr = 0.71), uniform wall temperature (T_w/T_O = 0.2 at M_∞ = 9 and 0.066 at M_∞ = 18), Sutherland viscosity law, and identical pressure distributions from an ideal-gas blunt body and characteristics solution at M_∞ = 9 or 18.

For computation purposes, three sets of conditions or cases were defined at M_∞ = 18 and five cases at M_∞ = 9. The free-stream and

---

[1]Unpublished comparisons between solutions in physical and transformed variables have shown identical results for all second-order effects except displacement and vorticity. Therefore, unless otherwise noted, the differences shown between second-order solutions were due entirely to the choice of viscosity law.

stagnation conditions used in the first- and second-order boundary-layer calculations are given in Tables I and II.

The second-order solutions for each vorticity and displacement based upon displacement pressure treatment were found to be numerically nonunique. The solutions were affected by both Δy or $\Delta \eta$ step sizes and η_∞ or its equivalent in physical variables. It was found, however, that the sum of both displacement and vorticity effects was unique and was equal to the displacement speed treatment of the sum of both effects. However, since the displacement speed treatment greatly magnifies both displacement and vorticity effects and since the effects of $\Delta \eta$ step size and η_∞ were certainly significant but not large, the second-order solutions shown were based upon the displacement pressure treatment. Moreover, since the sum of the two effects is unique, no loss in accuracy is involved when comparisons are made with their combined effects.

I. TRANSVERSE CURVATURE EFFECTS

A comparison of the results of the first- and second-order treatments of the transverse-curvature-induced friction drag at $M_\infty = 9$ and 18 is shown in Figures 11 and 12. At both Mach number conditions, the differences are small between second-order solutions with different viscosity laws; however, the approximate treatment of Clutter and Smith predicts an increment about 30 per cent less. This is a significant error, and the Clutter and Smith treatment cannot be

TABLE I
EXPANSION PARAMETER AND REYNOLDS NUMBER

Case	M_∞	ε	Re_∞	Re_*
187	18.0	0.0776	4844.9	429.1
185	18.0	0.2330	538.3	47.7
182	18.0	0.3516	236.2	20.9
95	9.0	0.1000	925.49	250.35
93	9.0	0.2401	160.26	43.35
90	9.0	0.3336	83.18	22.5
91	9.0	0.4398	47.87	12.95
92	9.0	0.5337	32.50	8.79

TABLE II
CONDITIONS USED IN THE BOUNDARY-LAYER CALCULATIONS

M_∞	18.0	9.0
H_e, ft^2/sec^2	4.988×10^7	3.261×10^7
p_o', lbf/ft^2	146.88	13.036
T_o', °R	8289.	5263.
$u_*^2/2h_{ref}$	0.03923	0.02565
u_∞, ft/sec	10074.8	7840.
p_∞, lbf/ft^2	0.35172	0.01244
ρ_∞, lbf-sec^2/ft^4	1.624×10^{-6}	2.367×10^{-7}
T_∞, °R	126.0	306.0
T_w, °R	547.0	1053.
g_w	0.066	0.20
B_{sh}	0.770	0.769
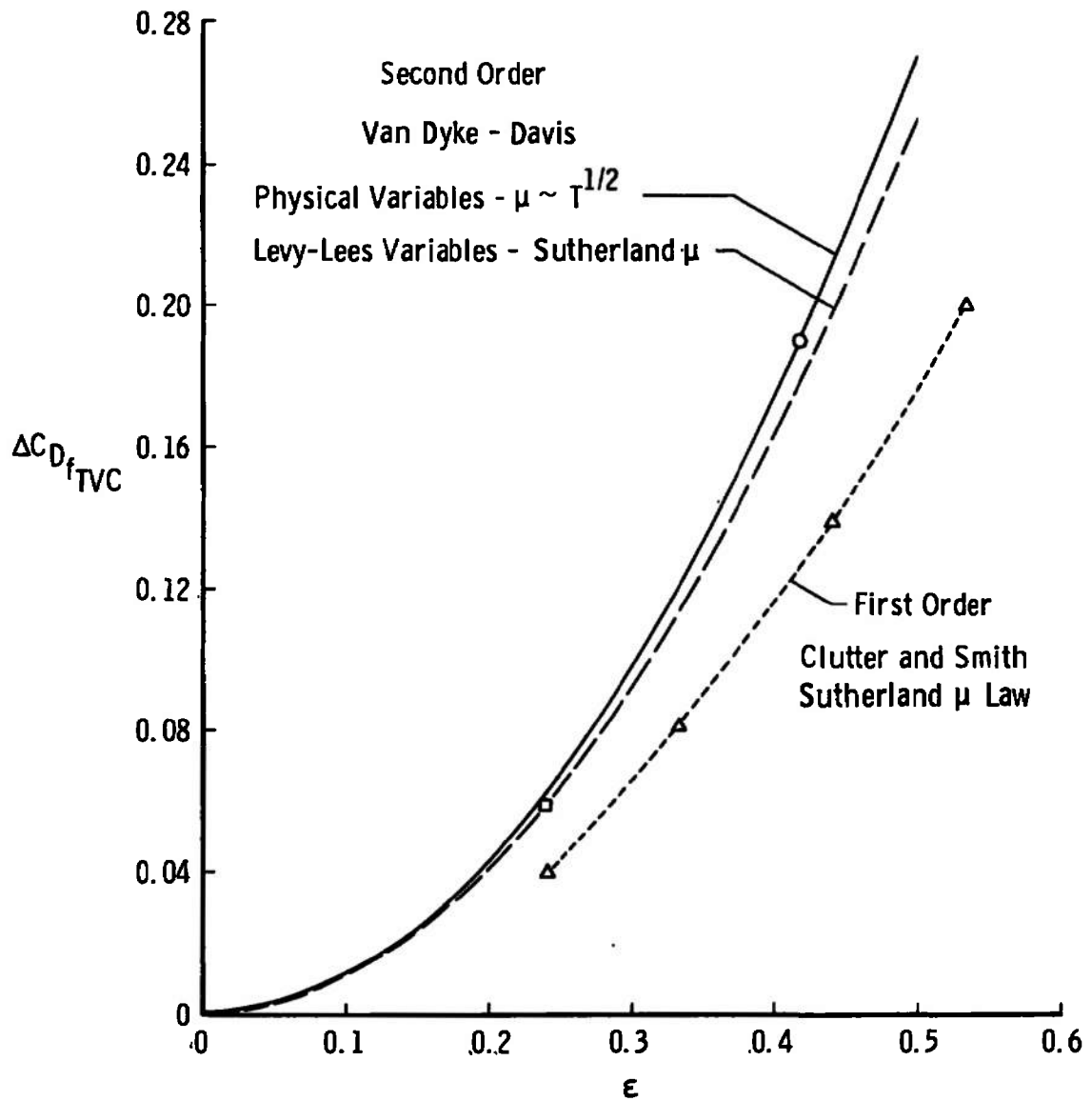
Fig. 11 Transverse-Curvature-Induced Friction Drag at $M_\infty = 9$, $T_w/T_o = 0.2$, and $r_n/r_b = 0.3$
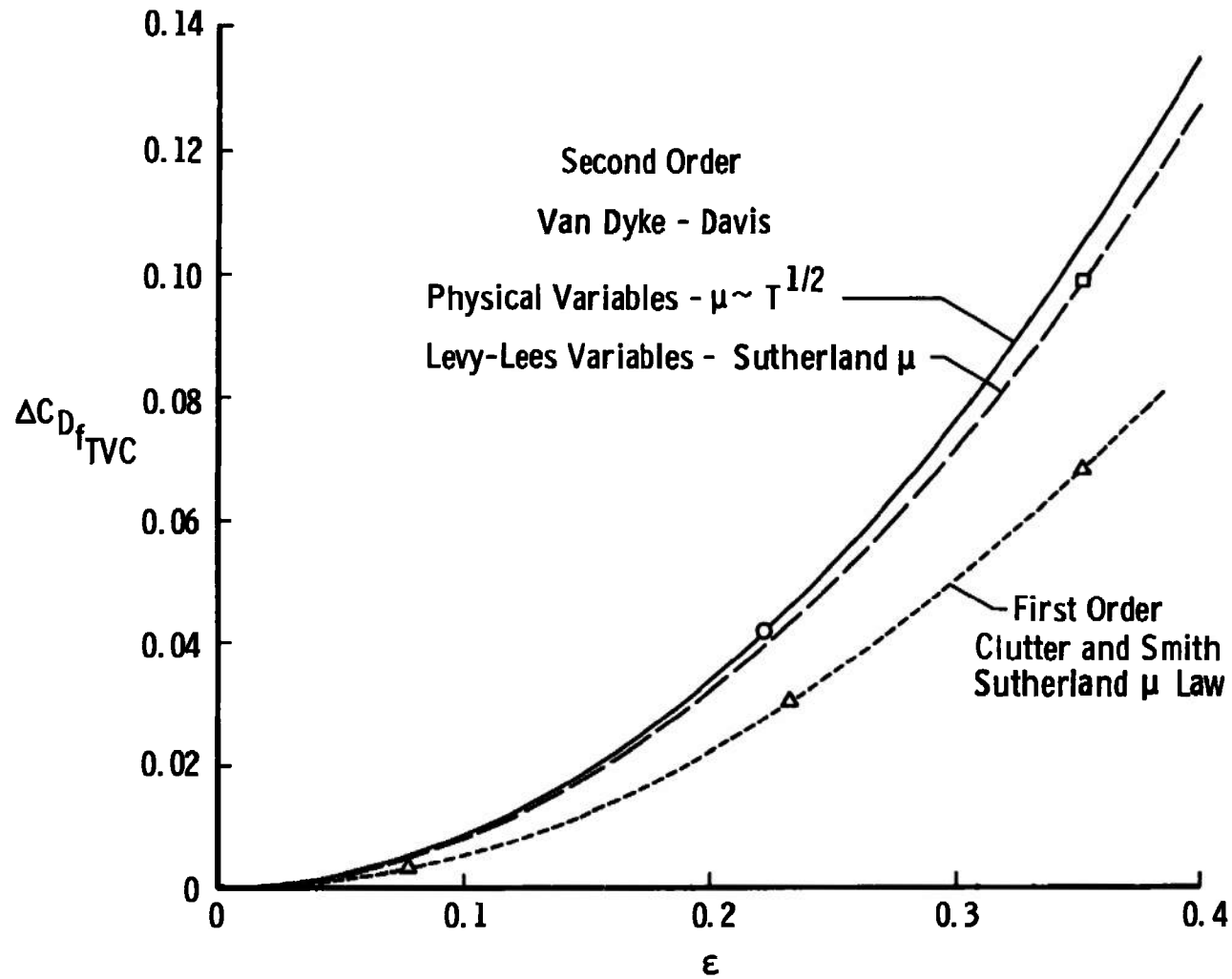
Fig. 12 Transverse-Curvature-Induced Friction Drag at $M_\infty = 18$, $T_w/T_o = 0.066$, and $r_n/r_b = 0.3$

recommended for calculations involving transverse curvature.[2]

II. VORTICITY INTERACTION EFFECTS

Figure 13 shows the local skin-friction coefficient predicted by first- and second-order methods. Good agreement exists for about 8.5 nose radii from the stagnation point. Beyond that point the first-order prediction increases whereas the second-order result remains approximately constant to the base of the cone (x = 16.4).

The effects of both Δx and $\Delta \eta$ step sizes were investigated for the first-order solutions. It was found that the solution was sensitive to $\Delta \eta$ but insensitive to Δx step sizes. This is explained as follows: First, the transformations used by Clutter and Smith are such that without vorticity effects the classical boundary layer was substantially reduced from $\eta_\infty = 6$ at x = 0 to $\eta_\infty = 2$ over much of the conical afterbody (for longer bodies or bodies with more favorable pressure gradient, values of $\eta_\infty = 1$ were not uncommon). The variation in boundary-layer thickness was less in the Levy-Lees transformed plane than in either the physical or Clutter and Smith transformed plane. Therefore, for classical boundary-layer solutions, the Clutter and Smith transformation is not optimum for bodies with strong favorable pressure gradients. Secondly, and more importantly, the extent

---

[2]Unpublished comparisons among numerical calculations of transverse curvature effects using a finite difference solution in Levy-Lees variables, the second-order results using the Davis and Flügge-Lotz method, and the first-order treatment of Jaffe, Lind, and Smith [22] showed that all three methods gave essentially the same results when identical conditions were used.
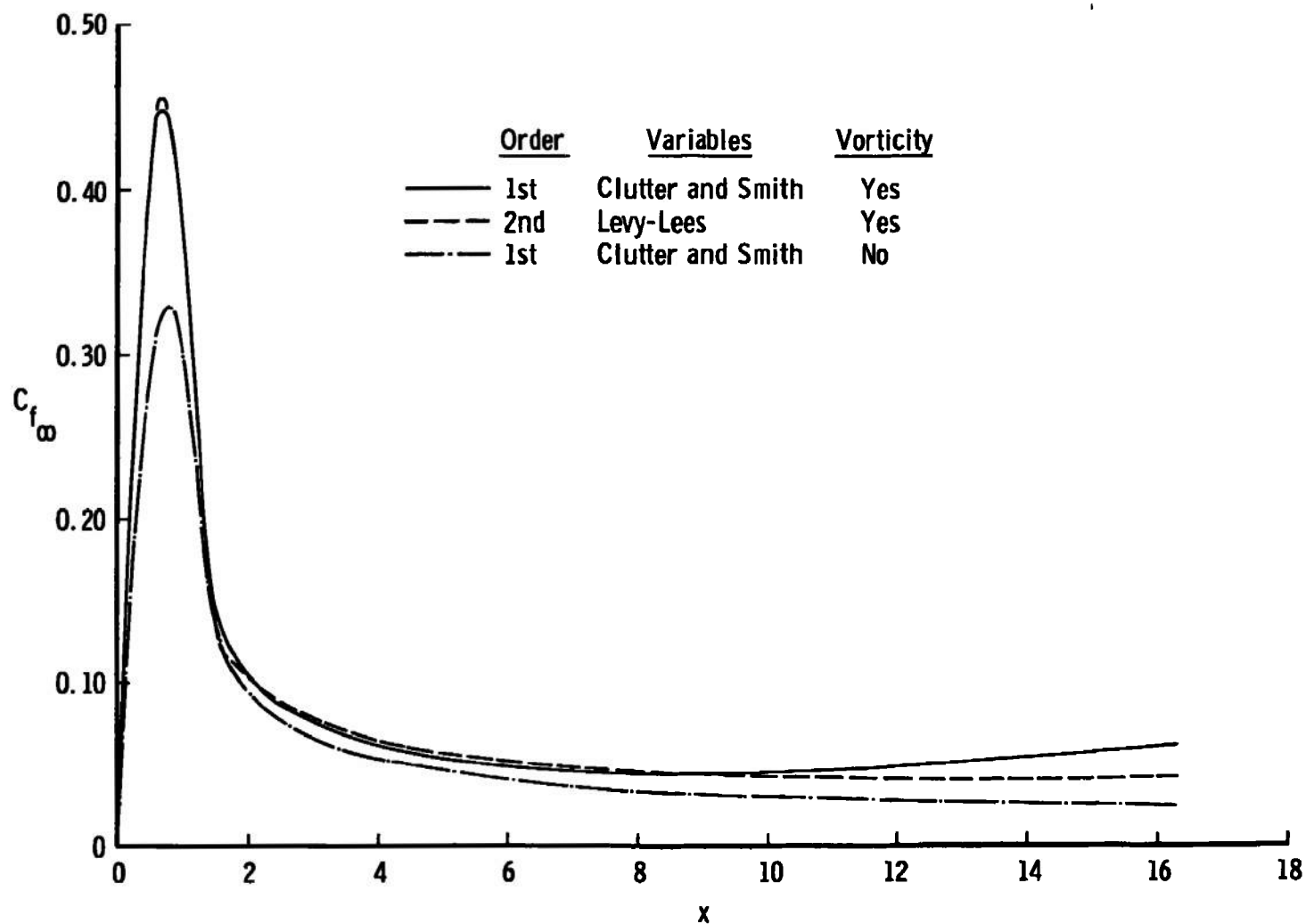
Fig. 13 Effects of External Vorticity on Skin Friction at $M_\infty = 18$, $T_w/T_o = 0.066$, and r/c 0.352

of the boundary layer with external vorticity is limited by a line of maximum velocity $f'_{max} = 1/(1-h_e/11_c)^{1/2}$ (see Appendix A). Along this line $T_i = 0$ and $\rho_i \to \infty$. This substantially reduces η_∞ below the allowed classical solution value. It was therefore necessary occasionally to reduce the $\Delta\eta$ step size as the solution proceeded along the body. The data normal to the surface were interpolated so that a minimum of 200 η points were used to integrate the momentum and energy equations. The solutions were accepted when similar calculations were made with reduced step sizes and no significant changes were observed in f''_w and g'_w. Similar reduction of Δx-step size significantly increased machine time without affecting the solution. Examination of the $f'(\eta)$ profiles showed they asymptotically approached a linear variation as $\eta \to \eta_\infty$.

The first-order solutions shown with vorticity were examined for step size effects and are believed to be unaffected of both Δx and $\Delta\eta$ step sizes. The divergence of solutions for $x > 8.5$ is believed to be a result of the first- and second-order boundary-layer treatments and not an accuracy or step size effect. This effect was observed for all solutions, but the divergence in solutions increased as the Reynolds number decreased or ϵ increased.

The good agreement between the values of C_{f_∞} from the first- and second-order treatments of the effects of vorticity for $x < 8.5$ is gratifying and might have been expected; however, to the author's knowledge, this is the first time the essential agreement between first- and second-order solutions has been demonstrated for conditions far from the stagnation region.

The importance of the difference in first- and second-order shear stress is shown in Figures 14 and 15. At $M_\infty = 9$ the first- and second-order solutions were in excellent agreement for $\epsilon < 0.2$ and departed rapidly as ϵ increased. For $\epsilon = 0.4$ the first-order prediction was approximately twice the second-order increment. The large difference in this the largest higher-order drag component is disappointing, and moreover, it will be shown by comparison with experimental data that both methods overpredict the total zero-lift drag for $\epsilon > 0.2$. The trends of the results at $M_\infty = 18$ were similar to those at $M_\infty = 9$, but the solutions tended to separate earlier and one of the first-order solutions fell below the second-order solution curve. The range of ϵ was chosen for numerical solution to cover generally the range of available experimental data, and thus the ranges differed for the two Mach numbers.

Figure 16 shows a convenient quantity introduced by Davis and Flügge-Lotz for a stretched nondimensionalized displacement thickness. The quantity (which they denoted as DISP) is defined here as $\delta_D^* = \delta^*/\epsilon$ and thus is independent of the expansion parameter. Comparisons of the results shown on Figure 16 indicate the effects of viscosity law on the two-dimensional displacement thickness, the effects of transverse curvature, and the effects of first-order vorticity interaction on the displacement thickness. Using a square-root viscosity law gave a slightly larger δ^* than the use of Sutherland's law predicted. The axisymmetric δ^* including TVC was slightly below the two-dimensional result. A dramatic effect occurred when the expression for the
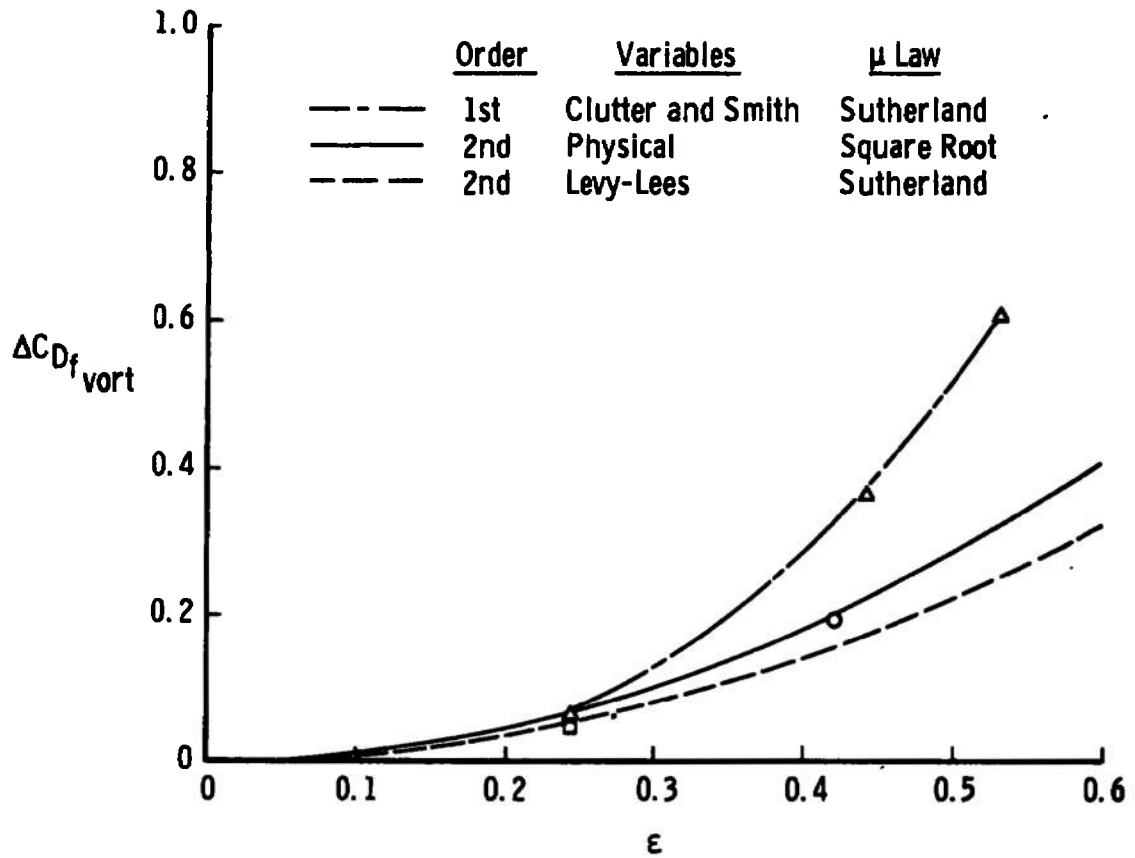
Fig. 14 First- and Second-Order Vorticity-Induced Friction Drag Predictions at
$M_\infty = 9$, $T_w/T_o = 0.2$, and $r_n/r_b = 0.3$
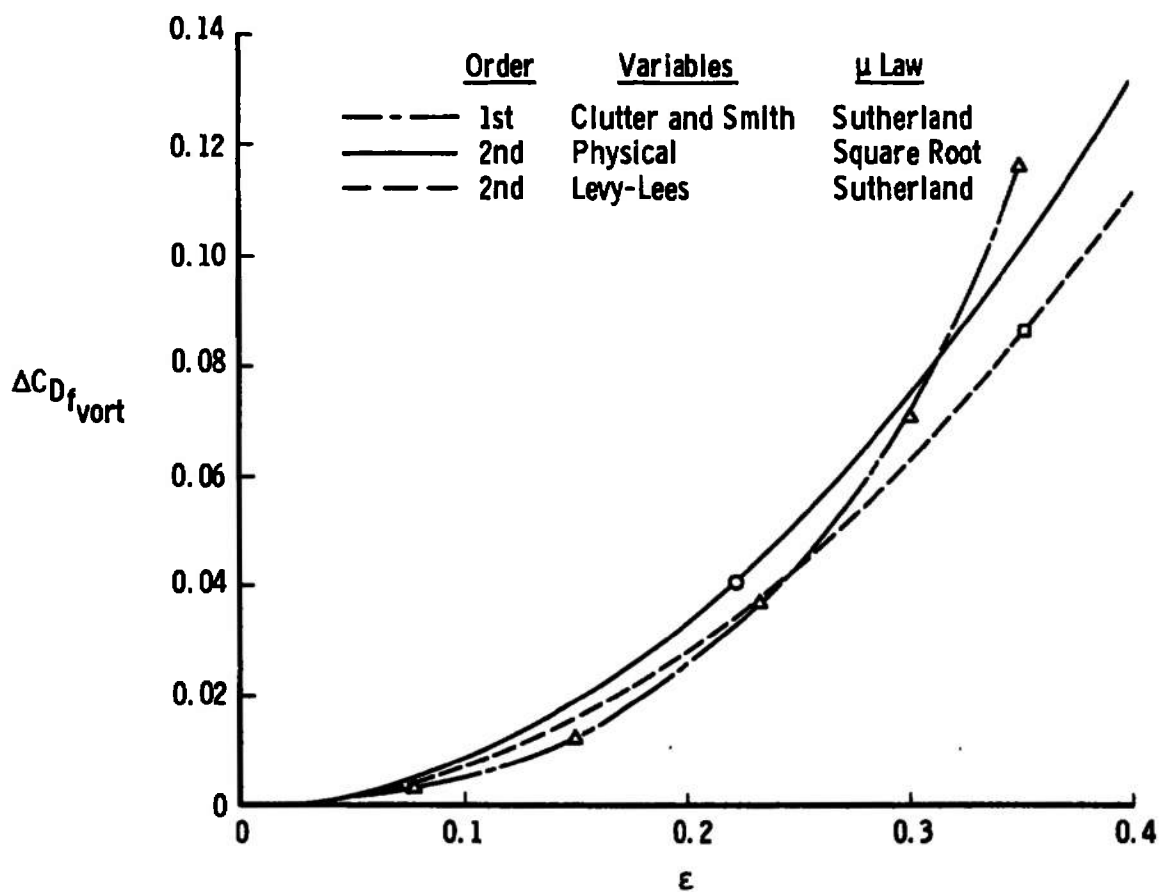
Fig. 15 First- and Second-Order Vorticity-Induced Friction Drag Predictions at $M_\infty = 18$, $T_w/T_o = 0.066$, and $r_n/r_b = 0.3$

AEDC-TR-68-148
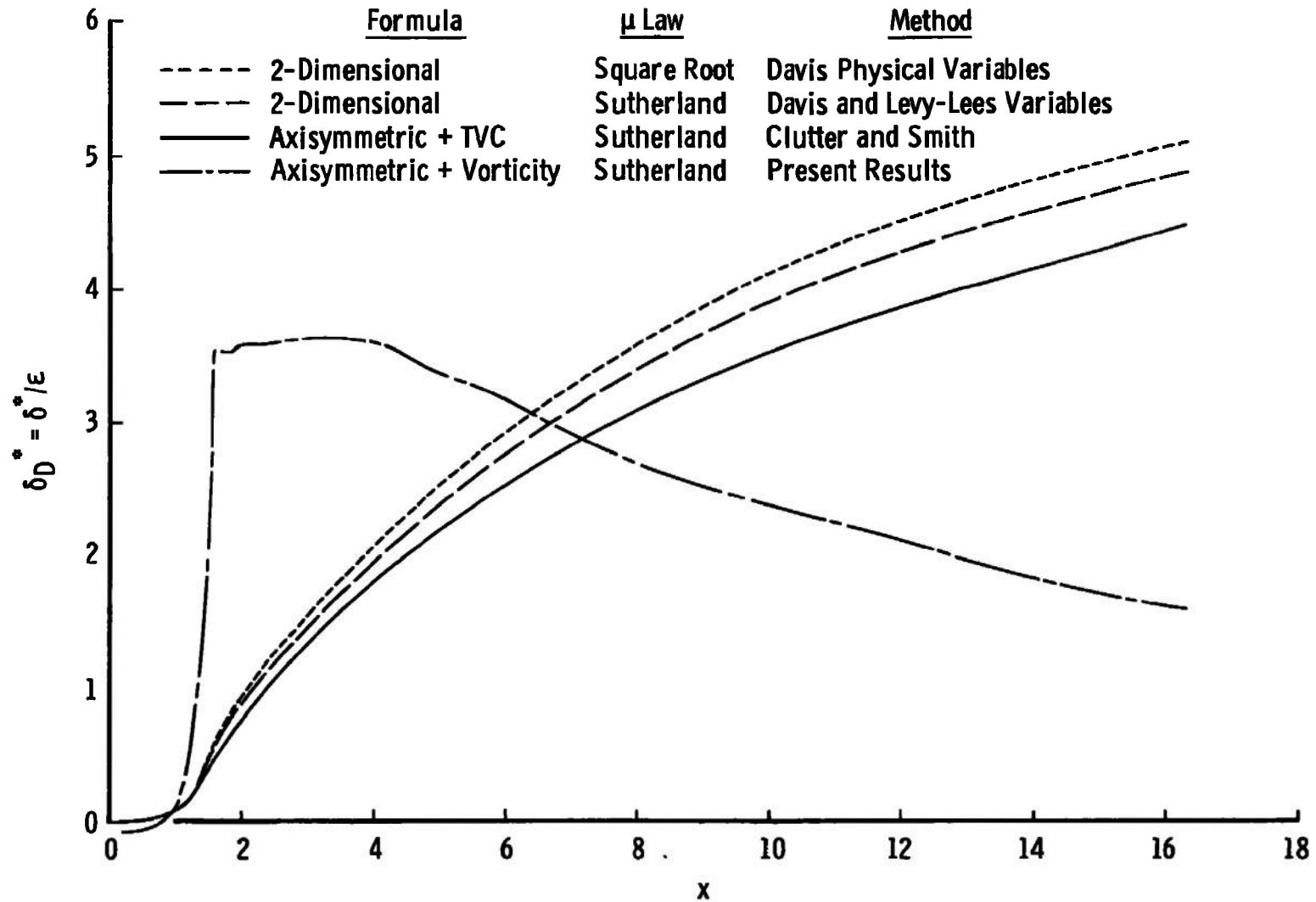
Fig. 16 Higher-Order Effects on Displacement Thickness at $M_\infty = 9$ and $T_w/T_o = 0.2$

displacement thickness δ_v^*, which is derived in Appendix C and includes vorticity interaction, was compared with the classical forms. Including vorticity produced a negative displacement thickness over the nose (whereas the values calculated using classical theory were slightly positive), substantially increased the rate of growth in the region of strong favorable pressure gradient, and caused a rapid decline in displacement thickness over much of the conical afterbody where the effects of vorticity on the velocity profile and wall shear were most important. The behavior of δ_v^* indicates the difficulty of realistically and consistently treating the combined effects of displacement and vorticity interactions by a first-order method without simultaneously treating the interaction of the entropy and boundary layers. Of course, in the second-order theory this interaction was not considered and its region of applicability was also limited. These limitations can also be seen in the next chapter from comparisons of the numerical results with some experimental data.

III. DISPLACEMENT EFFECTS

The first-order displacement-induced pressure distributions over the spherically blunted cone are shown in Figures 17 and 18. The large effect of displacement on the pressure distributions for the ranges in Reynolds number considered is evident from the figures. The bump in the pressure distribution for the lowest Reynolds number or largest ϵ considered at $M_\infty = 9$ can be seen in Figure 18. The bump is caused by the rapid increase in displacement thickness in the region $x = 1.0$ to
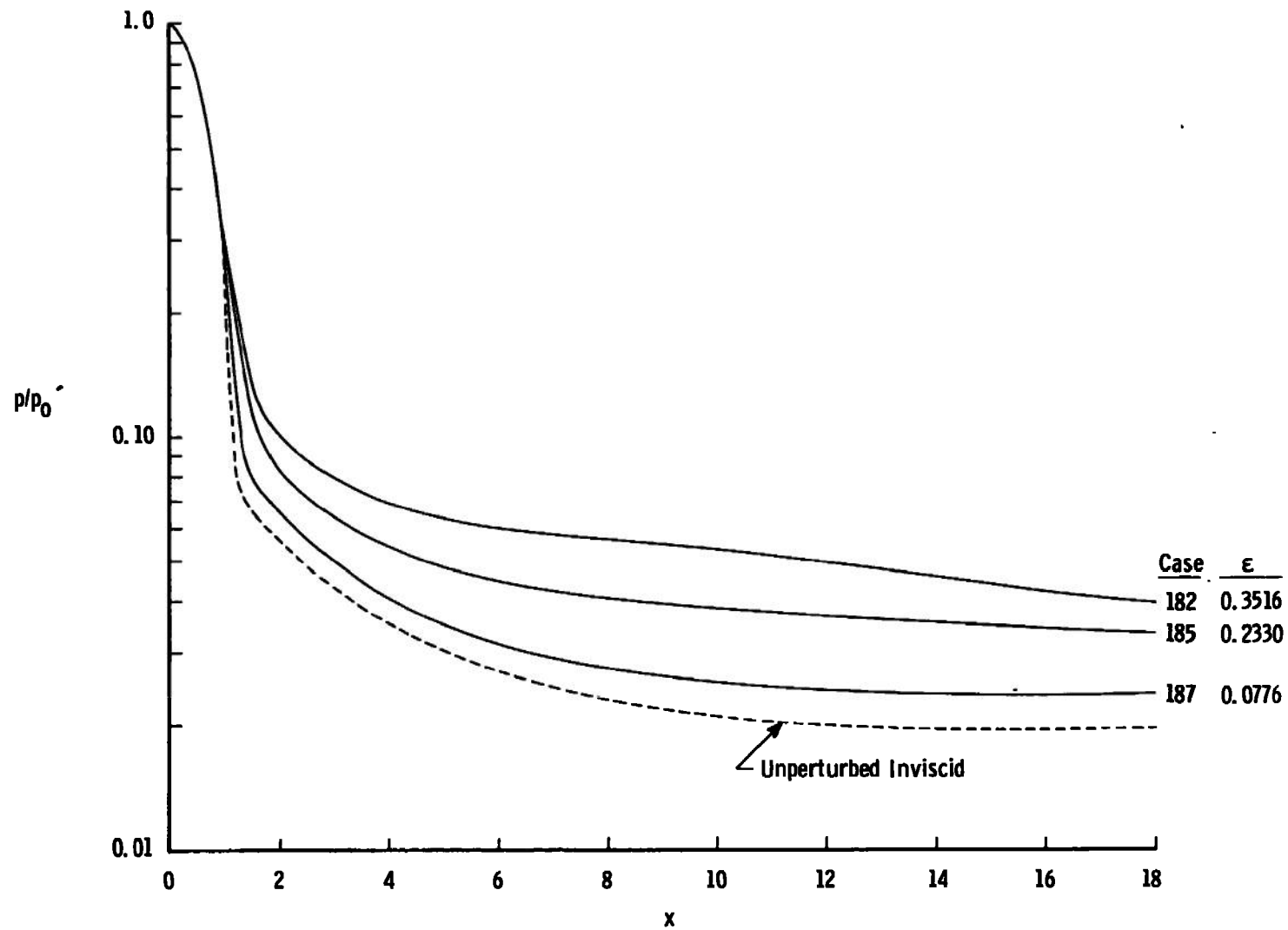
Fig. 17 First-Order Displacement-Induced Pressure Distribution Over a Spherically
Blunted Cone at $M_\infty = 18$ and $T_w/T_o = 0.066$

Case	ϵ
182	0.3516
185	0.2330
187	0.0776

Unperturbed Inviscid
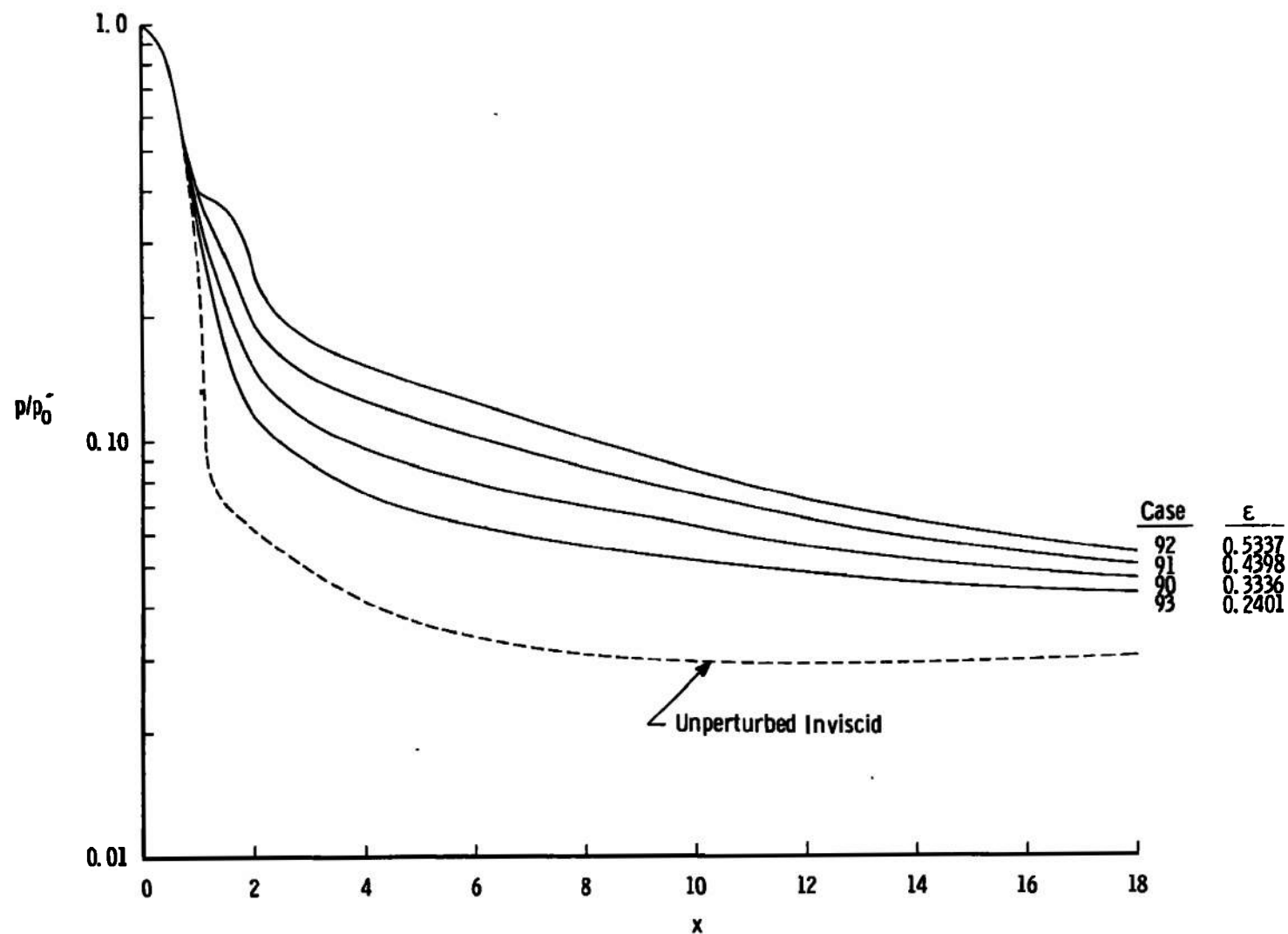
Fig. 18 First-Order Displacement-Induced Pressure Distribution Over a Spherically Blunted Cone at $M_\infty = 9$ and $T_w/T_o = 0.2$

2.0. As described in Appendix B, the curve fit of the effective body
in the region of rapid increase in displacement thickness was poorer
since inflection points were not allowed in the effective body curve
fits over this region. However, allowing inflection points in the
curve fits would only have caused larger bumps and induced secondary
shocks which would have further altered the pressure distributions
over the conical afterbody.

First- and second-order displacement-induced pressure and
friction-drag increments are shown in Figures 19 and 20. Perturbed
inviscid outer flow solutions were obtained for four values of ϵ
at $M_\infty = 9$ and three values at $M_\infty = 18$. The two predictions for the
displacement-induced pressure drag differed only by the effect of the
pressure gradient over the nose, where the effect was included in the
second-order but not in the first-order treatment.

The differences between the two treatments of displacement-
induced friction drag were larger, and the results are more interest-
ing. In the first-order treatment, only the effect of displacement
of the inviscid outer flow-field pressure was included. In the second-
order solutions, however, the effects of inviscid vorticity on the
outer edge velocity and temperature were also present.

Caution must be used when trying to generalize the results
shown in Figures 19 and 20. First, the second-order results for
displacement-induced pressure and friction-drag increments were not
simply linearly and quadratically dependent, respectively, on ϵ.
(It is interesting to note, however, that the first-order friction-drag
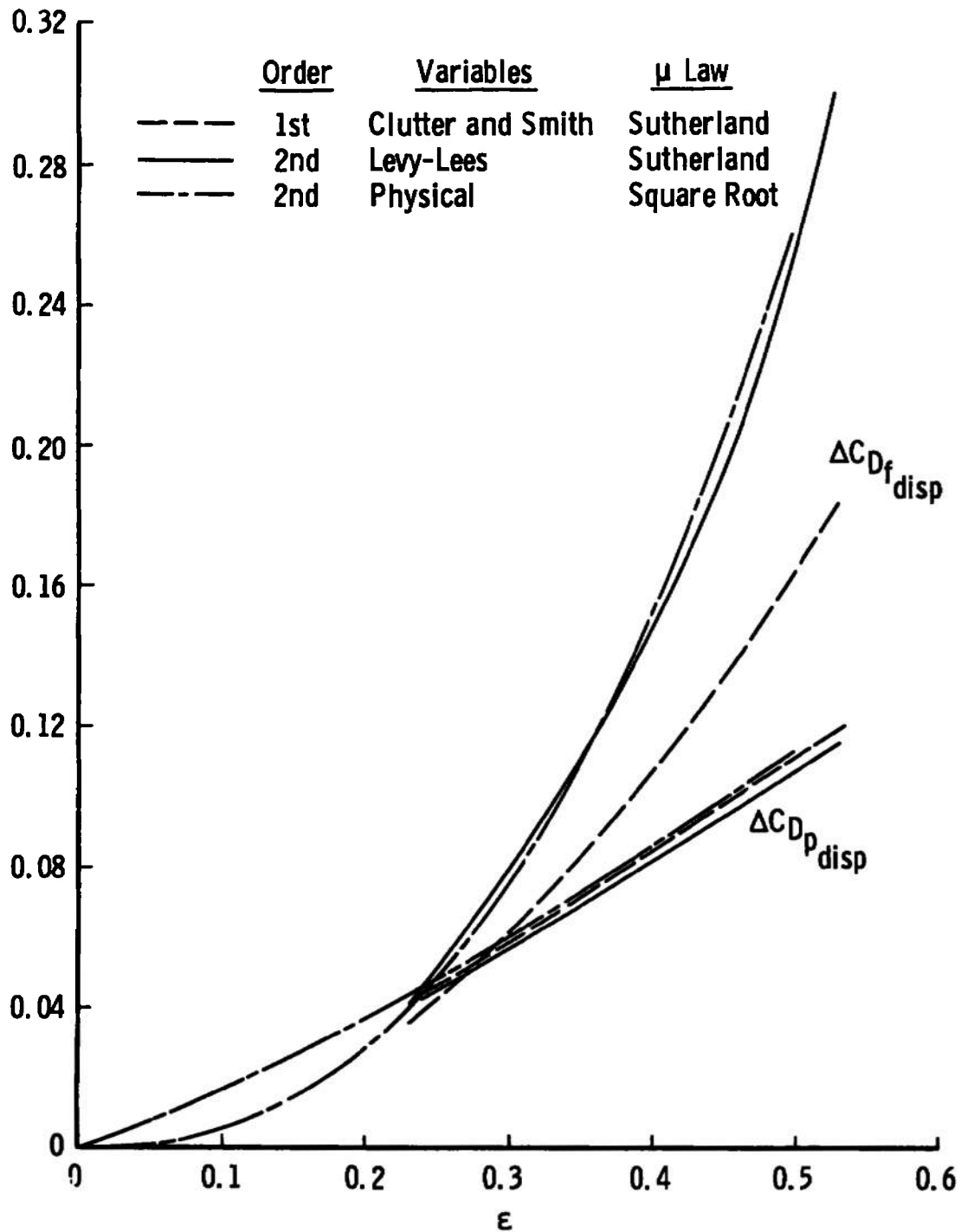
Fig. 19 First- and Second-Order Displacement-Induced Pressure and Friction-Drag Components at $M_\infty = 9$, $T_w/T_o = 0.2$, and $r_n/r_b = 0.3$
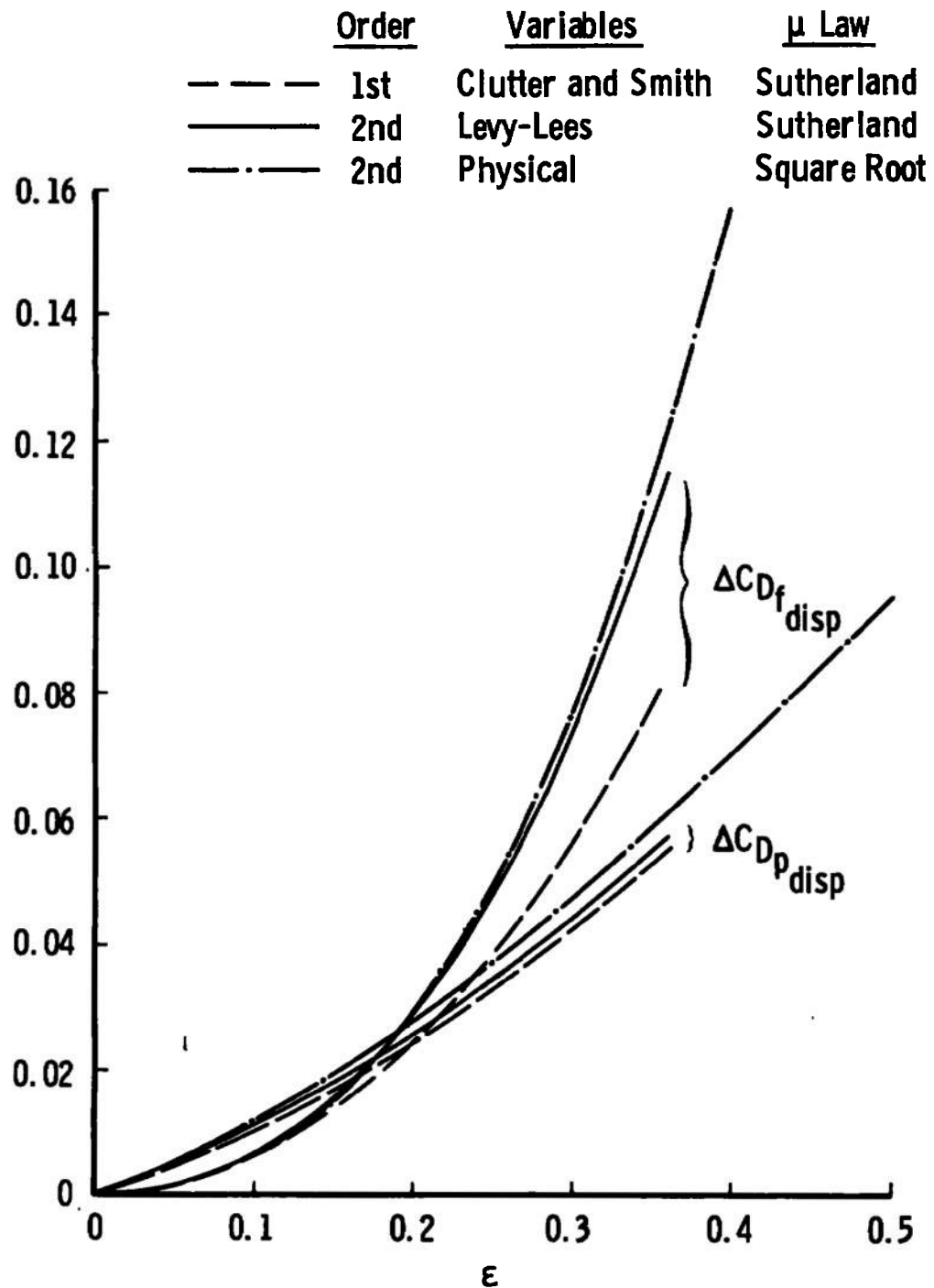
Fig. 20 First- and Second-Order Displacement-Induced Pressure and Friction-Drag Components at $M_\infty = 18$, $T_w/T_o = 0.066$, and $r_n/r_b = 0.3$

results were quadratically dependent on ε.) Secondly, for other bodies under different conditions, negative second-order displacement-induced friction drag has been found. The effects of geometry (both surface slope and length), wall-to-stagnation temperature ratio, and viscosity law used have the strongest influence on second-order wall shear stress distribution. For the conditions treated here, the effects of wall-to-stagnation temperature ratio caused small differences in the induced-drag increments for both first- and second-order treatments.

It is emphasized again that the second-order displacement-induced friction-drag results shown in Figures 19 and 20 were not unique. The results shown in Levy-Lees variables were obtained with an edge $\eta_\infty = 6$. Two conditions were recalculated using $\eta_\infty = 9$, and the displacement-induced friction drag was increased about 7 per cent without affecting the displacement-induced pressure drag. Therefore, the excellent agreement between the second-order solutions in physical and Levy-Lees variables was to some extent fortuitous since neither solution was independent of the outer matching point location.

IV. SLIP AND TEMPERATURE JUMP EFFECTS

Comparisons of first- and second-order wall slip velocity and temperature jump for one of the conditions at $M_\infty = 9$ are shown in Figures 21 and 22. The first-order slip velocity and temperature was lower than the second-order results by about 15 to 20 per cent. Figure 23 shows a comparison of the first- and second-order local (total) skin-friction coefficient. The differences in slip velocity and
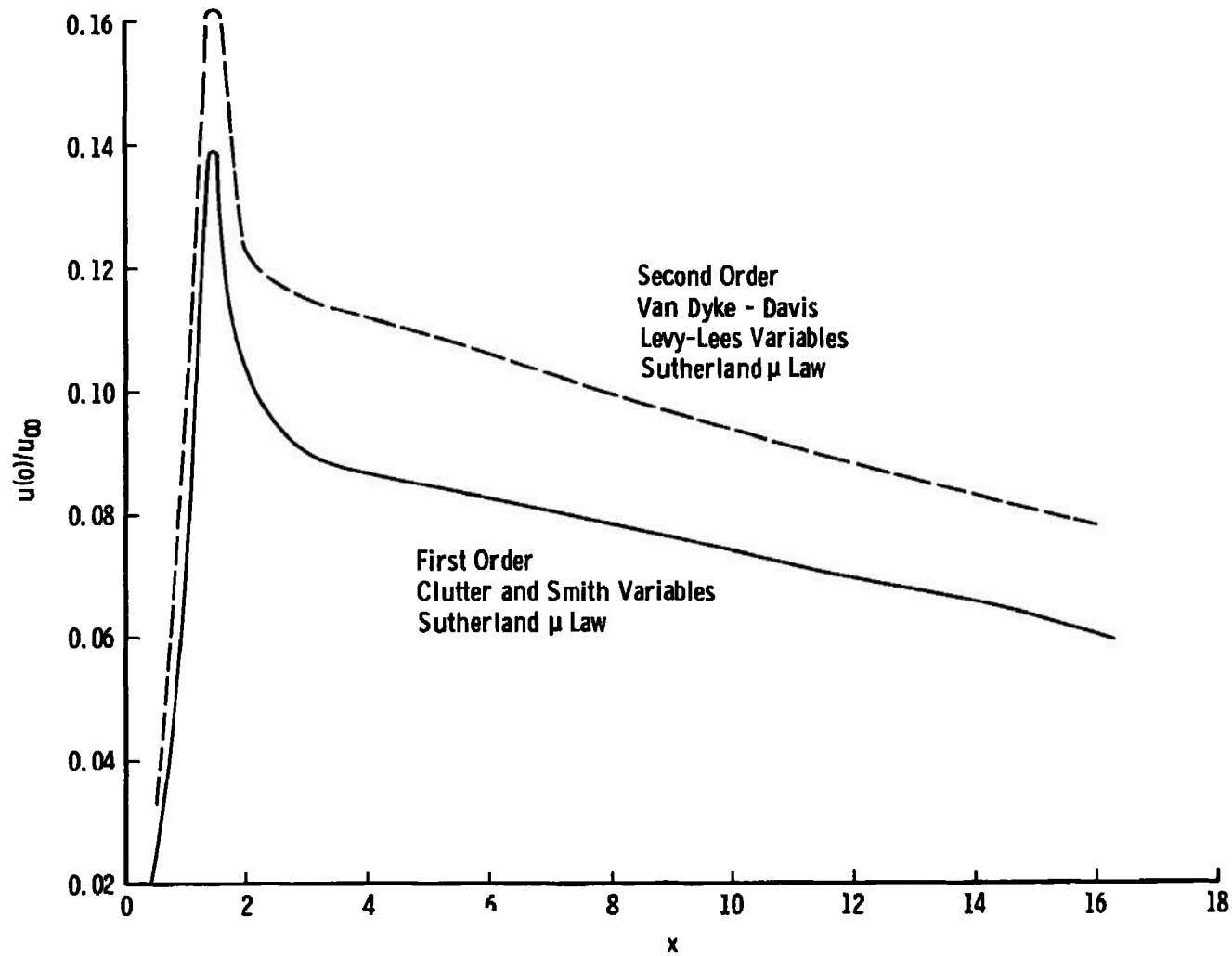
Fig. 21 First- and Second-Order Slip Velocity at M_∞ = 9, T_w/T_o = 0.2, and ϵ = 0.24
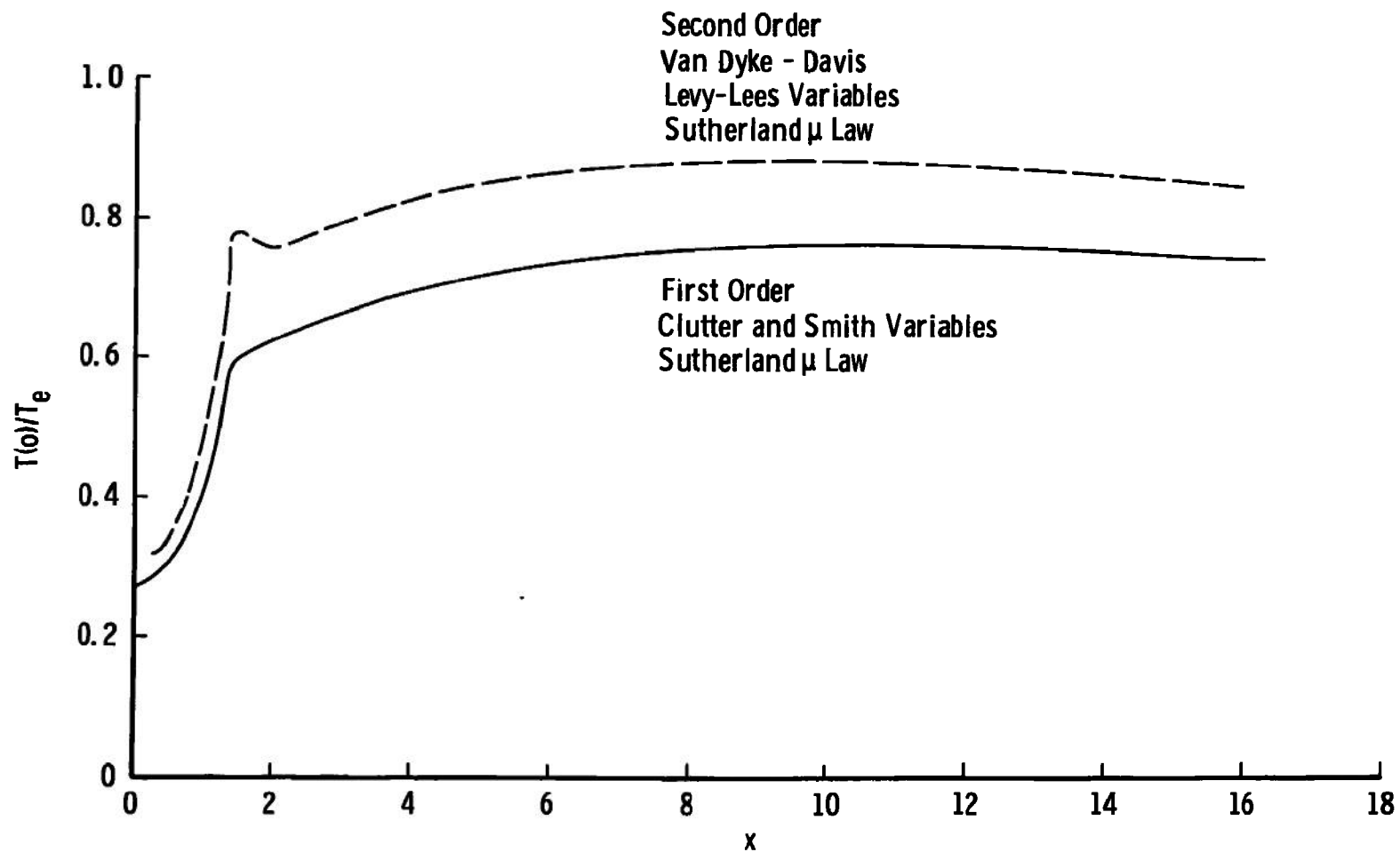
Fig. 22 First- and Second-Order Temperature Jump at M_∞ = 9, T_w/T_o = 0.2, and ϵ = 0.24
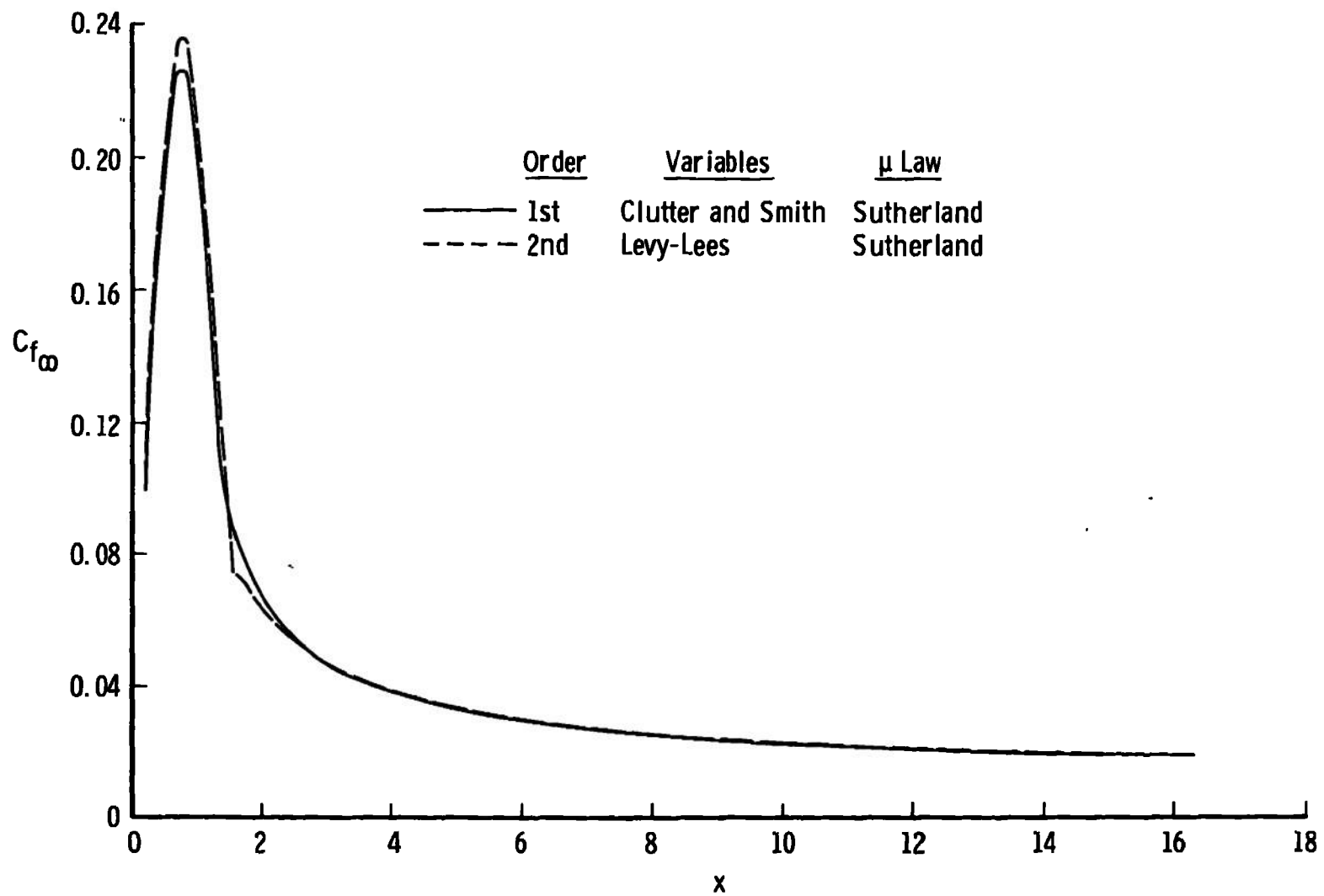
Fig. 23 Effects of Slip and Temperature Jump on Skin Friction at $M_\infty = 9$, $T_w/T_o = 0.2$, and $\epsilon = 0.24$

temperature caused a negligible effect on the wall shear stress distribution. Moreover, for the lowest Reynolds number condition considered ($Re_\infty/in. < 400$), the separate effects of slip and temperature jump were indeed small in comparison with other effects.

The slip-and-temperature-jump-induced friction-drag results are shown in Figures 24 and 25. At the highly cooled wall conditions at $M_\infty = 18$, the second-order solution in physical variables was step size dependent, and an acceptable solution was not obtained for this effect at these conditions using physical variables. In either the Clutter and Smith or Levy-Lees transformed planes, the highly cooled wall presented no difficulty, and stable solutions were obtained with reasonable ($\Delta\eta = 0.025$ or 0.05) step sizes. Both first- and second-order treatments evaluated the properties in the slip velocity and temperature at the no-slip wall conditions. The differences between first- and second-order treatments were larger for this separate effect. However, since this drag component was small compared with other second-order effects, the difference between the two treatments was not an important influence on the total drag prediction for $\varepsilon < 0.2$.

A comparison of the first- and second-order incremental friction-drag components at $M_\infty = 18$ is shown in Figure 26. The nonlinearities of the first-order vorticity-induced friction drag and the second-order displacement-induced friction-drag components are clearly visible as well as the empirically linear variation of the first-order displacement and TVC effects. The second-order results in physical variables using a square-root viscosity law are not shown since they were
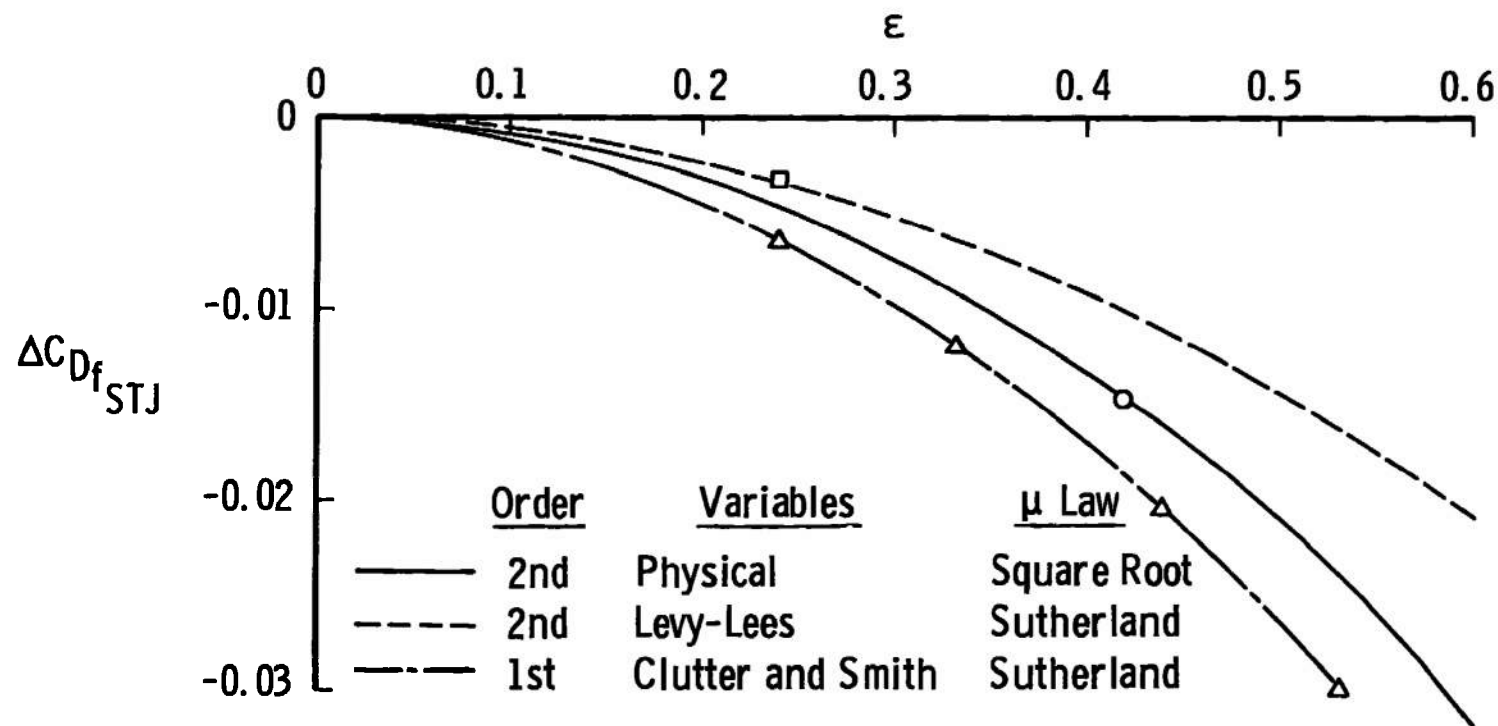
Fig. 24 First- and Second-Order, Slip-and-Temperature-Jump-Induced Friction Drag at $M_\infty = 9$, $T_w/T_o = 0.2$, and $r_n/r_b = 0.3$
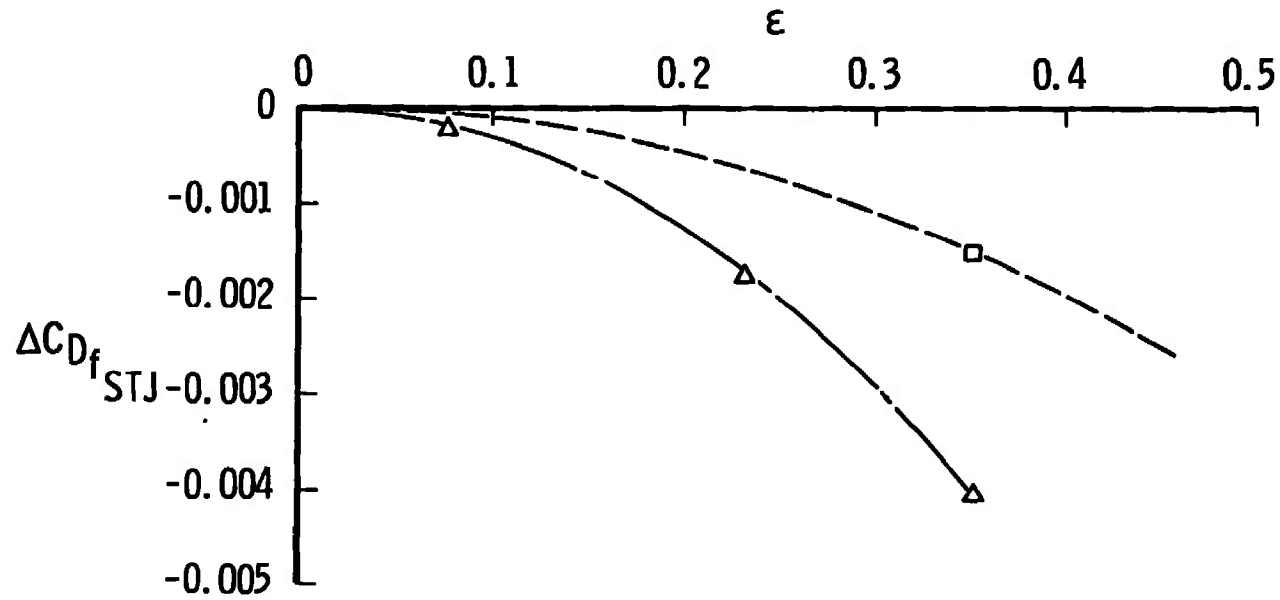
Fig. 25 First- and Second-Order, Slip-and-Temperature-Jump-Induced Friction Drag at M_∞ = 18, T_w/T_o = 0.066, and r_n/r_b = 0.3
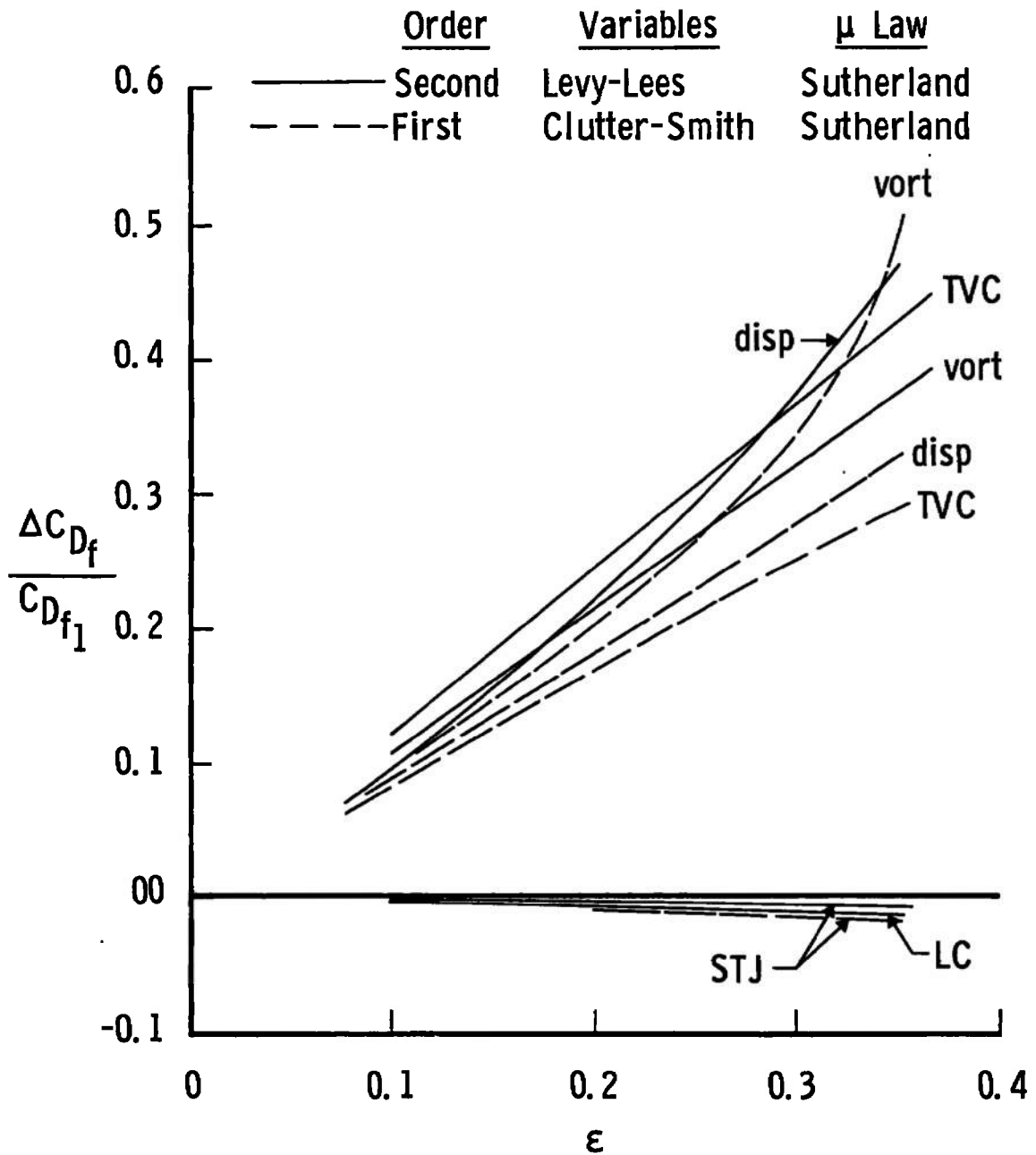
Fig. 26 Comparison of First- and Second-Order Incremental Friction Drag Components
at $M_\infty = 18$, $T_w/T_o = 0.066$, and $r_n/r_b = 0.3$

in good agreement with the second-order results presented. Displayed in this way, it is obvious that for the conditions considered all of the separate higher-order drag components can be classified as either major (TVC, displacement and vorticity) or minor (STJ and LC) effects. However, when the effects are coupled in the first-order treatment, no simple classification exists. The results of such a comparison at $M_\infty = 9$ showed qualitative agreement with the results at $M_\infty = 18$; therefore, the $M_\infty = 9$ data are not presented.

V. COUPLED EFFECTS

The first-order treatment of higher-order effects on the skin-friction coefficient at $M_\infty = 9$ is shown in Figure 27. The results are shown for a large value of the expansion parameter $\varepsilon = 0.533$ in order to magnify some of the effects and clearly establish the strong coupling influence of small individual effects.

The individual effects of transverse curvature (TVC), vorticity (vort), displacement (disp), and slip and temperature jump (STJ) on the skin-friction coefficient are seen by comparison with the classical first-order axisymmetric result. The bumps in the curves including displacement were caused by a displacement-induced compression region over the effective body and the resulting displacement of the inviscid outer flow. Although at the conditions considered in Figure 27, each separate higher-order effect had a significant influence on the skin-friction distribution, the separate effect of vorticity was clearly dominant. The strong effect of coupling displacement and vorticity can
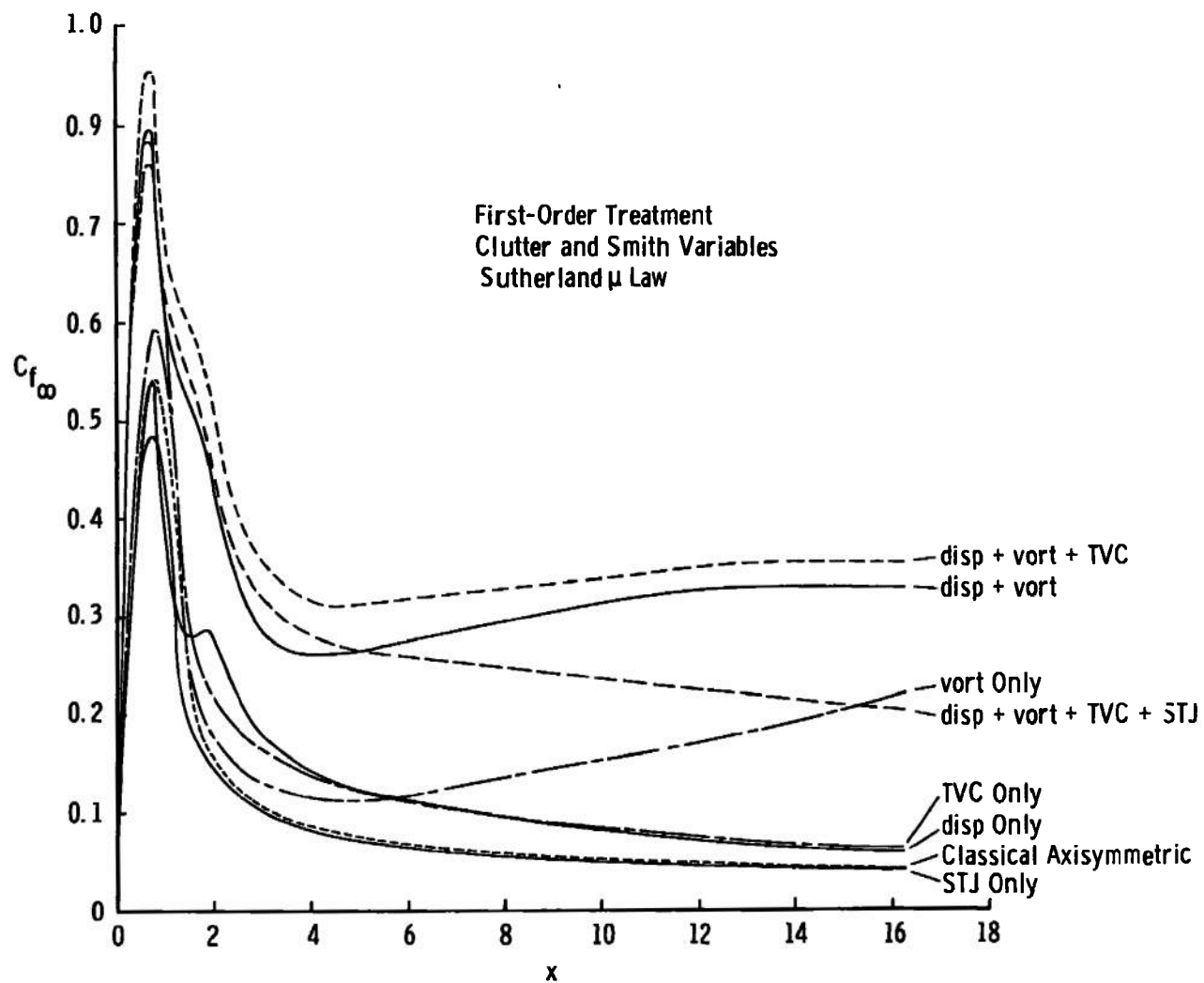
Fig. 27 Separate and Coupled Higher-Order Effects on Skin-Friction Coefficient, M_∞ = 9,
Friction Coefficient at M_∞ = 9, T_w/T_o = 0.2, and ϵ = 0.533

be seen by comparison of the results of these combined effects with the sum of the independent effects. Coupling displacement with vorticity approximately doubled the vorticity-induced skin-friction coefficient. The displacement-induced pressure strongly affected the vorticity index Ω which in turn controlled the vorticity effect. Coupling TVC with displacement and vorticity increased the coupled effects of the latter two by about the increment due to transverse-curvature-induced skin friction only. The most surprising result was found when slip and temperature jump effects were coupled with displacement, vorticity, and transverse curvature. Near the end of the body, the effects of STJ were larger than the combined effects of displacement and transverse curvature! The trends clearly indicate that if the body were longer the effects of slip and temperature jump would offset not only the effects of displacement and transverse curvature but vorticity as well. In Chapter III it was shown that $f'(\eta=0) \propto f''(\eta=0)$. Vorticity increased f'' which in turn increased the slip velocity $f'(\eta=0)$ which reduced the velocity gradient $f''(\eta=0)$. This coupling between vorticity and STJ can be seen by comparison of the almost linear increase in the vorticity-induced skin-friction coefficient with the almost linear decrease in the combined total effects including slip.

The effects of coupling first-order displacement and vorticity effects can be seen in Figures 28 and 29. The vorticity index $\Omega(x)$ is shown for the conditions at $M_\infty = 9$ and 18 both with and without the displacement effect. As the Reynolds number decreases, ϵ increases for both Mach numbers. The dependence of $\Omega(x)$ on the pressure can be seen
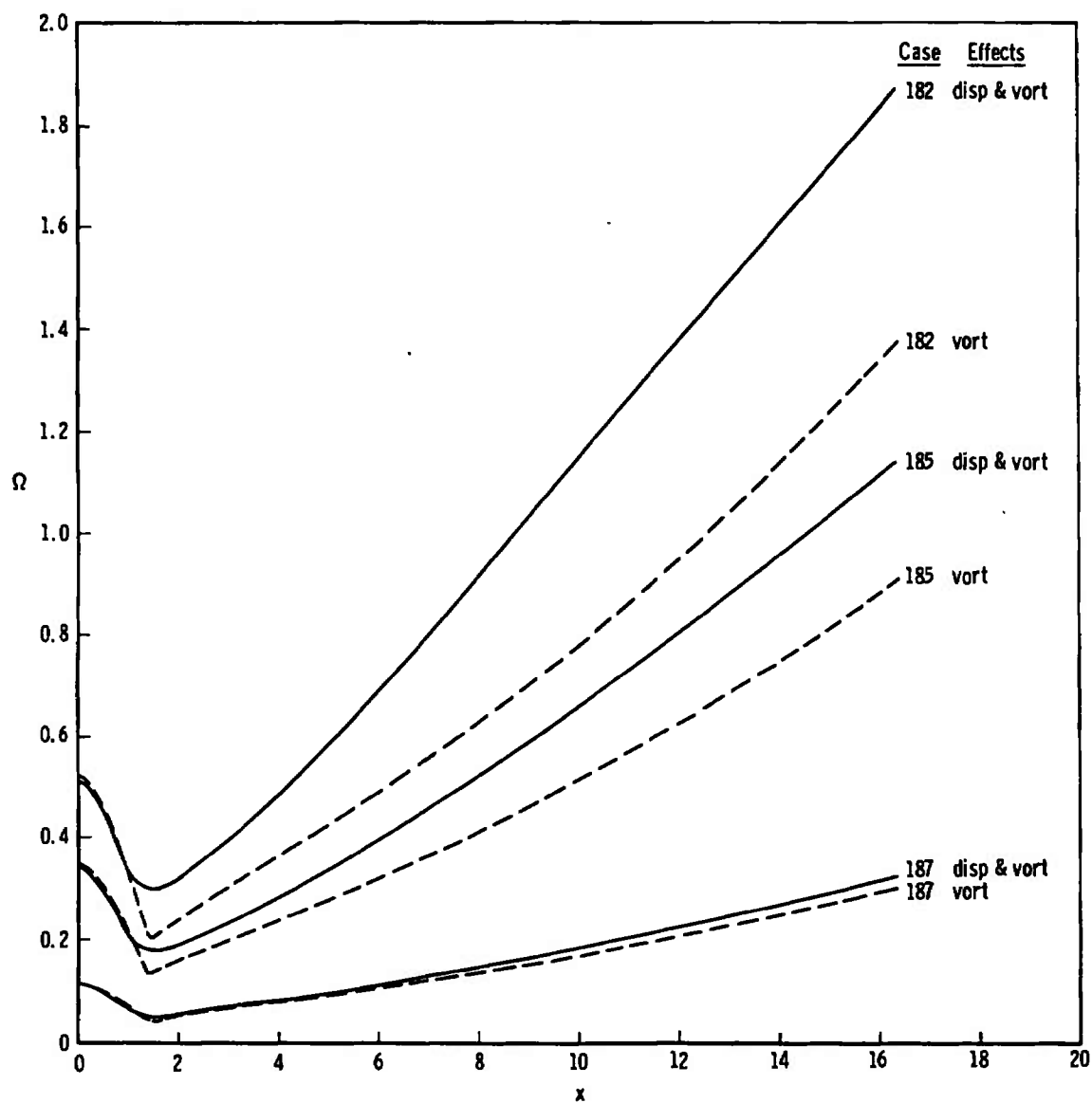
Fig. 28 The Vorticity Index $\Omega(x)$ With and Without Displacement Effects at $M_\infty = 18$ and $T_w/T_o = 0.066$
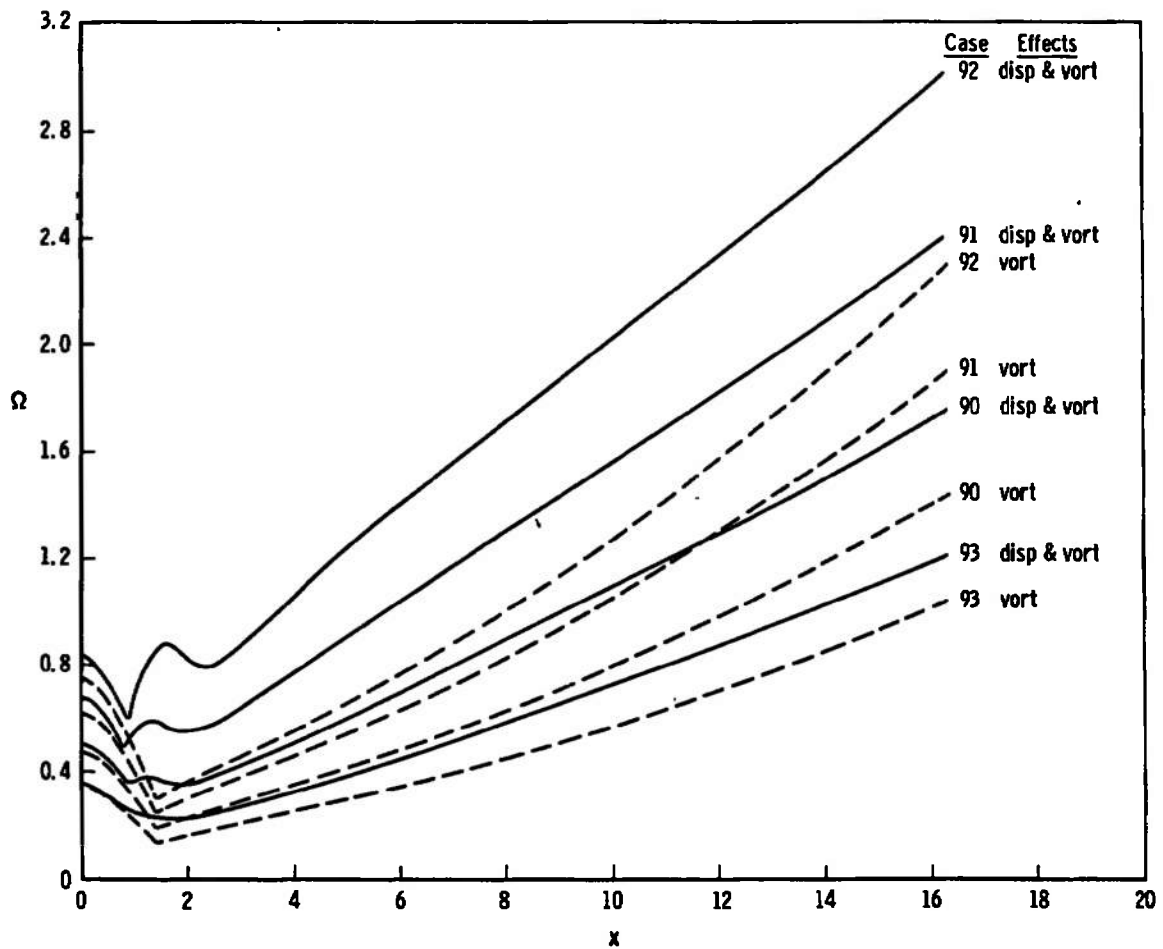
Fig. 29 The Vorticity Index $\Omega(x)$ With and Without Displacement Effects at $M_\infty = 9$ and $T_w/T_o = 0.2$

as follows: In Chapter III it was shown that

$$\Omega(x) \sim [(H_e/u_*{}^2) - \frac{1}{2} (u_e/u_*)^2] (u_*/u_e)^{3/2}$$

when x is held fixed and the pressure allowed to vary. From the perfect gas law and energy equation

$$p = \rho RT = \frac{\gamma-1}{\gamma} \rho h = \frac{\gamma-1}{\gamma} \rho (H_e - u_e{}^2/2)$$

Along a streamline $p \propto \rho^\gamma$, and also

$$\left(\frac{u_*}{u_e}\right)^2 = \frac{H_e - h_*}{H_e - h_e} = \frac{1/6}{1 - T_e/T_o} = \frac{1/6}{1 - \left(\frac{p}{p_o^!}\right)^{\frac{\gamma-1}{\gamma}}}$$

Therefore, one finds that

$$\Omega \sim \frac{p}{\rho} \left(\frac{u_*}{u_e}\right)^{3/2} \sim \left(\frac{p}{p_o^!}\right)^{\frac{\gamma-1}{\gamma}} \left[1 - \left(\frac{p}{p_o^!}\right)^{\frac{\gamma-1}{\gamma}}\right]^{-3/4}$$

$$\sim \left(\frac{p}{p_o^!}\right)^{\frac{\gamma-1}{\gamma}} \left[1 + \frac{3}{4} \left(\frac{p}{p_o^!}\right)^{\frac{\gamma-1}{\gamma}} + \frac{21}{32} \left(\frac{p}{p_o^!}\right)^{\frac{2(\gamma-1)}{\gamma}} + \ldots\right]$$

where the remaining terms are all positive and can be neglected in comparison with the three leading terms for $p/p_o^! < 0.1$.

As the Reynolds number is reduced or ϵ increases, the displacement thickness increases which produces a larger displacement-induced pressure (see Figures 17 and 18, pages 67 and 68). Thus, when the displacement and vorticity effects are coupled, the displacement-

induced pressure increases the vorticity effect by increasing $\Omega(x)$.

Because of the hotter wall at $M_\infty = 9$ ($T_w/T_0 = 0.2$ at $M_\infty = 9$, whereas $T_w/T_0 = 0.066$ at $M_\infty = 18$), the displacement thickness was positive over the spherical nose rather than negative as in the $M_\infty = 18$ cases. The rapid increase in displacement thickness at $M_\infty = 9$ for $0.8 < x < 2.5$ caused bumps in the $\Omega(x)$ curves which were not observed at the $M_\infty = 18$ highly cooled wall condition. It should be noted that $\epsilon = 0.33$ for Case 90 with a bump and $\epsilon = 0.35$ for Case 182 without a bump, and thus there was a region of overlap for comparison.

Although the coupling between displacement and vorticity was not as dramatic as the coupling between vorticity and STJ, the effect was important. Since the first-order treatment always produces an increase in displacement-induced pressure, the effects of displacement and vorticity coupling would be expected to increase with increasing wall-to-stagnation temperature ratio and increasing body length.

The results for the coupled higher-order effects were clearly not linearly independent as were the second-order effects of TVC, longitudinal curvature, vorticity, and slip and temperature jump according to Van Dyke's theory. The obvious result here was that small separate higher-order effects had a strong influence when coupled with other higher-order effects, and a simple linear combination of each first-order effect was not justified and could lead to erroneous results.

VI. RANGE OF APPLICABILITY

The range of applicability of the first- and second-order

theories must finally be determined by comparison with experimental data; however, it is instructive to consider the range of applicability predicted from the numerical results.

The first-order boundary layer-to-shock layer thickness ratio over the cone at M_∞ = 18 is shown in Figure 30. The boundary-layer thickness was defined to be the distance normal to the wall where $f' = u/u_e$ = 0.995 and y_{sh} is the first-order (nonperturbed) inviscid shock-layer thickness from the blunt body and characteristics solutions. The variation of δ/y_{sh} was small over the entire body, as shown in Figure 30, and a region is indicated between ε = 0.11 and 0.16 where δ/y_{sh} = 1. Beyond this region the shock layer is fully viscous and boundary-layer theory is not applicable.

The values of x shown in Figure 30 correspond to some of the stations along the body used in the first-order boundary-layer cal-culations in Clutter and Smith variables. The boundary layer-to-shock layer thickness ratio is minimum at the stagnation point (x = 0), a maximum at the sphere-cone tangent point (x = 1.409), and the variation over the entire body is rather small (about 30 per cent).

Since the boundary-layer thickness was arbitrarily defined, the effect of the definition of the boundary-layer thickness on δ/y_{sh} is shown in Figure 31. The results of the variation f'_δ = 0.90 to 0.999 are shown at the location x = 3.54. The results for f'_δ = 0.90 and 0.95 are shown only for interest since these values are too low for serious con-sideration. The range in c is not significantly affected by the variation f'_δ = 0.990 to 0.999, and thus the value of 0.995 appears to be
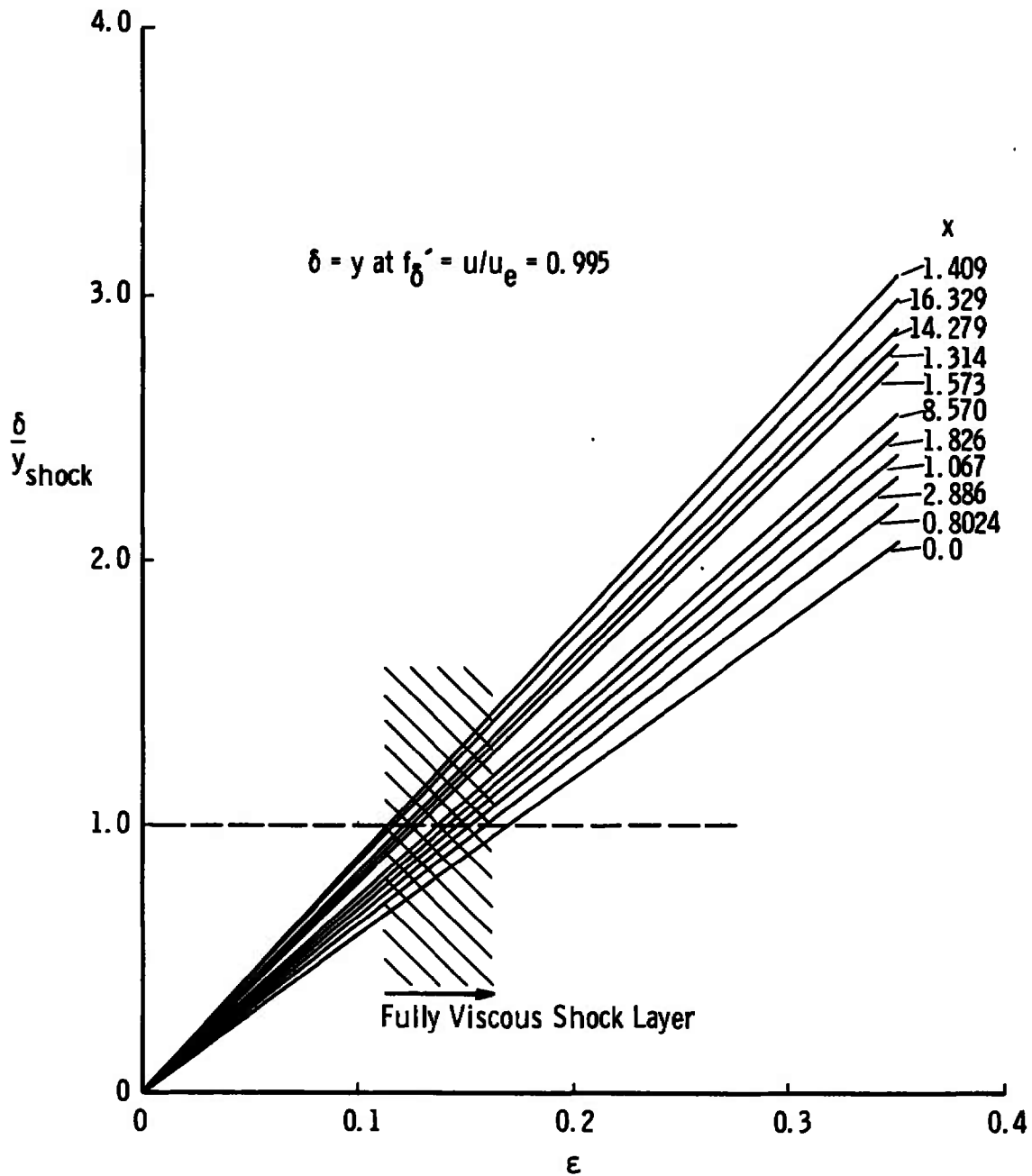
Fig. 30 Boundary Layer-to-Shock Layer Thickness Ratio Over the Cone at $M_\infty = 18$ and $T_w/T_o = 0.66$
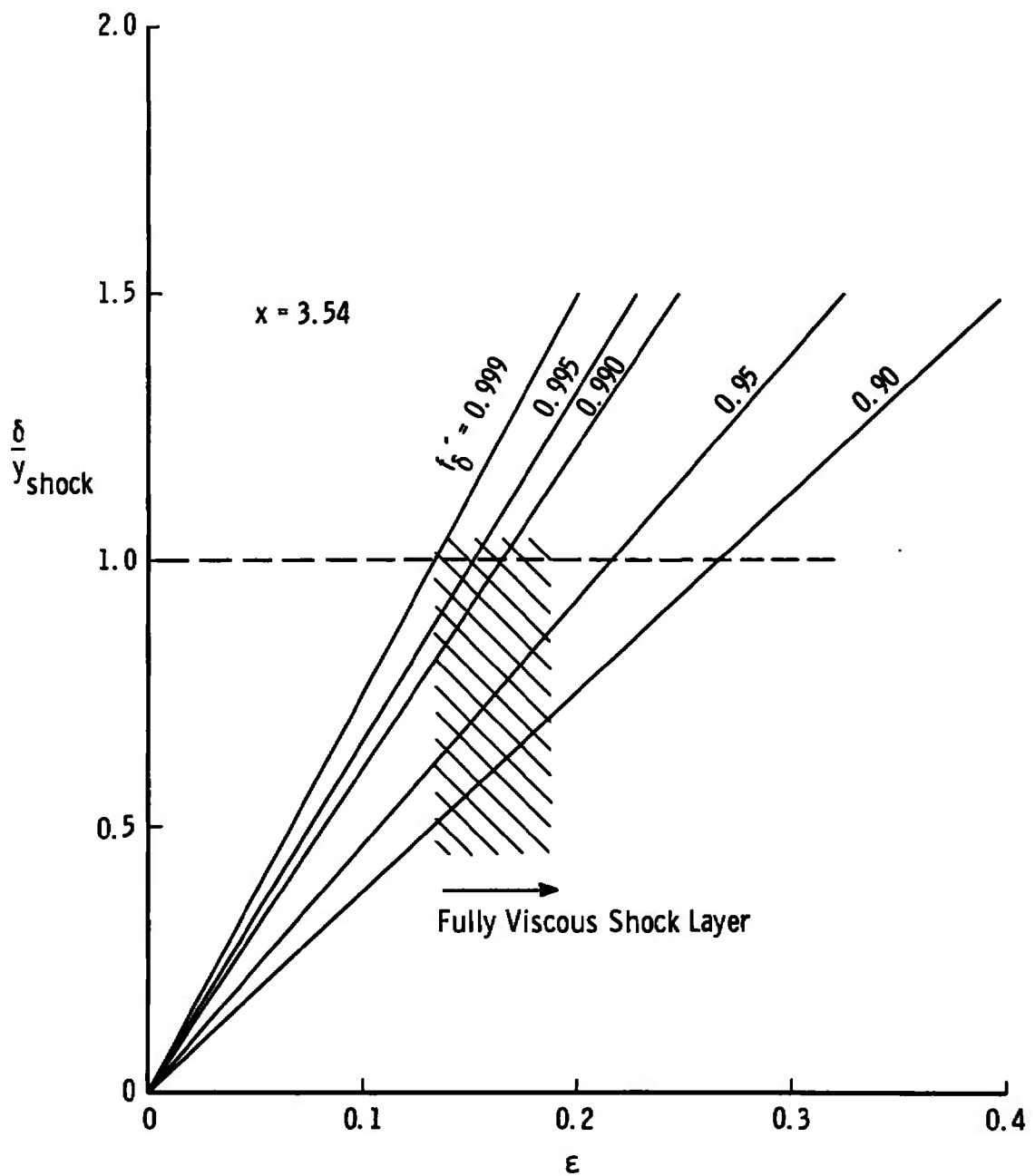
Fig. 31 Effects of the Definition of Boundary-Layer Thickness on the Range of
Applicability of Boundary-Layer Theory

a reasonable choice for the definition of boundary-layer thickness.

VII. COMPUTING TIME REQUIREMENTS

In concluding this chapter on the discussion of numerical results, a comparison is given of computing time required for the first- and second-order boundary-layer calculations. The times required for the calculations on a Control Data Corporation 1604-B digital computer are shown in Table III. The time required for the first-order treatment including the vorticity effect increased as the Reynolds number decreased (or as ε increased) for each of the free-stream Mach numbers considered. Therefore, the times shown in Table III are valid only for one set of conditions (Case 185), and the data are shown primarily for comparison of the machine time required for the first- and second-order boundary-layer calculations.[3]

From the results shown in Table III, the implicit finite-difference method in physical variables or Levy-Lees variables was approximately three times faster than the first-order solution in Clutter and Smith variables for treating the classical boundary-layer problem. It should be noted also that the number of stations used in the finite-difference solutions was approximately ten times the number used in the first-order treatment. Including the second-order effects in the finite-difference solutions approximately doubled the computing time required

---

[3]The computing time required for the blunt body and characteristics solutions (approximately 20 minutes for each case considered) was in addition to the time shown in Table III for the boundary-layer calculations.

TABLE III
COMPUTING TIMES FOR FIRST- AND SECOND-ORDER
TREATMENTS OF HIGHER-ORDER BOUNDARY-LAYER EFFECTS[a]

Effect	First-Order Clutter-Smith Variables	Second-Order Physical Variables	Second-Order Levy-Lees Variables
	Computing time, minutes[b]		
Classical[c]	75	25	26
TVC	75	50	55
STJ	75	50	55
disp	75	50	55
vort	100	50	55
disp + vort	120	--	--
disp + vort + TVC	165	--	--
disp+vort+TVC+STJ	180	50	55
	Supplementary Data		
Stations along the body	34	336	390
n_∞ (maximum)	3	---	6
Δn	0.025	---	0.05
ΔN	--	0.02	--

[a]Case 185, M_∞ = 18, ϵ = 0.233

[b]Time required on a Control Data Corporation 1604-B digital computer (computing speed approximately 60 per cent of IBM 7094) with an on-line printer.

[c]Calculations for axisymmetric body without any higher-order effects.

for the classical boundary-layer problem.

For engineering purposes, one would usually be interested in calculations which include all of the significant effects. In both first- and second-order treatments, at least two complete boundary-layer calculations were required since, using the methods described herein, the effects of displacement could not be obtained with a single calculation. Therefore, for the conditions shown in Table III, a minimum of 225 minutes was required for the first-order treatment including all effects and 75 or 81 minutes was required for the second-order treatment in physical or Levy-Lees variables, respectively. The substantial savings in computing time using the implicit finite-difference method makes this scheme attractive for other applications (for example, the chemically reacting boundary-layer problem).

CHAPTER V
COMPARISON OF NUMERICAL RESULTS AND EXPERIMENTAL DATA

Results of the first- and second-order treatments will be compared with some available experimental data on pressure and heat-transfer distributions and zero-lift drag of a spherically blunted cone at $M_\infty = 9$ and 18. The experimental data were obtained from Whitfield and Griffith [1] and [28], Lewis [29], and Griffith and Lewis [30]. Some previous numerical results of Lewis and Whitfield [7] will also be compared with the numerical results from the first- and second-order treatments and the experimental data.

I. PRESSURE DISTRIBUTIONS

The displacement-induced pressure over a spherically blunted cone at $M_\infty \simeq 20$ is shown in Figure 32. The first-order iterated results of Lewis and Whitfield [7] and the second-order results of Marchand, Lewis, and Davis [18] at $M_\infty = 18$ are compared with the experimental data of Lewis [29] and Griffith and Lewis [30]. It is obvious that the trends of the experimental results were not predicted by either first- or second-order treatments. The nonlinear character of the first-order results of Lewis and Whitfield was due to the effects of iterating the inviscid outer flow and the viscous boundary-layer flow fields. The effect of this iteration was always to reduce the displacement-induced pressure.

Experimental Data

Sym	M_∞	T_∞, °K	Re_{∞, r_n}
●	20.8	52	2,260
■	20.8	58	1,890
◆	20.5	43	6,590
▲	20.0	24	36,000

Numerical Results

$\begin{cases} \epsilon\ p_2/p_0' \text{; Marchand, Lewis and Davis} \\ \Delta p_{disp} \text{; First-Order Treatment} \end{cases}$

$--- \quad \Delta p^{(2)}$; Lewis and Whitfield

$\dfrac{P - P_1}{P_0'}$
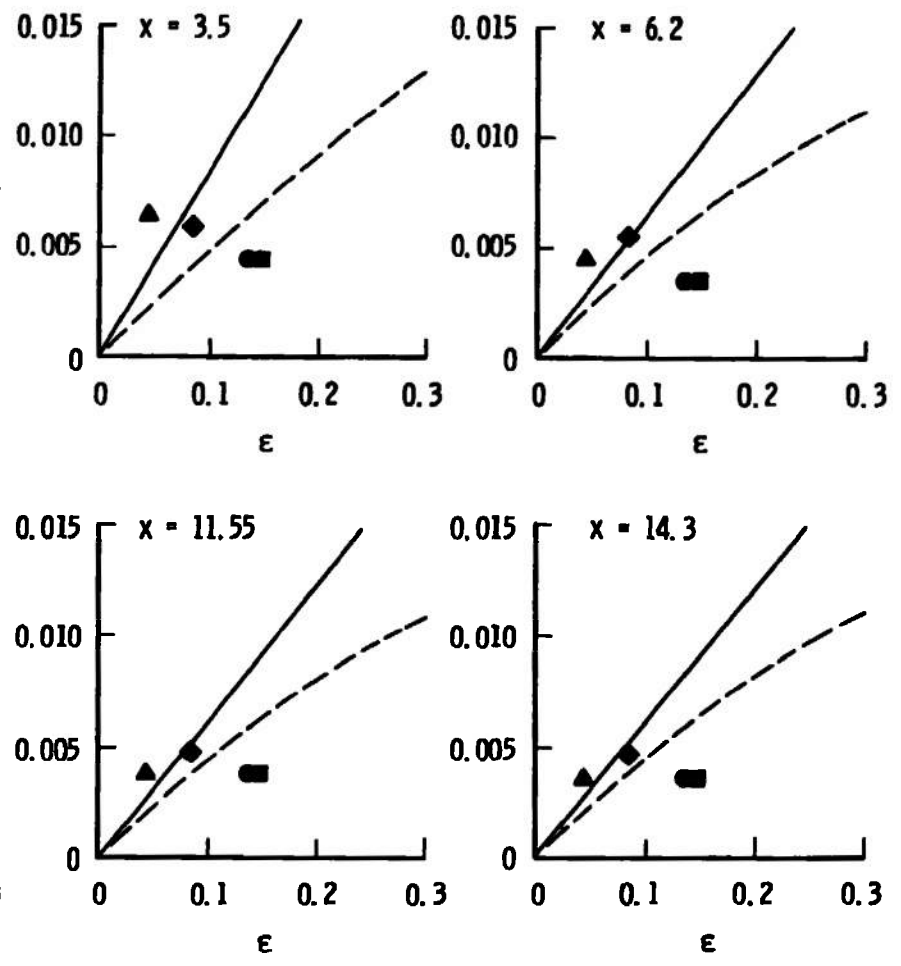
Fig. 32 Displacement-Induced Pressure Over a Spherically Blunted Cone at M_∞ = 18, T_w/T_0 = 0.066, θ_c = 9 degrees, and r_n/r_b = 0.3

The poor agreement between numerical results and experimental pressure data is not understood. The experimental data lay in a range where the second-order theory should have been applicable. Moreover, the experimental data and numerical results have been checked extensively, and the errors due to approximations in the numerical treatments and experimental scatter are believed to be small deviations.

II. HEAT-TRANSFER DISTRIBUTIONS

Figure 33 shows a comparison of first- and second-order heat transfer to a sphere-cone at $M_\infty \simeq 18$. In contrast with the pressure data discussed above, the first- and second-order results were in excellent agreement with the experimental data of Griffith and Lewis [30]. Because of the limited experimental data available, caution must be used in interpreting the comparison with the numerical results.

III. ZERO-LIFT DRAG

The final and most instructive comparisons between first- and second-order numerical results and experimental data are given in Figures 34 through 41. The total drag predicted by the two treatments is compared with the experimental data of Whitfield and Griffith [1] and [28].

The results from the first-order treatment of the higher-order effects on zero-lift drag are given in Table IV. Comparison of the sum of separate effects with the results including the coupled effects shows that the results were not linearaly independent, but strong coupling was involved especially at the highest ε. The relatively good agreement
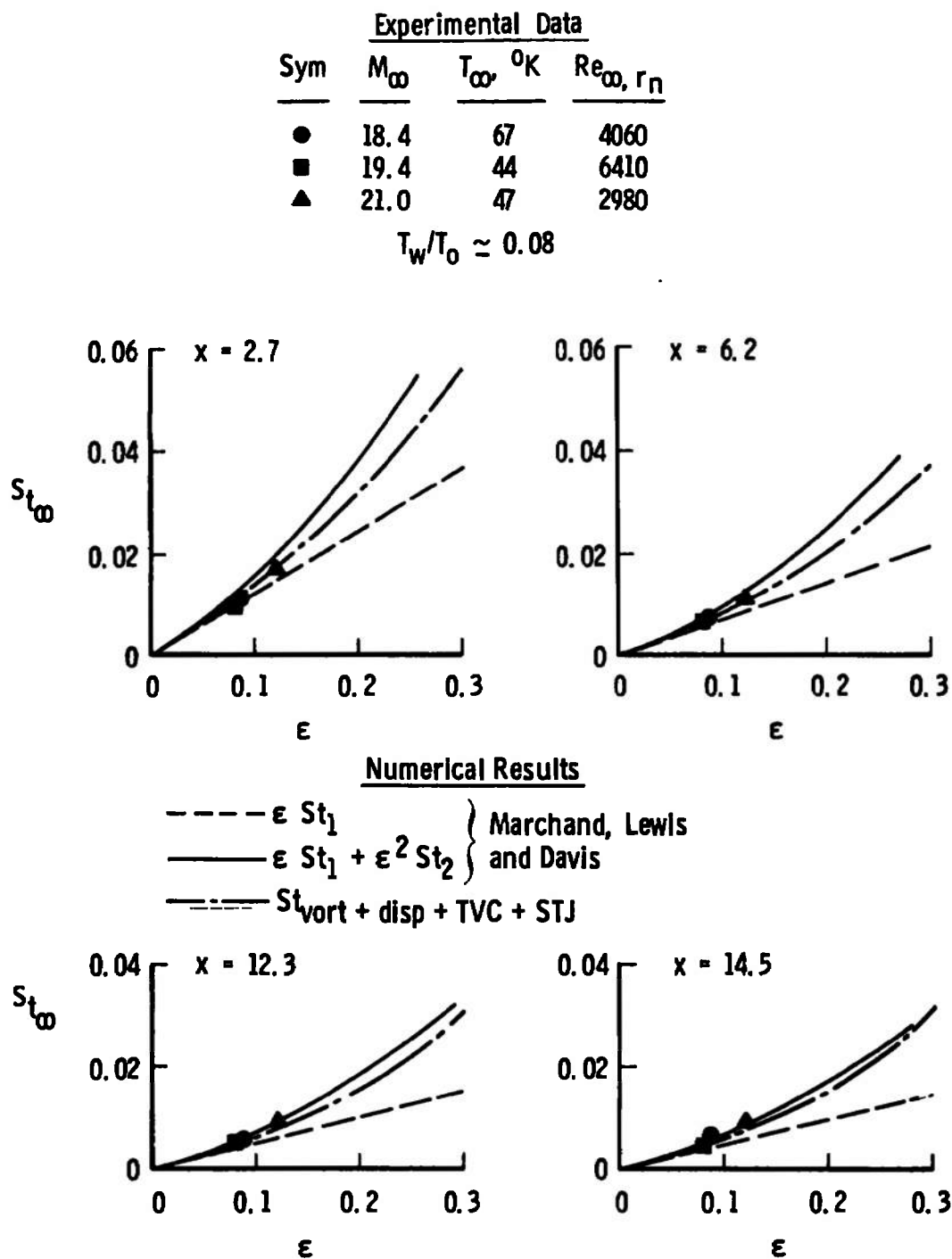
Fig. 33 Heat Transfer to a Spherically Blunted Cone at M_∞ = 18, T_w/T_o = 0.066, θ_c = 9 degrees, and r_n/r_b = 0.3

Fig. 34 Predictions of the Drag of a Spherically Blunted Cone at $M_\infty = 18$,
$T_w/T_o = 0.066$, and $r_n/r_b = 0.3$ Using Second-Order Boundary-Layer
Theory in Physical Variables

Fig. 35 Predictions of the Drag of a Spherically Blunted Cone at M_∞ = 18, T_w/T_o = 0.066, and r_n/r_b = 0.3 Using Second-Order Boundary-Layer Theory in Levy-Lees Variables

Fig. 36 Predictions of the Drag of a Spherically Blunted Cone at $M_\infty = 18$, $T_w/T_o = 0.066$, and $r_n/r_b = 0.3$ Using First-Order Boundary-Layer Theory in Clutter and Smith Variables

Fig. 37 Comparison of First- and Second-Order Predictions of the Drag of a
Spherically Blunted Cone at M_∞ = 18, T_w/T_o = 0.066, and
r_n/r_b = 0.3
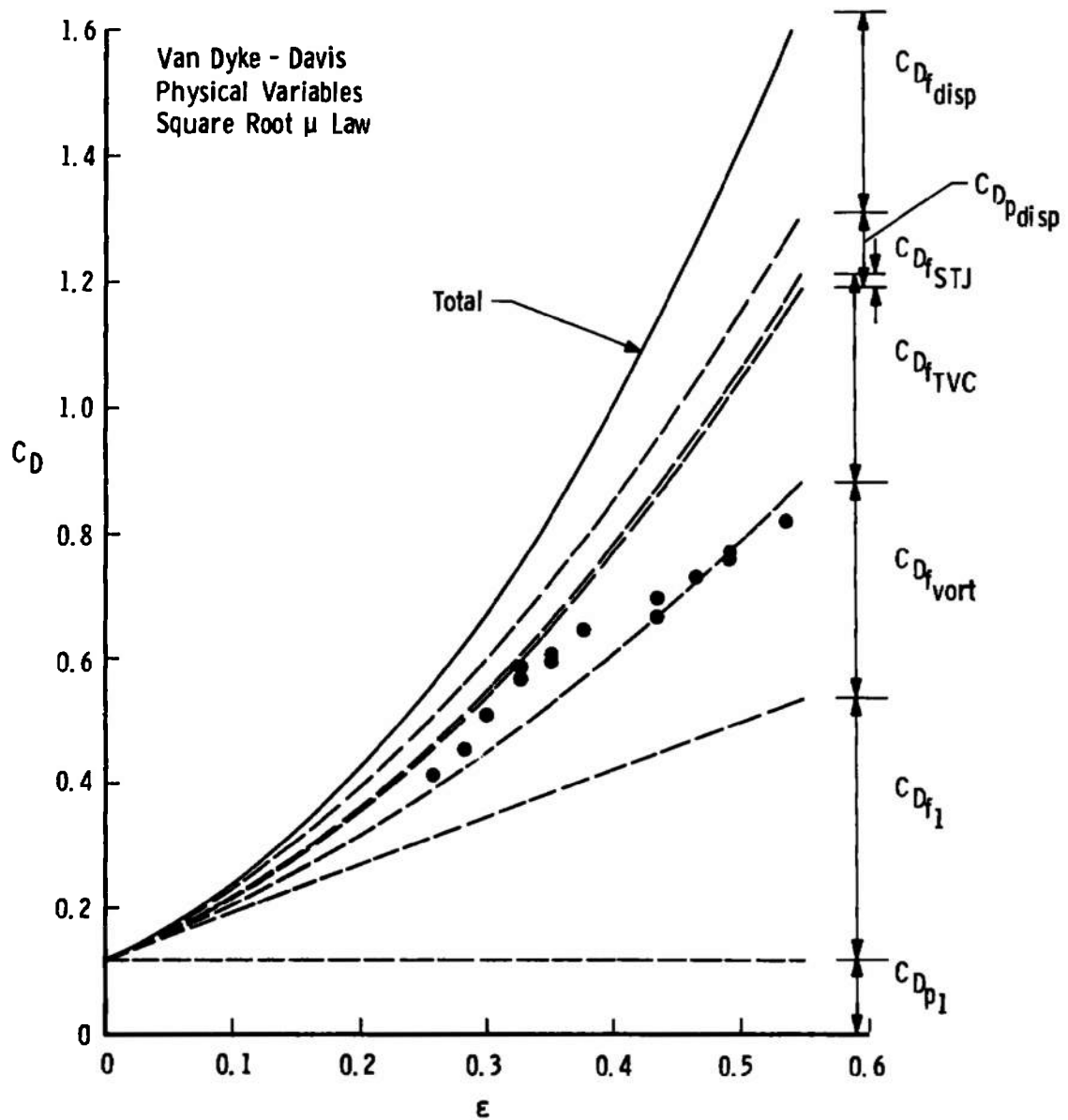
Fig. 38 Predictions of the Drag of a Spherically Blunted Cone at M_∞ = 9, T_w/T_o = 0.2, and r_n/r_b = 0.3 Based on Second-Order Boundary-Layer Theory in Physical Variables

Fig. 39 Predictions of the Drag of a Spherically Blunted Cone at $M_\infty = 9$, $T_w/T_o = 0.2$, and $r_n/r_b = 0.3$ Based on Second-Order Boundary-Layer Theory in the Levy-Lees Variables
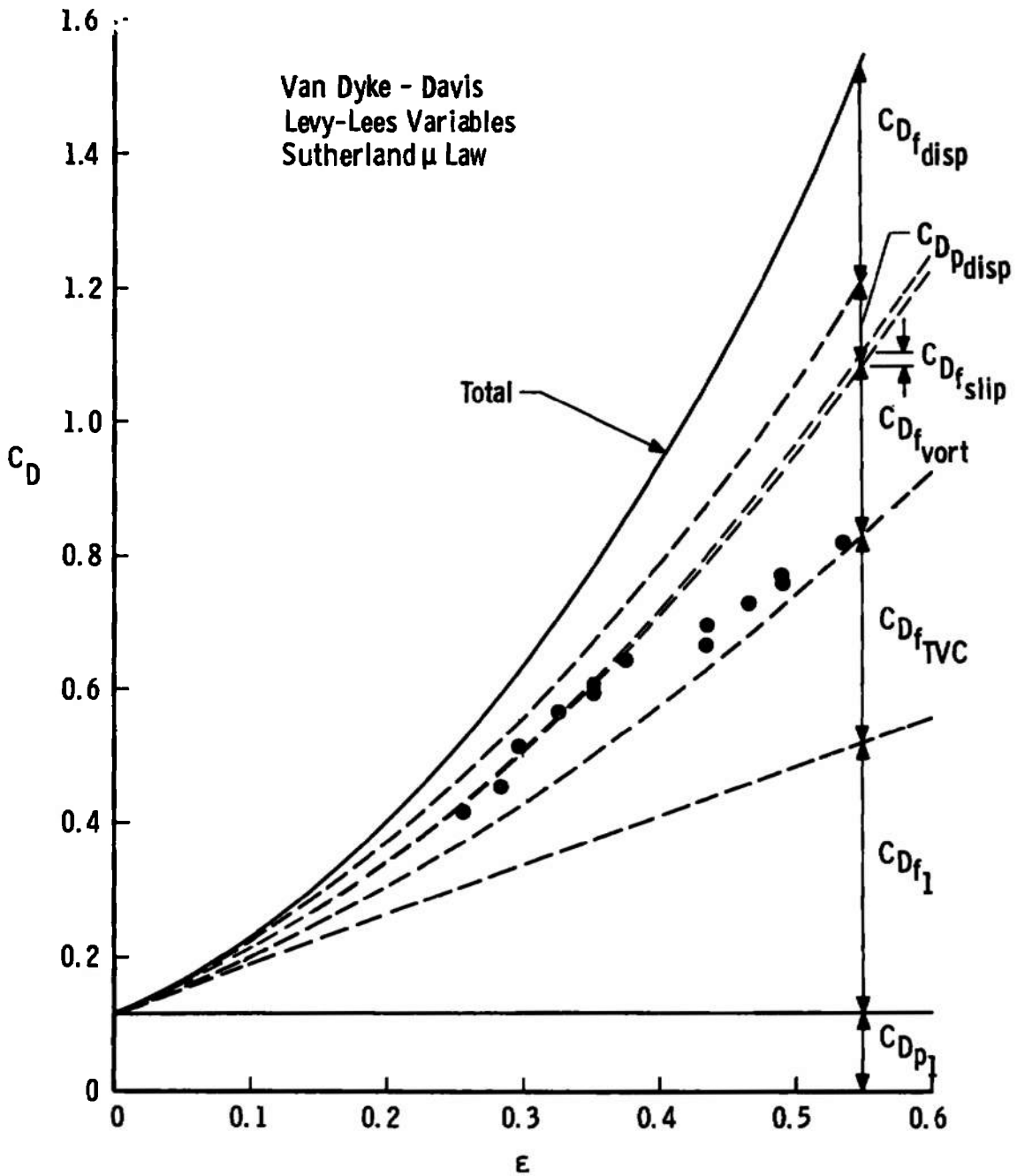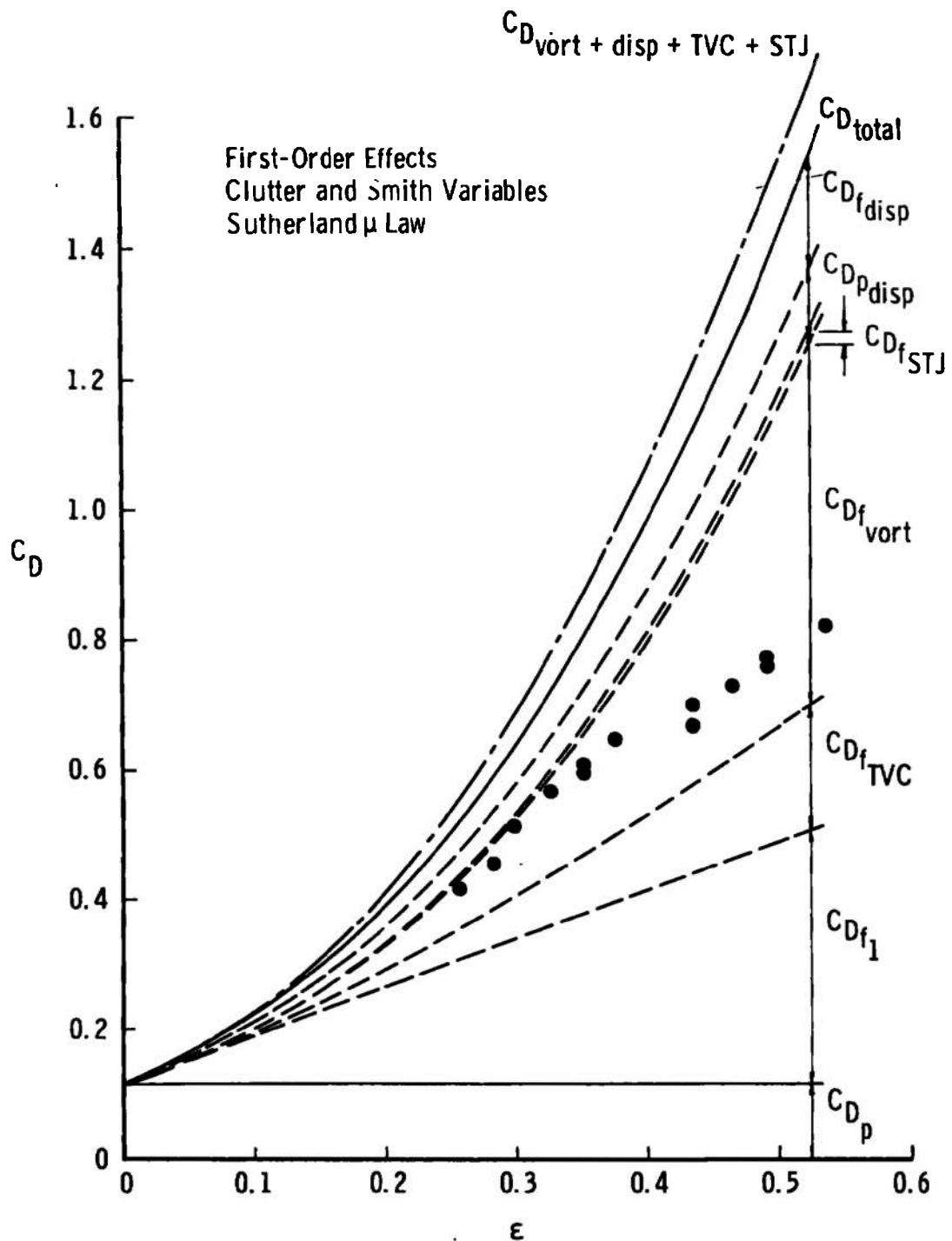
Fig. 40 Prediction of the Drag of a Spherically Blunted Cone at $M_\infty = 9$,
$T_w/T_o = 0.2$, and $r_n/r_b = 0.3$ Using a First-Order Boundary-
Layer Treatment in Clutter and Smith Variables

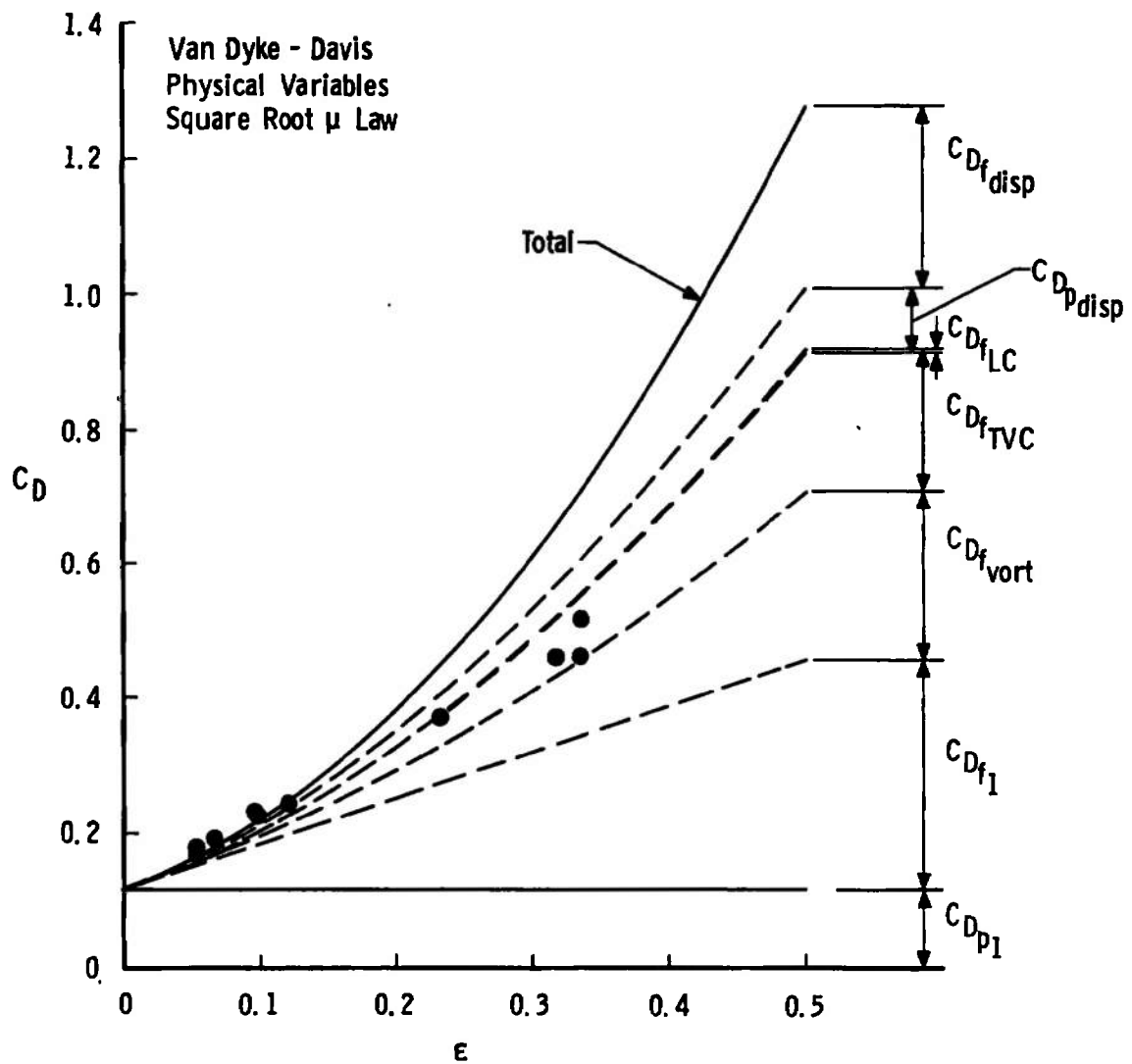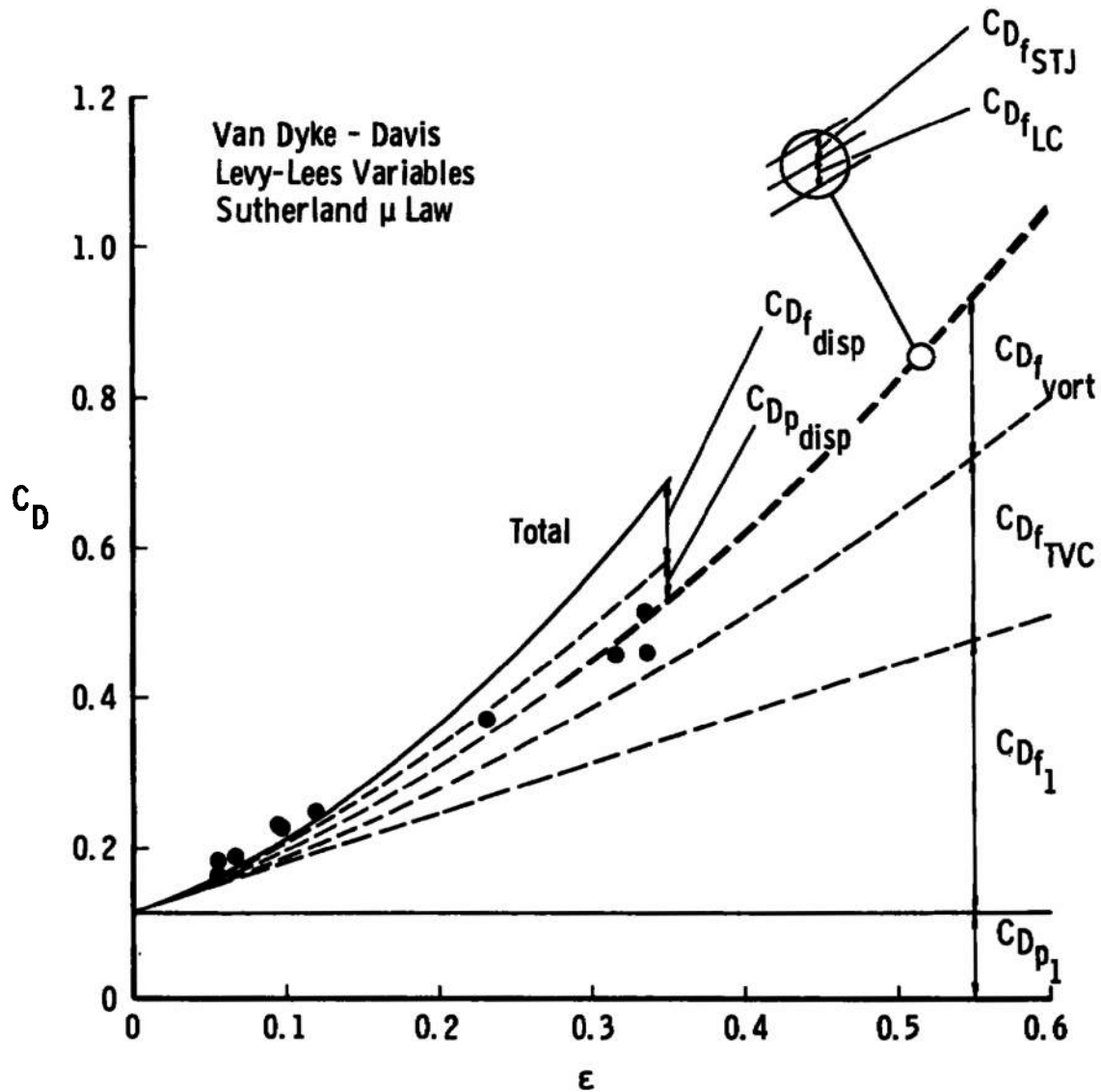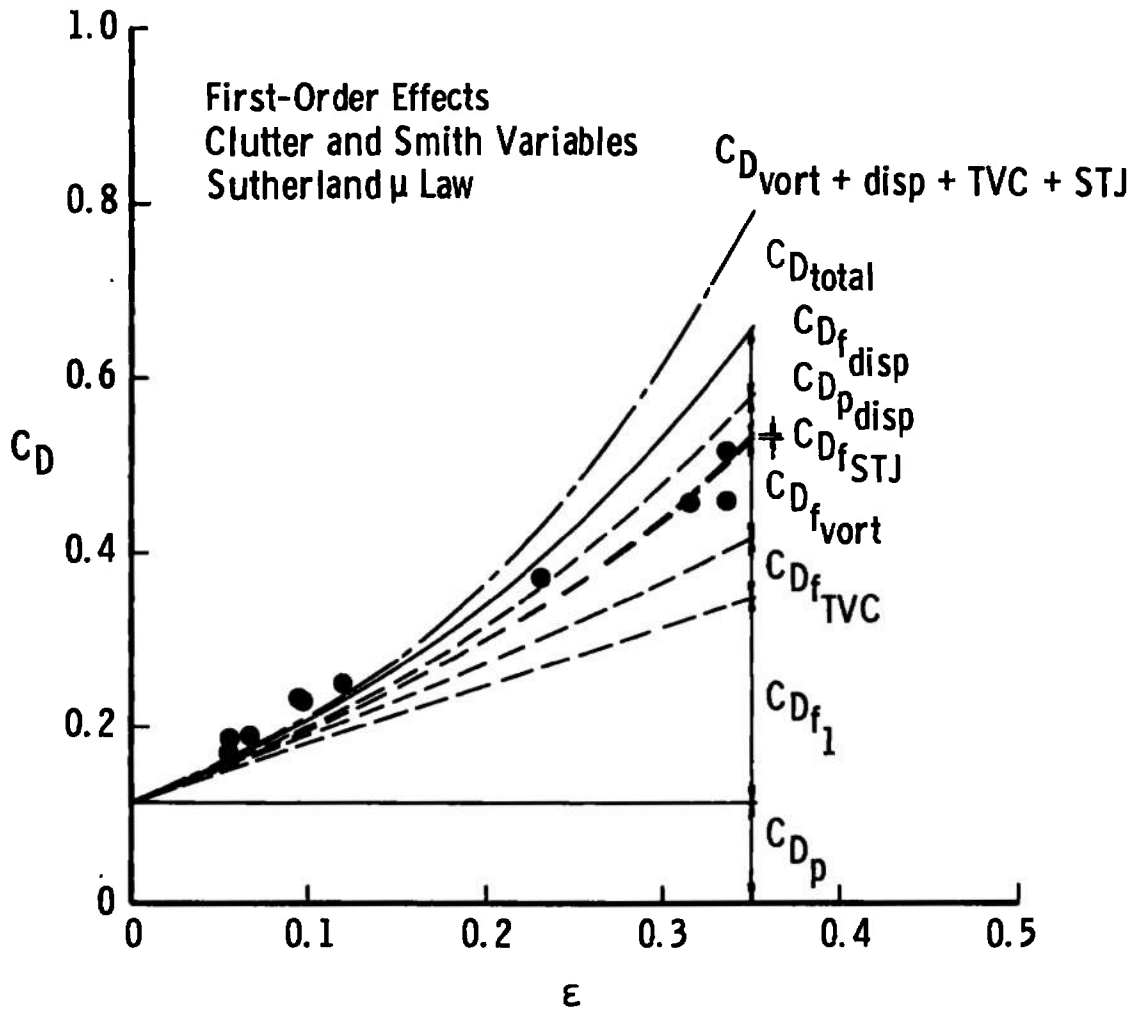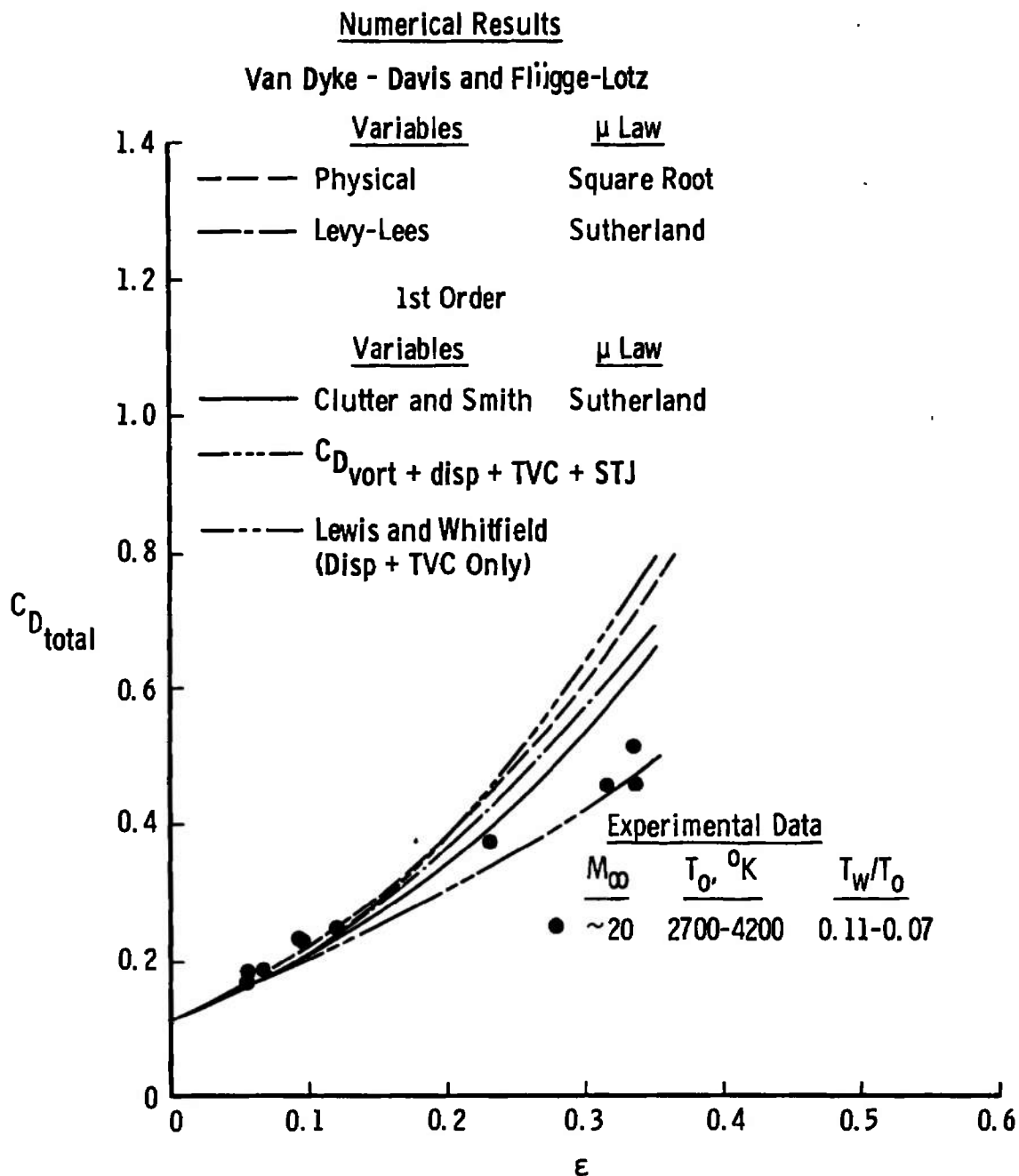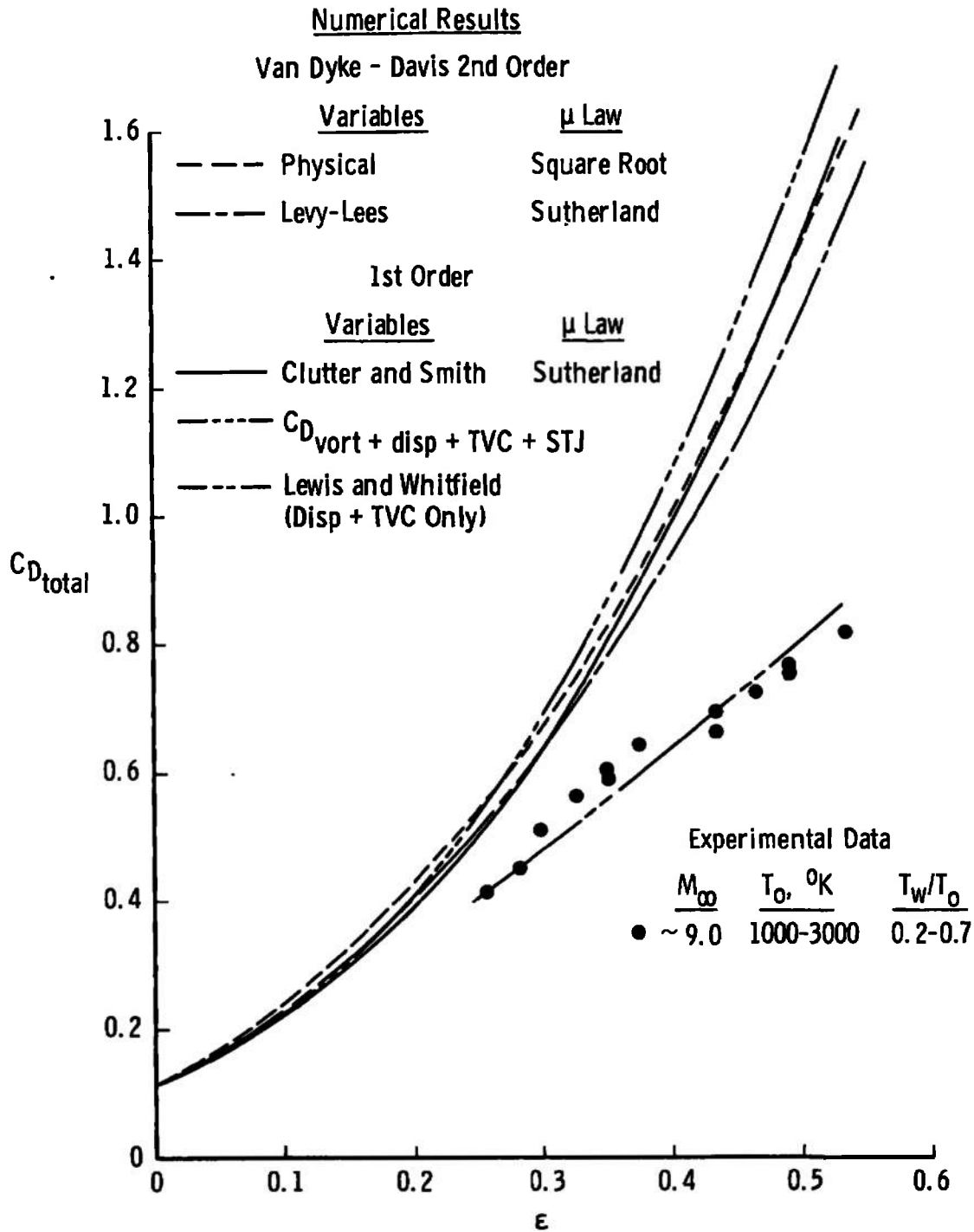Fig. 41 Comparison of First- and Second-Order Boundary-Layer Theory Predictions of the Drag of a Spherically Blunted Cone at $M_\infty = 9$, $T_w/T_o = 0.2$, and $r_n/r_b = 0.3$

TABLE IV
FIRST-ORDER RESULTS OF HIGHER-ORDER EFFECTS ON ZERO-LIFT DRAG

Case	ϵ	Effects[a]	c_{D_f}	c_{D_p}	$c_{D_{Total}}$
187	0.0776	TVC	0.0550	0.0550	0.1692
187	0.0776	STJ	0.0514	0.1142	0.1656
187	0.0776	vort	0.0555	0.1142	0.1697
187	0.0776	vort+TVC	0.0584	0.1142	0.1726
187	0.0776	disp	0.0552	0.1223	0.1775
187	0.0776	disp+vort	0.0600	0.1223	0.1823
187	0.0776	disp+vort+TVC	0.0633	0.1223	0.1856
187	0.0776	disp+vort+TVC+STJ	0.0630	0.1223	0.1853
185	0.2530	TVC	0.1851	0.1142	0.2993
185	0.2530	STJ	0.1529	0.1142	0.2672
185	0.2530	vort .	0.1915	0.1142	0.3057
185	0.2530	vort+TVC	0.2206	0.1142	0.3348
185	0.2530	vort+TVC+STJ	0.2106	0.1142	0.3248
185	0.2530	disp	0.1878	0.1437	0.3315
185	0.2530	disp+vort	0.2558	0.1437	0.3995
185	0.2530	disp+vort+TVC	0.2873	0.1437	0.4310
185	0.2530	disp+vort+TVC+STJ	0.2856	0.1437	0.4293
182	0.3516	Classical[b]	0.2335	0.1142	0.3477
182	0.3516	TVC	0.3018	0.1142	0.4160
182	0.3516	STJ	0.2295	0.1142	0.3437
182	0.3516	vort	0.3497	0.1142	0.4639
182	0.3516	vort+TVC	0.4268	0.1142	0.5410
182	0.3516	disp	0.3118	0.1667	0.4785
182	0.3516	disp+vort	0.5628	0.1667	0.7295
182	0.3516	disp+vort+TVC	0.6304	0.1667	0.7971
182	0.3516	disp+vort+TVC+STJ	0.6229	0.1667	0.7896
95	0.1000	TVC	0.0811	0.1667	0.1977
95	0.1000	vort	0.0819	0.1667	0.1985
95	0.1000	disp	0.0798	0.1320	0.2118
95	0.1000	disp+vort	0.0905	0.1320	0.2225
95	0.1000	disp+vort+TVC	0.0973	0.1320	0.2293
95	0.1000	disp+vort+TVC+STJ	0.0961	0.1320	0.2281
93	0.2401	TVC	0.2185	0.1166	0.3351
93	0.2401	STJ	0.1724	0.1166	0.2890
93	0.2401	vort	0.2464	0.1166	0.3630

between the first- and second-order results of the total drag predictions shown in Figures 37, page 100, and 41, page 104, should be considered fortuitous in view of the strong effects of first-order coupling.

On Figures 36, page 99, and 40, page 103, the curves labeled $C_{D_{total}}$ were obtained by summation of the separate effects treated independently (that is, no coupling of effects was considered). Separate curves labeled $C_{D_{vort+disp+TVC+STJ}}$ are shown which included all effects coupled simultaneously. For both Mach number conditions, the results show excellent agreement between the uncoupled and coupled drag predictions for $\varepsilon \lesssim 0.1$ and somewhat surprisingly good agreement for $\varepsilon > 0.1$ considering the strong coupling effects on the skin-friction coefficient shown in Figure 27, page 81.

For $M_\infty = 18$ and $\varepsilon < 0.15$, good agreement was found between numerical results and the available experimental data, but for $\varepsilon > 0.2$ the agreement was poor. Recalling that in the second-order theory it was assumed that $\varepsilon << 1$, one should expect that as ε increases at some value the theory will no longer be applicable. For conditions considered here, this point appears to be near $\varepsilon = 0.15$. From this comparison the range of applicability of the theory is consistent with the range predicted from consideration of boundary layer-to-shock layer thickness ratio, δ/y_{sh}.

The previous first-order results of Lewis and Whitfield [7] are also shown for comparison in Figures 37 and 41. The apparently good agreement between their prediction and experimental data was simply fortuitous since only approximate transverse curvature (Clutter and Smith)

and displacement (iterated inviscid-viscous flow fields) were included.
The comparisons of transverse-curvature-induced friction drag showed that
the approximate Clutter and Smith treatment led to an error of about 30
per cent in that component. Also, iteration of the inviscid-viscous flow
fields reduced the displacement-induced pressure and friction drag. In a
first-order sense, it can be argued that iteration was allowable until
there was negligible change in $p(x)$. The fact remains, however, that in
the earlier work a sizable error existed in the transverse curvature term
and the important contribution of external vorticity was not considered.
It is interesting to note that the improved theoretical model and numerical
technique gave results in poorer agreement upon comparison of "theoreti-
cal" results and experimental data. However, the application of highly
approximate schemes outside the range where they have been extensively
compared with experimental data can lead to erroneous results.

CHAPTER VI
CONCLUSIONS AND SUMMARY

Based upon comparison of first- and second-order treatments of transverse curvature, vorticity, displacement, and slip and temperature jump, and comparisons of numerical results with experimental data, the following conclusions are drawn:

1. The approximate treatment of transverse curvature by Clutter and Smith led to errors in wall shear stress which in turn led to errors in transverse-curvature-induced friction drag of about 30 per cent.

2. The first- and second-order treatments of vorticity interaction were in substantial agreement over the forward half of the body, and the first-order treatment predicted higher wall shear and thus higher total vorticity-induced friction drag than the second-order results gave. Including vorticity interaction in the evaluation of displacement lead to unrealistic displacement thickness distributions over the body.

3. The first- and second-order treatments of slip and temperature jump led to significant differences in slip velocity and temperature but small differences in skin-friction coefficient. The differences in the friction-drag predictions for the two treatments were significant for this separate effect, but the effect on the linear combination of effects was not large. A strong effect of first-order slip and temperature jump was observed when coupled with all other higher-order effects at very low Reynolds number. However, in the range of applicability of the theory,

the effects were small.

4. The first- and second-order treatments predicted substantially the same displacement-induced pressure drag; however, the second-order treatment predicted substantially higher displacement-induced friction drag. The difference was attributed to the effects of normal pressure gradient and external vorticity on the second-order outer edge velocity and temperature since these effects were neglected in the first-order treatment.

5. The second-order displacement-pressure treatment used was not unique numerically, but the error was small (about 5 per cent) and gave physically realistic results for comparison of this separate effect with the first-order results. Because of the nonuniqueness of the results, only the sum of all second-order effects should be considered and the combined vorticity-displacement interaction based upon the displacement speed treatment should be used.

6. Both first- and second-order treatments substantially over-predicted the experimentally measured pressure distribution for a sphere-cone at $M_\infty \approx 18$. These differences are not understood since the comparisons were made under conditions where the second-order theory should be applicable. More extensive experimental data are needed to clearly establish the differences, and further improvements in the theoretical model are needed to improve the agreement with experimental observations.

7. The agreement between first- and second-order predictions of Stanton number and experimental data was excellent for $M_\infty = 18$. Caution must be used in interpreting these results since limited experimental data

were available for the conditions treated.

8. For M_∞ = 18 and ε < 0.15, good agreement was found between second-order predictions of zero-lift drag and experimental results. For ε > 0.2 at both M_∞ = 9 and 18, the second-order treatment substantially overpredicted the total drag, and higher-order effects are needed to improve agreement between theory and experiment.

9. For the conditions treated, the range of applicability of first- and second-order boundary-layer theories is predicted theoretically by the ε corresponding to $\delta/y_{shock} \approx 1$ and from comparison with experimental zero-lift drag data was found to be $\varepsilon \approx 0.15$.

In summary, it has been shown that, except for the pressure data in the expected range of applicability of the second-order theory ($\varepsilon \ll 1$), both first- and second-order treatments of higher-order boundary-layer effects were in substantial agreement with the experimental data. Beyond the expected ranges of applicability, the results from the numerical treatments substantially overpredicted the experimentally observed data. Since boundary-layer treatments higher than second order would introduce viscosity into the outer flow field and thus substantially complicate the outer as well as the inner flow-field solutions, it is clear that boundary-layer treatments higher than second order are not the correct approach. A theoretical model is needed which properly takes into account all higher-order effects such as a viscous "external" flow and the effects of transport properties on the shock wave. The fully viscous shock-layer treatment described by Davis [31] should provide a valuable tool for investigating this interesting and difficult problem.

BIBLIOGRAPHY

1. Whitfield, J. D. and Griffith, B. J., "Viscous Effects on Zero-Lift Drag of Slender Blunt Cones," AEDC-TDR-63-35, Arnold Air Force Station, Tennessee, 1963.

2. Cohen, C. B. and Reshotko, E., "Similar Solutions for the Compressible Laminar Boundary Layer with Heat Transfer and Pressure Gradient," NACA TR 1293, Washington, D. C., 1956.

3. Cohen, C. B. and Reshotko, E., "The Compressible Laminar Boundary Layer with Heat Transfer and Arbitrary Pressure Gradient," NACA TR 1294, Washington, D. C., 1956.

4. Lees, L. and Probstein, R. F., "Hypersonic Viscous Flow Over A Flat Plate," Princeton University Aeronautical Engineering Laboratory Report Number 195, Princeton, New Jersey, 1952.

5. Probstein, R. F., "Interacting Hypersonic Laminar Boundary Layer Flow Over A Cone," Brown University Division of Engineering Report Number AF 2798/1, Providence, Rhode Island, 1955.

6. Probstein, R. F. and Elliott, D., "Transverse Curvature Effect in Compressible Axially Symmetric Laminar Boundary-Layer Flow," J. Aeron. Sci., Vol. 23, No. 3, March 1956, pp. 208-224,236.

7. Lewis, C. H. and Whitfield, J. D., "Theoretical and Experimental Studies of Hypersonic Viscous Effects," AEDC-TR-65-100, Arnold Air Force Station, Tennessee, 1965.

8. Clutter, D. W. and Smith, A.M.O., "Solution of the General Boundary-Layer Equations for Compressible Laminar Flow, Including Transverse Curvature," Douglas Aircraft Company Report Number LB 31088, Long Beach, California, 1963.

9. Inouye, M., Rakich, J. V., and Lomax, H., "A Description of Numerical Methods and Computer Programs for Two-Dimensional and Axisymmetric Supersonic Flow over Blunt-Nosed and Flared Profiles," NASA TN D-2970, Washington, D. C., 1965.

10. Ferri, A. and Libby, P. A., "Note on an Interaction Between the Boundary Layer and the Inviscid Flow," J. Aeron. Sci., Vol. 21, No. 2, February 1954, p. 130.

11. Hayes, W. D., "On Laminar Boundary Layers with Heat Transfer," Jet Propulsion, Vol. 26, No. 4, April 1956, pp. 270-274.

12. Hayes, W. D. and Probstein, R. F., Hypersonic Flow Theory, Academic Press, New York, 1959.

13. Davis, R. T. and Flügge-Lotz, I., "Laminar Compressible Flow Past Axisymmetric Blunt Bodies (Results of a Second-Order Theory)," Stanford University Division of Engineering Mechanics Report Number 143, Stanford, California, 1963.

14. Van Dyke, M., "Second-Order Compressible Boundary-Layer Theory with Application to Blunt Bodies in Hypersonic Flow," Stanford University Department of Aeronautical Engineering Report Number SUDAER 112, Stanford, California, 1961.

15. Flügge-Lotz, I. and Blottner, F. G., "Computation of the Compressible Laminar Boundary-Layer Flow Including Displacement Thickness Interaction Using Finite-Difference Methods," Stanford University Division of Engineering Mechanics Report Number 131, Stanford, California, 1962.

16. Adams, J. C., Jr., "Higher Order Boundary-Layer Effects on Analytic Bodies of Revolution," Paper read at the AGARD Seminar on "Numerical Methods for Viscous Flows" at the National Physical Laboratory, Teddington, England, September 18-21, 1967.

17. Lees, L., "Laminar Heat Transfer over Blunt-Nosed Bodies at Hypersonic Flight Speeds," Jet Propulsion, Vol. 26, No. 4, April 1956, pp. 259-269,274.

18. Marchand, E. O., Lewis, C. H., and Davis, R. T., "Second-Order Boundary-Layer Effects on a Slender Blunt Cone at Hypersonic Conditions," AIAA Paper Number 68-54, January 1968.

19. Van Dyke, M., Perturbation Methods in Fluid Mechanics, Academic Press, New York, 1964.

20. Street, R. E., "A Study of Boundary Conditions in Slip-Flow Aerodynamics," Rarefied Gas Dynamics (Edited by F. M. Devienne), Pergamon Press, New York, 1960.

21. Van Dyke, M., "Higher Approximations in Boundary-Layer Theory Part 1. General Analysis," J. Fluid Mech., Vol. 14, Part 2, October 1962, pp. 161-177.

22. Jaffe, N. A., Lind, R. C., and Smith, A.M.O., "Solution to the Binary Diffusion Laminar Boundary-Layer Equations Including the Effect of Second-Order Transverse Curvature," Douglas Aircraft Company Report Number LB32613, Long Beach, California, 1966.

23. Clutter, D. W. and Smith, A.M.O., "Solution of the General Boundary-Layer Equations for Compressible Laminar Flow, Including Transverse Curvature," Douglas Aircraft Company Report Number LB31088, Long Beach, California, 1964.

24. Patterson, G. N., Molecular Flow of Gases, John Wiley and Sons, Inc., New York, 1956.

25. Mayne, A. W., Gilley, G. E., and Lewis, C. H., "Binary Boundary Layer on Sharp Cones in Low Density Supersonic and Hypersonic Flow," AIAA Paper Number 68-66, January 1968.

26. Van Dyke, M., "A Survey of Higher-Order Boundary-Layer Theory," Paper read at the AGARD Seminar on "Numerical Methods for Viscous Flows" at the National Physical Laboratory, Teddington, England, September 18-21, 1967.

27. Prandtl, L., "The Mechanics of Viscous Fluids," Aerodynamic Theory (Edited by W. F. Durand), Division G., Vol. 3, Springer, Berlin, 1935.

28. Whitfield, J. D. and Griffith, B. J., "Viscous Drag Effects on Slender Cones in Low-Density Hypersonic Flow," AIAA J., Vol. 2, No. 6, June 1965, pp. 1165-1166.

29. Lewis, C. H., "Pressure Distribution and Shock Shape Over Blunted Slender Cones at Mach Numbers from 16 to 19," AEDC-TN-61-81, Arnold Air Force Station, Tennessee, 1961.

30. Griffith, B. J. and Lewis, C. H., "Laminar Heat Transfer to Spherically Blunted Cones at Hypersonic Conditions," AIAA J., Vol. 2, No. 3, March 1964, pp. 438-444.

31. Davis, R. T., "The Hypersonic Fully Viscous Shock Layer Problem," Paper read at the AGARD Seminar on "Numerical Methods for Viscous Flows" at the National Physical Laboratory, Teddington, England, September 18-21, 1967.

32. Lomas, H. and Inouye, M., "Numerical Analysis of Flow Properties About Blunt Bodies Moving at Supersonic Speeds in an Equilibrium Gas," NASA TR R-204, Washington, D. C., 1964.

APPENDIXES

A. NUMERICAL METHODS FOR SOLVING
FIRST-ORDER BOUNDARY-LAYER EQUATIONS

B. FIRST- AND SECOND-ORDER BOUNDARY-LAYER
DISPLACEMENT EFFECTS

C. EFFECTS OF VORTICITY ON DISPLACEMENT
THICKNESS

APPENDIX A
NUMERICAL METHODS FOR SOLVING FIRST-ORDER
BOUNDARY-LAYER EQUATIONS

The treatment of the first-order boundary-layer effects was based on the method of Clutter and Smith [8] since considerable work had previously been done by Lewis and Whitfield [7] using the original method without vorticity interaction or slip and temperature jump.

The essential features of the method will first be desribed, and then the modifications required to include STJ and vorticity will be discussed.

The nonsimilar terms in the momentum and energy equation were replaced with two-point difference expressions, and the resulting equations were ordinary differential equations. The split boundary-value problem was then reduced to an initial-value problem for numerical solution.

· The procedure used for solving the boundary-layer equations is shown in Figure 42. The momentum equation is coupled to the energy equation through the fluid properties, and when the momentum equation solution is known, the energy equation is a linear differential equation in $\psi = g - 1$. The method then was as follows: First, fluid properties were assumed either crudely to initiate the solution or from the solution at the previous station or x location. Then, the momentum equation was integrated from the wall $\eta = 0$ to the outer edge of the boundary layer $\eta = \eta_\infty$. (The technique used for integrating the momentum equation is
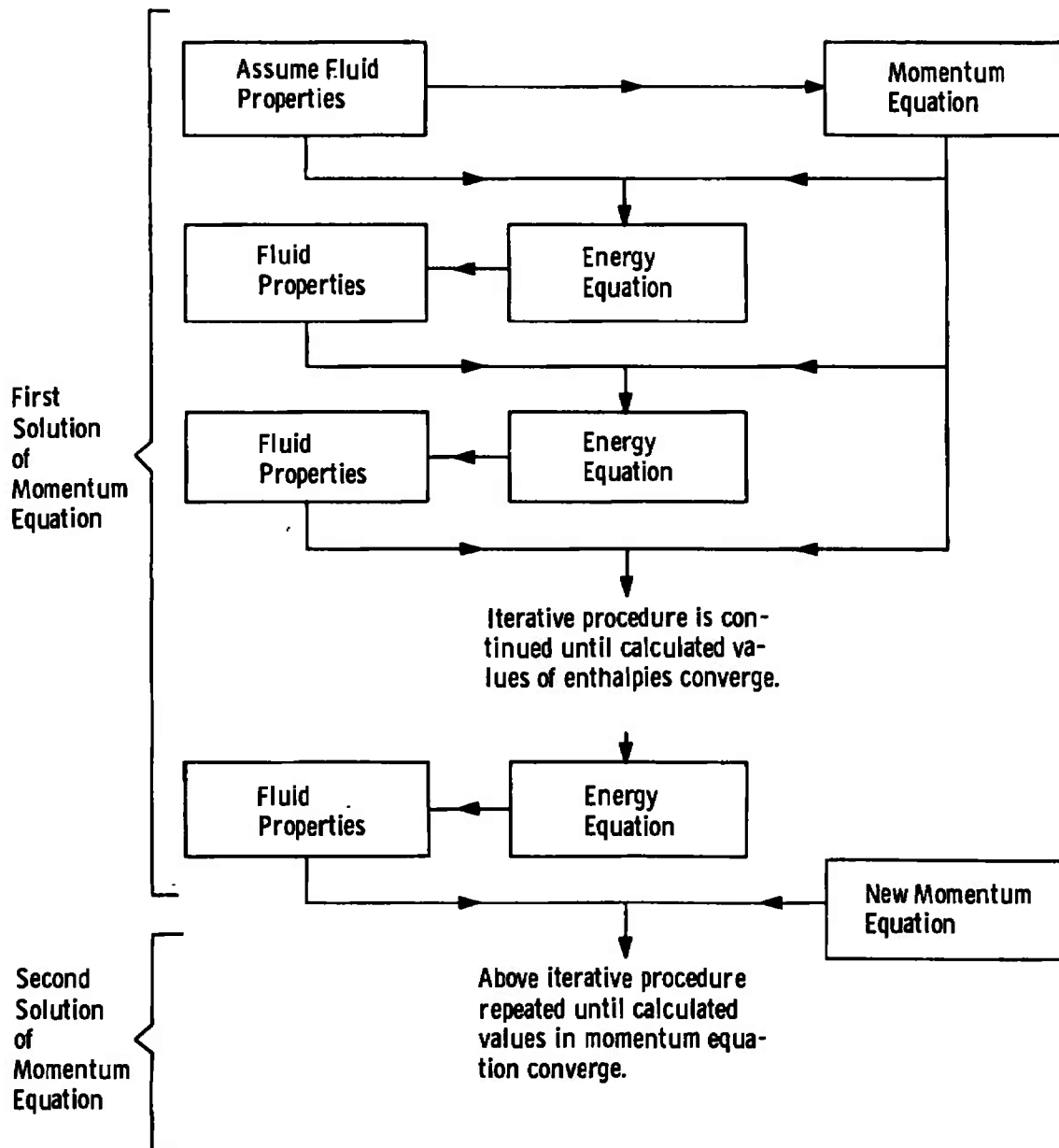
Fig. 42 Clutter and Smith's Procedure for Solving the Coupled Momentum
and Energy Equations (from Clutter and Smith [8])

described below.) Using the assumed fluid properties and the resulting trial solution of the momentum equation, two linearly independent solutions were obtained for the energy equation. Since the energy equation is linear, a linear combination of these two solutions was obtained satisfying the wall and outer edge boundary conditions. New fluid properties were obtained, and a new solution was obtained for the energy equation using the same solution of the momentum equation. This process was repeated a prescribed number of times or until two successive solutions of the energy equation agreed within a prescribed test, that is, until $|\psi_w'^{(j+1)} - \psi_w'^{(j)}| < e_e$ where j is the iteration index. Then a new solution of the momentum equation was obtained based on the updated fluid properties. The procedure for solving the system was repeated a prescribed number of times or until $|\phi''_w{}^{(k+1)} - \phi''_w{}^{(k)}| < e_m$. Typical values used in the calculations without vorticity or STJ were as follows:

Equation	Iterations	Convergence Test
Momentum	5	0.001
Energy	3	0.001

The values listed above were input data and could be changed as required; however, the machine program is large and the machine time required was affected by the choice of data. Therefore, the tests were made as loose as consistent with the problems solved.

The choice of method used to solve the momentum equation was important since the equation is nonlinear and under certain conditions the solutions were found not to converge. Figure 43 shows typical trial
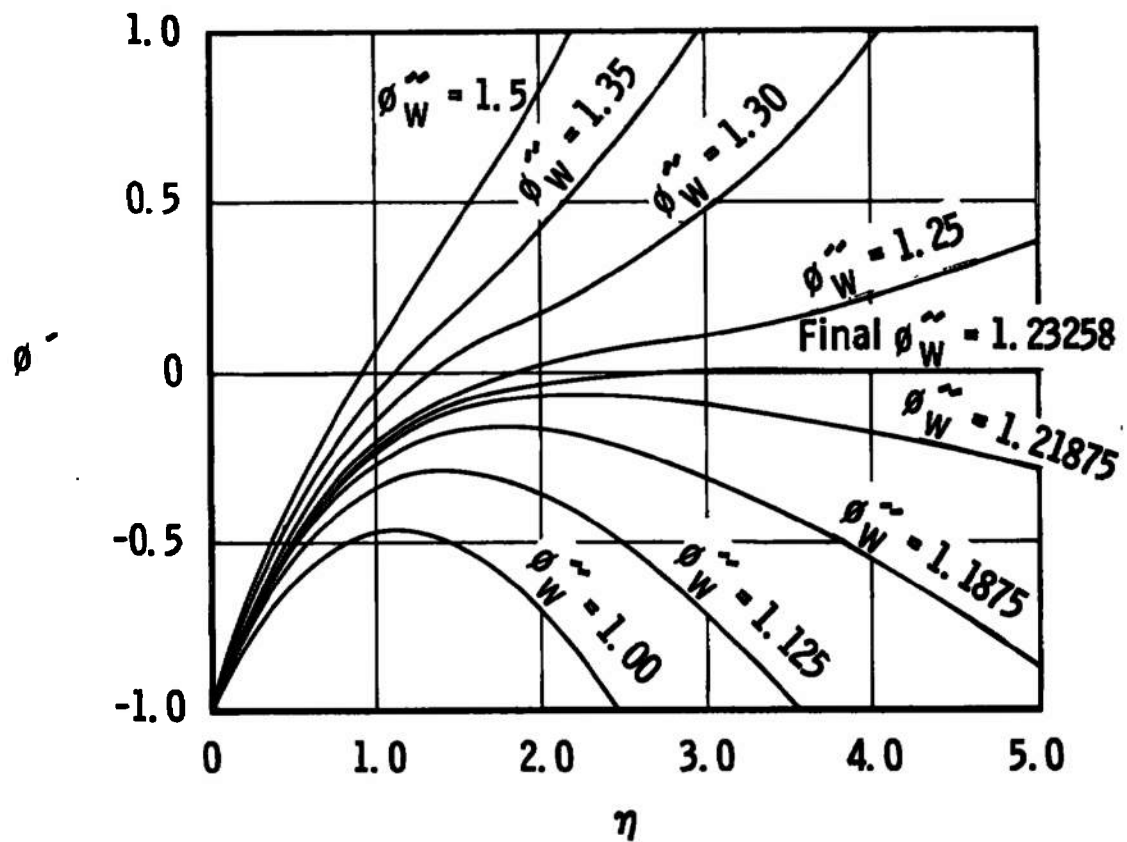
Fig. 43 Transformed Velocity Profiles Resulting from Trial Solutions of
the First-Order Momentum Equation in Clutter and Smith Variables
(from Clutter and Smith [8])

solutions for the momentum equation. The technique used is called "shooting" or "hunting" since solutions are sought which satisfy the wall and outer boundary conditions, namely $\phi'(0) = -1$ and $\phi'(\eta_\infty) = 0$ neglecting vorticity and STJ.

Briefly the method used was as follows: A trial guess of the solution ϕ''_w was made (either input or from a previously converged solution). The momentum equation was integrated from the wall $\eta = 0$ to $\eta = \eta_\infty$ or until $|\phi'| > K$ where K was an input constant which was typically $K = 0.5$ (in Figure 43, $K = 1.0$). The value of ϕ''_w was increased or decreased if $\phi'(\eta_{max}) < K$ or $\phi'(\eta_{max}) > K$, respectively, until $\eta_{max} = \eta_\infty$. The procedure was continued until three solutions were found, one of which was a high solution with $K > \phi'_\infty > 0$, and one a low solution $-K < \phi'_\infty < 0$, and the third solution was either high or low. The three solutions were then interpolated for a solution which satisfied the outer boundary condition at η_∞.

The method used to integrate both the momentum and energy equations was described by Clutter and Smith as a four-point extrapolation and interpolation formula, and they gave the details of the methods used.

Because of the iterative technique used by Clutter and Smith for solving the momentum and energy equation, it was easy to modify the boundary conditions to include vorticity and/or STJ. With vorticity the outer boundary condition becomes

$$\phi'_\infty = \Omega(x) \int_0^\infty \rho_e/\rho \ d\eta$$

and with STJ the wall boundary condition becomes

$$\phi'_w + 1 = f'_w = [\rho\mu/(\rho_*\mu_*)](\rho_*/\rho)F_s \, f''(\eta=0)$$

and

$$\psi_w + 1 = g_w = \frac{1}{H_e}\left[h_w + \frac{15}{8}\frac{\rho\mu}{\rho_*\mu_*}\frac{\rho_*}{\rho}F_s\frac{\partial h}{\partial \eta} + \frac{u_e^2}{2}f'^2_w\right]_w$$

where F_s is defined in Equation 86c.

The remaining significant change occurred in the density profile when vorticity was included. Since the pressure is constant across the boundary layer, the density profile becomes (for a perfect gas)

$$\frac{\rho_e}{\rho} = \frac{h}{h_e} = \frac{2(H/u_e^2) - f'^2}{2(H_e/u_e^2) - 1}$$

Since with vorticity $f'(\infty) > 1$, the boundary layer cannot extend to infinity because at some distance $h \to 0$ or $T \to 0$ and $\rho \to \infty$. Setting the static enthalpy h to zero in the above equation and solving for f' gives the maximum or limiting edge velocity possible

$$f'_{max} = 1/(1 - h_e/H_e)^{1/2}$$

The edge of the boundary layer (η_∞) must lie below this line of infinite density. Thus for large vorticity effects (large Ω), the value of η_∞ was reduced as the solution progressed along the body. It was often necessary to reduce the $\Delta\eta$ step size in the integration of the momentum and energy equations since values of $\eta_\infty < 1$ were not uncommon.

In order to reduce the step size $\Delta\eta$, it was necessary to stop the calculation, interpolate all quantities which were functions of η, and continue the calculation with the new step size. The procedure was straightforward but time consuming, especially when it was necessary to interpolate the results several times for a given set of conditions.

APPENDIX B
FIRST- AND SECOND-ORDER BOUNDARY-LAYER DISPLACEMENT EFFECTS

In both first- and second-order treatments it was necessary to obtain a solution for the perturbed inviscid outer flow. The outer flow solution was obtained over the geometric body perturbed by the first-order displacement thickness defined as follows:

$$\delta^* = \int_0^\infty [1 - \rho u/(\rho_e u_e)]dy$$

Inverse blunt body and characteristics solutions were obtained over the effective body. The method used was a modification of one developed by Lomax and Inouye [32]. The modification was necessary to properly describe the effective body since, in general, no simple means was available to describe the entire body. An accurate approximate scheme was developed which permitted fitting the body by three separate curve-fit procedures with proper matching conditions.

Approximate treatments have been used in the past to perturb the outer flow field. Davis and Flügge-Lotz perturbed the first-order inviscid flow solutions by assuming the effective body to be a body approximated by shifting and expanding the original geometric body. This treatment had the desirable feature of being independent of the expansion parameter ϵ, and thus the results were quite general. The disadvantage which ruled out this method was that the shifted and expanded body technique was limited to the nose region (see [13]).

Since inviscid solutions were required over the entire effective body and especially over the conical afterbody, a new and more general method of solution was developed.

A crude attempt was previously developed by Lewis and Whitfield [7] to treat the displacement effect. In that treatment, the spherical nose was expanded or contracted by the displacement thickness at the initial data line just downstream of the sonic line, and an approximate curve was faired between the spherical nose and a curve fit of the downstream effective body data. That method worked reasonably well except at very low Reynolds numbers in which case the displacement thickness became large and the region covered by the approximate curve fit became large in extent.

The method used herein was an improvement on the scheme of Lewis and Whitfield [7] in that the numerical accuracy was substantially improved. The perturbed spherical nose was approximated with small error by a conic where the bluntness ratio was computed by fitting the effective body at the initial data surface. This surface was determined by a rotationally symmetric line normal to the body where M = 1.05 at the inviscid wall. A curve was then fitted to the effective body data such that r, dr/dz, and d^2r/dz^2 were continuous on the surface at the initial line (M = 1.05) and also at the point where the curve joined the curve which fitted the data over the conical afterbody. The intermediate curve fit was also required to have no inflection points, and the best fit of the data in the least-squares sense which satisfied the other criteria was chosen.

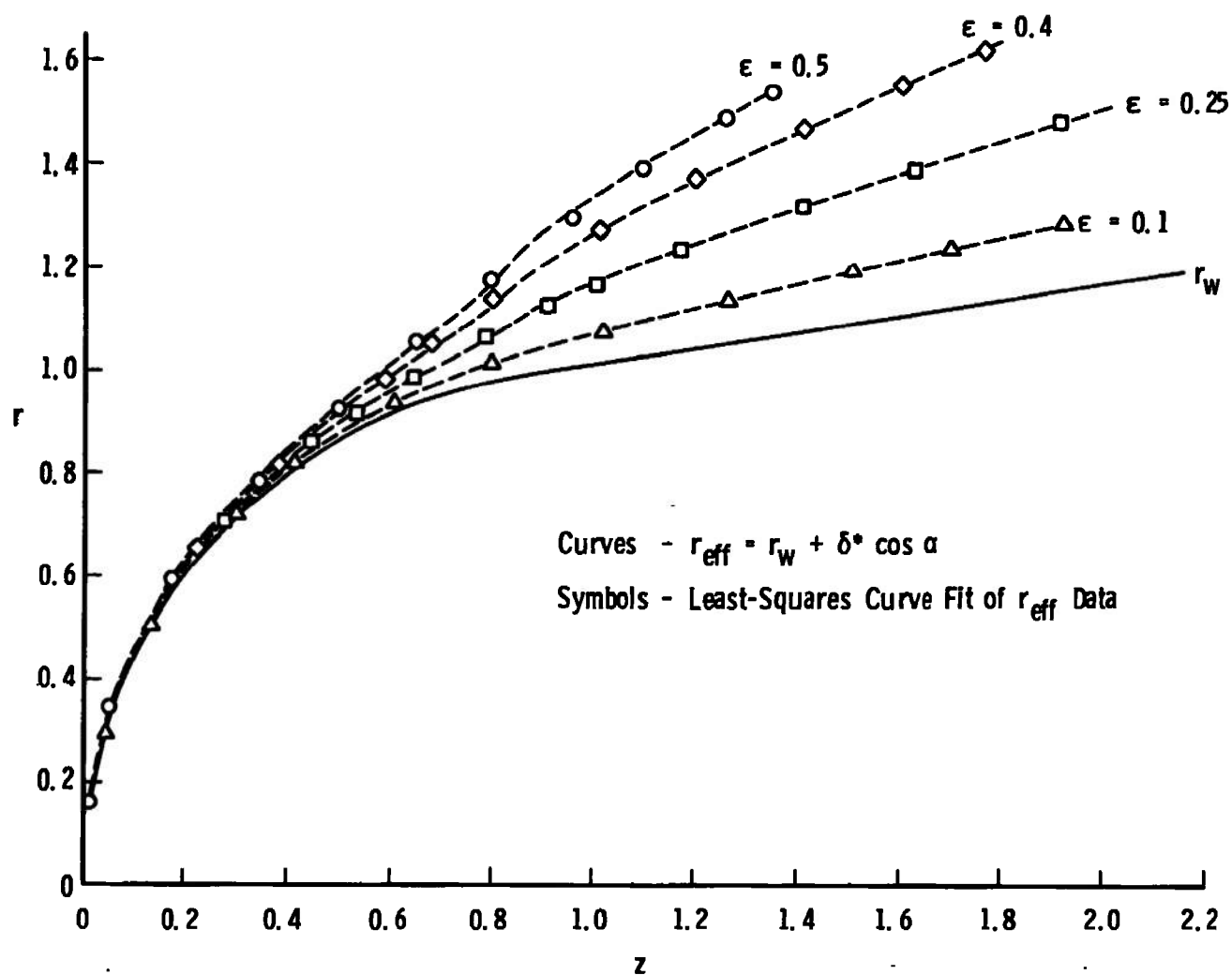The results of the curve-fit procedure are shown in Figure 44.

Fig. 44 Curve Fit of Effective Body Data for Blunt Body and Characteristics
Solutions at $M_\infty = 9$ and $T_w/T_o = 0.2$

The fit became poorer as values of ε increased from 0.1 to 0.5 since an inflection in the effective body curve occurred at the higher values. However, in a least-squares sense the fit remained good even though the extent of region increased substantially. Allowing inflection points to occur in the region near $z = 0.8$ would have induced a secondary shock and substantially altered the flow field over the conical afterbody. Experimental data did not indicate any such secondary shock, and such a shock was not allowed.

The perturbed inviscid outer flow solution method (blunt body and characteristics solution) was identical for both first- and second-order boundary-layer treatments. The difference in application were: (1) the way in which the outer boundary conditions are obtained, (2) the effects of the normal pressure gradients, and (3) the effects of inviscid vorticity.

I. FIRST-ORDER TREATMENT

The perturbed inviscid outer flow pressure was imposed on the first-order boundary-layer equations, and consistent with the first-order theory, the normal pressure gradient was neglected. The edge velocity was obtained from Bernoulli's equation, and the derivative was obtained numerically. The effects of inviscid vorticity were only implicitly involved through the blunt body and characteristics solution. Through the positive viscous-induced pressure increment, the first-order displacement treatment always produced an increase in both pressure and friction drag. This result is to be contrasted with the second-order treatment described below.

II. SECOND-ORDER DISPLACEMENT PRESSURE TREATMENT

The skin-friction coefficient C_f is defined as follows:

$$C_{f_\infty} = [2/\rho_\infty^* U_\infty^{*2}] \; (\mu^* \; \partial u^*/\partial n^*)_{n=0}$$

$$= 2\epsilon \; \tau_1(s,0) + 2\epsilon^2 \; \tau_2(s,0)$$

where

$$\tau_1(s,0) = (\mu u_{1N})_{N=0}$$

$$\tau_2(s,0) = (\mu u_{2N} + \mu' \; t_2 \; u_{1N})_{N=0}$$

Therefore, if $\tau_2(s,0)$ is independent of ϵ, then the friction-drag component will be independent of ϵ, and the total second-order friction drag $C_{Df2} = \int C_{f_\infty 2} \cos \alpha \; 2\pi \; r_w ds/A_b$ will be quadratically dependent on ϵ. The first-order friction drag is given by $C_{Df1} \propto \epsilon$. The dependence was easily seen by inspection of the second-order equations except in the case of the displacement effect. For all second-order effects except displacement, ϵ did not appear in the calculation. However, the outer edge boundary conditions for the second-order displacement pressure effect depended on ϵ through the extrapolation of the inviscid outer flow pressure and velocity from the effective body to the geometric wall. Therefore, a perturbed inviscid outer flow solution was obtained for different values of ϵ over the range of interest, whereas the other effects were simply scaled by ϵ^2 from a single calculation for given geometry and free-stream conditions (see also Marchand, Lewis, and Davis [18]).

The discontinuity in surface curvature, κ , caused difficulties

in numerically evaluating the x-derivative of the extrapolated inviscid outer flow pressure. The discontinuity was replaced by an exponential fairing between $\kappa = 1$ and 0. The constant in the exponential term was varied as the x-step size was changed until a smooth transition in shear stress was obtained in the region of the sphere-cone tangent point. This scheme reduced some large oscillations induced by the discontinuity without substantially affecting the total displacement-induced friction drag.

III. COMPARISON OF FIRST- AND SECOND-ORDER TREATMENTS

The significant difference between the first- and second-order treatments was in the normal pressure gradient. In the second-order theory, the second-order normal momentum equation was used to extrapolate the pressure along the effective wall to the geometric wall or body surface. Consistent with the original first-order boundary-layer equations, the normal component of momentum was not considered in the first-order treatment, and the pressure was assumed constant throughout the boundary layer normal to the surface. Therefore, in the first-order treatment the perturbed inviscid outer flow pressure was impressed upon the first-order boundary layer as the edge pressure.

The comparative effects on the first- and second-order solutions were as follows:

1. Over the nose where the longitudinal curvature $\kappa = 1$, the pressure on the surface from the second-order theory was either increased or decreased from the effective wall value, depending on

129

whether the displacement thickness was negative (highly cooled wall) or positive. Over the conical afterbody, where $\kappa = 0$, the first- and second-order treatments yielded the same surface pressure, assuming equivalent displacement thicknesses. However, because of the effects of the inviscid vorticity along the wall, the velocity at the surface was always less over the conical afterbody based upon the second-order theory. This effect due to inviscid vorticity was <u>independent</u> of inclusion or exclusion of the vorticity effect in the second-order boundary-layer treatment. Again, the coupling between displacement and vorticity is seen, but this time through the inviscid flow fields.

2. The first-order displacement treatment always induced an increase in friction and pressure drags. The second-order effects could be either positive or negative, depending on the sign and magnitude of displacement thickness, and the effects of longitudinal curvature and inviscid external vorticity.

These two major factors can cause the first- and second-order displacement treatments to yield substantially different effects on such global quantities as drag and total heat transfer; however, for the length of the cone and other conditions treated here, the first- and second-order treatments predicted induced-drag effects in good agreement.

APPENDIX C
EFFECTS OF VORTICITY ON DISPLACEMENT THICKNESS

Assuming the following form for the inviscid velocity profile,

$$u_i = u_e \ (1 + U_i' \ y)$$

where $U_i' = (f'(\infty) - 1)/y(\infty)$; then the definition of displacement thickness

$$\int_0^{\delta^*} \rho_i u_i r^j dy = \int_0^\infty \rho_i u_i r^j dy - \int_0^\infty \rho u r^j dy$$

leads to the following integral equation:

$$B \int_0^{\delta_v^*} (\rho_i/\rho_e)(1 + U_i' \ y)(r_w + y \cos \alpha)^j \ dy$$

$$= B \int_0^\infty (\rho_i/\rho_e)(1 + U_i' \ y)(r_w + y \cos \alpha)^j \ dy$$

$$- \int_0^\infty f'(r_w + y \cos \alpha)^j \ d\eta$$

where $B = [Re_* \ (u_e/u_*)/x]^{1/2} \ \rho_e/\rho_*$.

When the vorticity is neglected, $U_i' = 0$ and the integral equation for δ_v^* reduces to the classical axisymmetric form of the equation with TVC. Results are shown in Chapter IV for the variation of δ_v^* over the body.

DOCUMENT CONTROL DATA - R & D

(Security classification of title, body of abstract and indexing annotation must be entered when the overall report is classified)

1. ORIGINATING ACTIVITY (Corporate author)	2a. REPORT SECURITY CLASSIFICATION
Arnold Engineering Development Center ARO, Inc., Operating Contractor Arnold Air Force Station, Tennessee	UNCLASSIFIED
	2b. GROUP N/A

3. REPORT TITLE

COMPARISON OF A FIRST-ORDER TREATMENT OF HIGHER-ORDER BOUNDARY-LAYER EFFECTS WITH SECOND-ORDER THEORY AND EXPERIMENTAL DATA

4. DESCRIPTIVE NOTES *(Type of report and inclusive dates)*

June 1, 1966 to January 1, 1968 – Final Report

5. AUTHOR(S) *(First name, middle initial, last name)*

Clark H. Lewis, ARO, Inc.

6. REPORT DATE	7a. TOTAL NO. OF PAGES	7b. NO. OF REFS
October 1968	151	32

8a. CONTRACT OR GRANT NO. F40600-69-C-0001	9a. ORIGINATOR'S REPORT NUMBER(S)
b. PROJECT NO. 8953	AEDC-TR-68-148
c. Program Element 6540223F	9b. OTHER REPORT NO(S) (Any other numbers that may be assigned this report)
d.	N/A

10. DISTRIBUTION STATEMENT

This document has been approved for public release and sale; its distribution is unlimited.

11. SUPPLEMENTARY NOTES	12. SPONSORING MILITARY ACTIVITY
Available in DDC.	Arnold Engineering Development Center, Air Force Systems Command, Arnold Air Force Station, Tennessee

13. ABSTRACT The axisymmetric nonsimilar compressible laminar boundary-layer equations including approximate transverse curvature terms were modified to treat inviscid external vorticity, slip and temperature jump as first-order quantities, and this is referred to as the first-order treatment. The effects of boundary-layer displacement were also treated. Primary interest was in predicting experimentally measurable quantities over the entire body length of nonanalytic shapes, and the analysis was not confined to the nose or stagnation region. A review is included of second-order boundary-layer theory and of recent developments in the numerical solution of second-order boundary-layer effects. Comparisons of predicted displacement-induced pressure distributions, heat-transfer distributions and zero-lift drag were made with results from second-order boundary-layer theory and experimental data for a spherically blunted 9-deg half-angle cone at free-stream Mach numbers of 9 and 18. At moderate to high Reynolds numbers, the comparisons showed good agreement between first- and second-order predictions and experimental results for drag and heat-transfer distributions; however, poor agreement was found between predicted and experimental displacement-induced pressure distributions. At low Reynolds numbers, both first- and second-order treatments substantially overpredicted the zero-lift drag. The range of applicability of the theories was established for the conditions treated by inspection of the numerical results and by comparison of the numerical results with experimental zero-lift drag data.

DD FORM 1473
1 NOV 65

14. KEY WORDS.	LINK A		LINK B		LINK C	
	ROLE	WT	ROLE	WT	ROLE	WT
boundary-layer theory						
laminar flow						
vorticity						
slip						
temperature jump						
displacement						
pressure distribution						
heat-transfer distribution						
zero-lift drag						
hypervelocity flow						

1. Flow Boundary Layer -- Mathematical analyses

2. " " -- Pressure distribution

3. " " -- Heat transfer

1 ~ 2.